UNIVERSITY OF OKLAHOMA

GRADUATE COLLEGE

STRUCTURE – FUNCTION ANALYSIS OF HUMAN ONCOSTATIN M

A DISSERTATION

SUBMITTED TO THE GRADUATE FACULTY

in partial fulfillment of the requirements for the

Degree of

DOCTOR OF PHILOSOPHY

By

SRINIVAS CHOLLANGI
Norman, Oklahoma
2009

Downloaded from SHAREOK. Persistent Handle URL: https://hdl.handle.net/11244/319327

STRUCTURE – FUNCTION ANALYSIS OF HUMAN ONCOSTATIN M

A DISSERTATION APPROVED FOR THE
DEPARTMENT OF BIOENGINEERING

BY

Dr. Mathias U. Nollert, Chair

Dr. John D. Ash

Dr. Timothy Mather

Dr. Edgar A. O'Rear III

Dr. Roger G. Harrison

Dr. Alberto Striolo

© Copyright by SRINIVAS CHOLLANGI 2009
All Rights Reserved.

Dedicated to

Nishitha & My Parents

Acknowledgements

Throughout my degree program, I am honored to have worked in the company of many wonderful researchers both at the University of Oklahoma, Norman campus and the Health Sciences Center campus in Oklahoma City. I am greatly indebted to my advisor Dr. John D. Ash for giving me an opportunity to work in his lab and for his support throughout my work. Thank you Dr. Ash for always challenging me to aim for nothing short of a high quality research and, for always being there when I needed help. The knowledge I have gained in this lab is invaluable and I am very thankful to you for all those thought-provoking discussions and helping me develop critical thinking in addressing the research questions.

I would like to express my thanks to Dr. Timothy Mather for teaching me the basics of protein structural analysis and for patiently helping me in designing and characterizing the mutant proteins. Also, I would like to thank the rest of all my committee members Dr. Mathias U. Nollert, Dr. Edgar A. O'Rear III, Dr. Roger G. Harrison and Dr. Alberto Striolo for their stimulating discussions and valuable suggestions throughout.

I would like to thank Dr. Karla Rodgers and Ruby Rehman for all their help in conducting Circular Dichroism experiments and Nathan Gillock at ICX Technologies for his help in conducting the SPR experiments. And, thank you Dr.

Michael Elliott, for all your help in going through my manuscripts and helping me with corrections. I am also very thankful to all my lab members, Dr. Jiangang Wang, Ray Archer, Anisse Saadi, Yumi Ueki, Ana Chucair, Lei Xu and Fatemeh Shariati for providing a nice amicable environment to work in. Particularly, I am greatly indebted to Dr. Jiangang Wang for all his help in conducting animal experiments also providing me with the moral support when I am low.

And finally, I am very thankful to Nishitha, my parents and all other family members for inspiring me and for always being there for me. This work would not have been possible without your support.

Thank you all very much !!

TABLE OF CONTENTS

ABSTRACT XVI

1. INTRODUCTION 1

1.1. Oncostatin M and IL-6 family cytokines 1

1.1.1. IL-6 family Cytokines 1

1.1.2. gp130 family of cytokine receptors 9

1.1.3. Ligand-Receptor Interaction 14

1.1.4. Mapping Binding Sites on the Cytokines 17

1.1.5. Stoichiometry of Signaling Complexes 32

1.2. Biological activities of OSM & other IL-6 family cytokines 37

1.2.1. Inflammation 37

1.2.2. Neuroprotection 39

1.2.3. Hematopoiesis 42

1.2.4. Other Functions of Oncostatin M 43

1.3. Controlled Drug Delivery 45

1.3.1. Hydrogels 49

1.3.2. Types of Hydrogels 51

1.3.3. Polymers in Controlled Drug Delivery 54

1.3.4. Mechanisms of Drug Delivery 57

1.4. Outline 63

2. MATERIALS AND METHODS 65

2.1. Mutation of human Oncostatin M 65

2.2. Recombinant protein expression and purification 70

2.3. Circular Dichroism 71

2.4. Cell culture and cytokine stimulation 72

2.5. Cell proliferation 72
2.6. Animals and bright cyclic light preconditioning 73
2.7. Bright Light Damage 74
2.8. Real-time RT-PCR 75
2.9. Electroretinograms (ERGs) 77
2.10. Intravitreal Injections 78
2.11. Histological analysis 78
2.12. Western Blots 79
2.13. Surface Plasmon Resonance (SPR) 80
2.14. Enzyme-linked immunosorbent assay (ELISA) 83
2.15. Synthesis of PEG hydrogels 85
2.16. Theoretical Estimation of Drug Release 88
2.17. Evaluation of Drug Release – *In vitro* 90
2.18. Evaluation of Drug Release – *In Vivo* 90
2.19. Statistical Analysis 92

3. RESULTS AND DISCUSSION 93
3.1. Preconditioning-Induced Protection from Oxidative Injury is Mediated by Leukemia Inhibitory Factor Receptor (LIFR) and its Ligands in the Retina 93
3.1.1. Introduction 93
3.1.2. Results 96
3.1.2.1. Preconditioning-Induced Protection 96
3.1.2.2. Expression of neuroprotective factors during preconditioning 98
3.1.2.3. Antagonism of LIFR attenuates preconditioning-induced STAT3 activation 101

3.1.2.4. Antagonism of LIFR blocks preconditioning-induced protection 103
3.1.2.5. Effect of LIF05 on normal retinal function 106
3.1.2.6. LIF05 inhibits LIF induced STAT3 activation 109
3.1.2.7. LIF forms a high affinity stable complex with LIFR and gp130 111
3.1.3. Discussion 114
3.2. A Unique Loop Structure in Oncostatin M Reduces Binding Affinity Towards Oncostatin M Receptor and Leukemia Inhibitory Factor Receptor 117
3.2.1. Introduction 117
3.2.2. Results 119
3.2.2.1. Structural analysis of hLIF and hOSM: Identification of the BC loop. 119
3.2.2.2. Structural characterization of OSM-M1 and OSM-M2 125
3.2.2.3. Functional Evaluation of wild-type* and mutant OSMs in their activation of OSMR:gp130 complexes 127
3.2.2.4. Functional Evaluation of wild-type and mutant OSMs in their activation of LIFR:gp130 complexes. 130
3.2.2.5. Removal of BC loop does not alter the requirement of core FXXK motif in active site III. 132
3.2.2.6. Reducing the size of BC loop improves OSM's affinity towards LIFR and OSMR 134
3.2.2.7. Inhibition of A375 melanoma cell proliferation 143
3.2.2.8. Protection of retinal photoreceptors 145
Discussion 148
3.3. Sustained Delivery of human Oncostatin M (hOSM) to Retina using poly(ethylene glycol) (PEG) based hydrogels 152
3.3.1. Introduction 152
3.3.2. Results 156

3.3.2.1. Estimation of volumetric swelling ratio (Q), mesh size (ξ) and diffusivity of the drugs in hydrogel (Dg) 156
3.3.2.2. Theoretical Estimation of Drug Diffusion from Hydrogels 162
3.3.2.3. Drug Release Studies – *In Vitro* 168
3.3.2.4. Drug Release Studies – *In Vivo* 173
3.3.3. Discussion 177

4. CONCLUSIONS AND RECOMMENDATIONS 180

BIBLIOGRAPHY 189

APPENDIX 211
A1. Concentration profile as a function of position (x) and time (t): 211
A2. Fractional Release of Drug as a function of time (t) 217

LIST OF TABLES

Table 1.1 Site III amino acid sequences of various IL-6 family cytokines. 26
Table 1.2 Composition of IL-6 family cytokine receptor complexes 33
Table 1.3 Examples of natural and synthetic polymers commonly used in synthesis of hydrogels 50
Table 1.4 Chemical structure and desirable properties of some of the common polymers used in synthesis of hydrogels. 55
Table 2.1 Primers used for PCR amplification of hOSM gene and conducting point mutations thereafter 69
Table 2.2 Forward and reverse primers used in RT-PCR analysis. (F – Forward, R – Reverse, bp – base pairs) 76
Table 3.1 Comparison of association (k_a), dissociation (k_d) and estimated equilibrium dissociation (K_D) constants for LIFR and gp130 binding to LIF and LIF05. 113
Table 3.2 Comparison of association (k_a), dissociation (k_d) and equilibrium dissociation (K_D) constants for LIFR and gp130 binding to LIF, OSM-WT, OSM-M1 and OSM-M2. 137
Table 3.3 Comparison of apparent equilibrium dissociation constant ($K_{D,App}$) values (nM) for direct interaction of LIFR and OSMR with LIF, OSM-WT*, OSM-M1 and OSM-M2 or the interaction of LIFR and OSMR with gp130 bound LIF, OSM-WT*, OSM-M1 and OSM-M2) 142

LIST OF FIGURES

Figure 1.1 Protein sequence of full length and mature human OSM 3
Figure 1.2 Crystal structure of mature human OSM with its N and C terminals indicated. 4
Figure 1.3 Structure of IL-6 with the α-helices A, B, C and D identified 5
Figure 1.4 Crystal structures of IL-2, IL-6 and IFN-γ. 7
Figure 1.5 Receptor complexes of IL-6 family cytokines 8
Figure 1.6 Domain composition of receptor subunits involved in IL-6 family cytokine signaling. 10
Figure 1.7 Crystal structure of LIF in complex with the cytokine binding domain (CBD) of gp130 13
Figure 1.8 IL-6 signaling via the gp130/jak/STAT pathway 16
Figure 1.9 Comparison of site II residues on hLIF and hOSM 18
Figure 1.10 Complementarity between the interaction surfaces of hOSM and gp130 21
Figure 1.11 Site II residues of IL-6 and IL-11 responsible for gp130 binding. 22
Figure 1.12 Surface representations showing the site III interfaces of OSM, LIF CNTF and IL-6. 25
Figure 1.13 Site I residues of IL-6 that participate in IL-6Rα binding. 28
Figure 1.14 Water molecules (red spheres) in the region between the helix D and the A-B loop of IL-6 30
Figure 1.15 Site I residues of CNTF and IL-11 that play a key role in binding CNTFRα and IL-11Rα respectively 31
Figure 1.16 Schematic diagram of the hexameric receptor complex assembly for IL-6 35
Figure 1.17 Three-dimensional model structures for IL-6 family cytokines in complex with their receptors. 36
Figure 1.18 Changes in systemic levels of drug concentrations with traditional methods of repeated cyclic administration 46

Figure 1.19 Changes in systemic levels of drug concentrations with ideal modes of controlled drug delivery 48
Figure 1.20 Schematic of methods for forming physical and chemical hydrogels 52
Figure 1.21 Mechanisms of controlled drug delivery from A) matrix and B) reservoir devices 59
Figure 1.22 Mechanisms of drug delivery from a surface eroding vs. bulk eroding device. 61
Figure 2.1 Amino acid sequence of human OSM. 67
Figure 2.2 SDS-PAGE analysis of OSM with or without the 'AGA' modification after subjection to thrombin cleavage. 68
Figure 2.3 STAT3 activation in human Müller cells in response to stimulation with GST fused wild type (GST-hOSM (WT)) or AGA modified human OSM (GST-hSOM (modified). 68
Figure 2.4 Schematic diagram of bright cyclic light preconditioning. 74
Figure 2.5 Schematic representation of cytokine – receptor interaction on SPR chip 82
Figure 2.6 Chemical structures of poly(ethylene glycol) (PEG) and poly(ethylene glycol) diacrylate (PEGDA) macromers 87
Figure 2.7 Schematic representation of photopolymerization. 87
Figure 2.8 Schematic representation of a lateral section of circular disc uniformly dispersed with drug (shown in blue color) at a concentration C_o. 89
Figure 2.9 Schematic representation of sub-conjunctival hydrogel implantation in a mouse eye 91
Figure 3.1 Schematic representation of cellular architecture in the retina 94
Figure 3.2 Functional and morphological evaluation of preconditioning-induced protection of retinal photoreceptors 97
Figure 3.3 Preconditioning with bright cyclic light leads to strong upregulation of neuroprotective factors. 100

Figure 3.4 LIF05 inhibited preconditioning-induced STAT3 activation. 102
Figure 3.5 LIF05 inhibited preconditioning-induced protection of retinal photoreceptors. 105
Figure 3.6 Evaluation of LIF05 toxicity towards retinal function and morphology 108
Figure 3.7 LIF05 inhibits LIF stimulated STAT3 activation *in vivo*. 110
Figure 3.8 Kinetic analysis of LIFR and gp130 interaction towards LIF and LIF05 112
Figure 3.9 A, B) Crystal structures of LIF (PDB: 1EMR) and OSM (PDB: 1EVS) with their active sites and helices A, B, C and D identified. 121
Figure 3.10 Amino acid sequences of wild type OSM and the mutant variants of OSM with truncated BC loops 123
Figure 3.11 SDS-PAGE analysis of purified proteins 124
Figure 3.12 Modifications in the BC loop area of OSM did not induce a global change in the protein's structure. 126
Figure 3.13 Human Müller cells express LIFR, gp130 while A375 melanoma cells express OSMR, gp130 on their cell surface. 128
Figure 3.14 Activation of STAT3 and Erk 1/2 in A375 melanoma cells in response to different doses of wild type (OSM-WT) and the mutant forms of OSM (OSM-M1 and OSM-M2). 129
Figure 3.15 Activation of STAT3 and Erk 1/2 in human Müller cells in response to different doses of wild type (OSM-WT) and mutant forms of OSM (OSM-M1 and OSM-M2) 131
Figure 3.16 OSM with truncated BC loop still utilizes the FXXK motif to activate LIFR and OSMR. 133
Figure 3.17 Kinetic analysis of LIFR and gp130 interaction towards LIF, OSM-WT, OSM-M1 or OSM-M2 136

Figure 3.18 Neither wild type (OSM-WT) nor the mutant forms of OSM with truncated BC loop (OSM-M1 and OSM-M2) exhibit a direct affinity towards OSMR. 140
Figure 3.19 ELISA analysis of OSMR and LIFR binding towards LIF, OSM-WT*, OSM-M1 and OSM-M2 or gp130 bound LIF (gp130:LIF), OSM-WT* (gp130:OSM-WT*), OSM-M1 (gp130:OSM-M1) and OSM-M2 (gp130:OSM-M2). 141
Figure 3.20 A375 melanoma cell proliferation in the presence or absence of OSM-WT, OSM-M1 and OSM-M2. 144
Figure 3.21 Mutant OSM's with truncated BC loop (OSM-M1 and OSM-M2) are more potent than the wild-type* OSM (OSM-WT) in protecting the photoreceptor cells from light damage (LD). 147
Figure 3.22 Schematic representation of the eye. 154
Figure 3.23 Changes in mass swelling ratio, volumetric swelling ratio and mesh size of PEG hydrogels as a function of macromer content 160
Figure 3.24 Changes in diffusivity (D_g) of hOSM through PEG 5000 DA hydrogels as a function of macromer content in the hydrogel. 161
Figure 3.25 Theoretical predictions for changes in the concentration profile of hOSM through a hydrogel slab as a function of time. 164
Figure 3.26 Theoretical predictions for fractional release (A) and average release rate (B) of hOSM through 10 wt% and 50 wt% PEG hydrogels. 167
Figure 3.27 Percent release of hOSM from a 10% and 50% PEG hydrogel as a function of time. 170
Figure 3.28 Percent release of BSA from a 10% and 50% PEG hydrogel as a function of time. 171

Figure 3.29 STAT3 activation profile in mouse retina after sub-conjunctival implantation with PEG hydrogels releasing hOSM. 175
Figure 3.30 Comparison of STAT3 activation in the retina with theoretical predictions for release rate from the hydrogel (Figure 3.30 with Figure 3.27B). 176
Figure 4.1 Schematic representation of hypothesized model for stress induced protection of photoreceptor cells. 183

ABSTRACT

Oncostatin M (OSM) is a pleiotropic cytokine that belongs to the interleukin-6 (IL-6) family of cytokines. These cytokines play crucial role in diverse biological events like inflammation, neuroprotection, hematopoiesis, metabolism and development. For example, when exposed to moderate levels of oxidative stress (i.e. bright cyclic light), IL-6 family cytokines are strongly upregulated in the retina. Using inhibition studies, we show that these upregulated cytokines play an essential role in protecting the neuronal cells from succumbing to subsequent lethal doses of oxidative stress. These wide ranges of functions elicited by IL-6 family cytokines are mediated by the formation of multimeric receptor complexes, which include a common receptor glycoprotein 130 (gp130). OSM is unique in this family since it can signal via two different receptor complexes i.e. LIFR:gp130 (type I) and OSMR:gp130 (type II). We have identified a unique helical loop on OSM between its B and C helices, which is not found on other IL-6 family cytokines. Based on its size and location, we hypothesized that the BC loop is responsible for OSM's unique ability to bind and activate OSMR. However, our experiments with mutated OSM molecules that have truncated BC loops showed that the BC loop does not play a role in OSM's unique ability to bind OSMR, but instead presents a steric hindrance for OSM's strong interaction with OSMR and LIFR. Kinetic and equilibrium binding analyses using surface plasmon resonance (SPR) and enzyme-linked immunosorbent assay (ELISA) support the evidence for improved binding and stability between mutant OSMs

and the receptor complexes. Also, as a consequence of improved binding, these structurally modified OSMs exhibit enhanced ability in suppressing the proliferation of A375 melanoma cells and also protecting the neuronal cells in retina from oxidative stress, demonstrating that improved binding has functional consequences. Finally, we have evaluated the applicability of poly(ethylene glycol) (PEG) based hydrogels for delivering these molecules in a controlled manner. Using *in vitro* and *in vivo* studies in mice, we show that PEG hydrogels fabricated with PEG-diacrylate macromers with a molecular weight of 5000 Da can be used to deliver these cytokines in a sustained manner for ~12 days. And, for transscleral transport, a release rate of at least 0.5 μg/day is required for OSM to cross the scleral barriers and reach the retina to induce STAT3 activation.

1. INTRODUCTION

1.1. Oncostatin M and IL-6 family cytokines

Human Oncostatin M (hOSM) is a pleitropic cytokine that belongs to the Interleukin-6 (IL-6) family of cytokines. It was originally isolated in 1986 from the growth media of phorbol 12-myristate 13-acetate (PMA) treated U-937 histiocytic lymphoma cells and identified by its ability to inhibit the growth of melanoma cell lines (1). OSM cDNA encodes for a 252 amino acid precursor protein, the first 25 residues of which function as a secretory signal peptide which upon removal yields the soluble 227 amino acid pro-OSM (2). Cleavage of the c-terminal 31 residues from this pro-OSM yields the fully functional mature OSM with 196 residues and a molecular weight of 28 kDa (3) (Figure 1.1). This mature OSM contains two intra-molecular disulfide bonds (C6-C127 and C49-C167) resulting in the formation of a 'four α-helix bundle' like structure (Figure 1.2), a typical characteristic of the IL-6 family cytokines (4). In addition to tumor suppression, recent evidences have shown that OSM acts on a wide variety of cells *in vivo* and elicits diverse biological responses involved in inflammation, neuroprotection, haematopoiesis, tissue remodeling and development (5,6).

1.1.1. IL-6 family Cytokines

Cytokines represent a diverse group of small soluble proteins that when secreted by one cell can act on the same cell, in an autocrine fashion, or on another cell, in a paracrine fashion. Through binding to specific cell surface receptors, they

initiate signals that are critical to a diverse spectrum of functions including induction of immune responses, cell proliferation, differentiation, and apoptosis. The defining structural feature of the cytokine family is a 'four-α-helix bundle' like structure (7-9), which is composed of four amphipathic helices having solvent-facing hydrophilic sides and hydrophobic sides that form the core of the helical bundle. These four helices are oriented into a unique 'up-up-down-down' topology (Figure 1.3) (7).

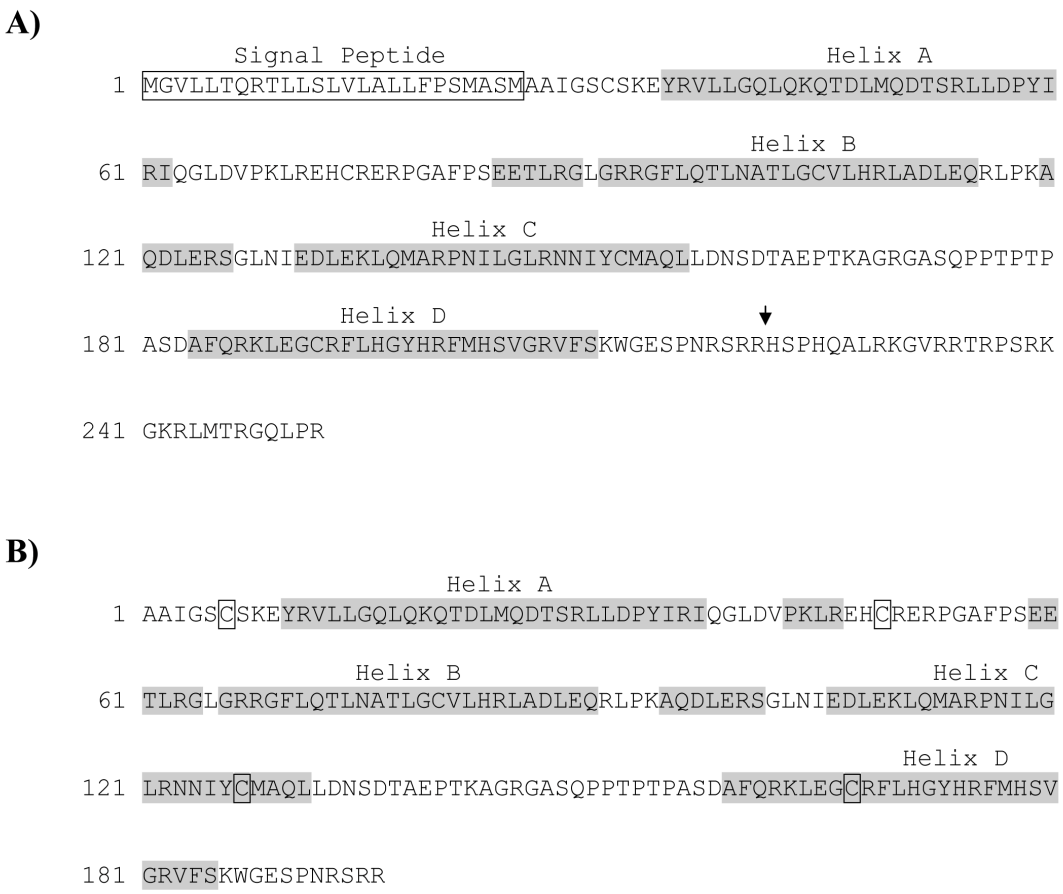


Figure 1.1 Protein sequence of full length and mature human OSM

Alpha helical regions in both sequences are highlighted in gray A) Full length hOSM consists of a 25 amino acid secretory signal peptide (shown in box) at the N-terminal. Cleavage of this secretory signal peptide yields pro-OSM. Cleavage of C-terminal 31 amino acids from this pro-OSM (shown with arrow) yields the fully functional mature OSM. B) Mature OSM consists of five cysteines (C6, C49, C80, C127,C167), four of which (C6-C127; C49-C167) (shown in boxes) participate in formation of disulfide bonds stabilizing the four-α-helix bundle like structure of OSM

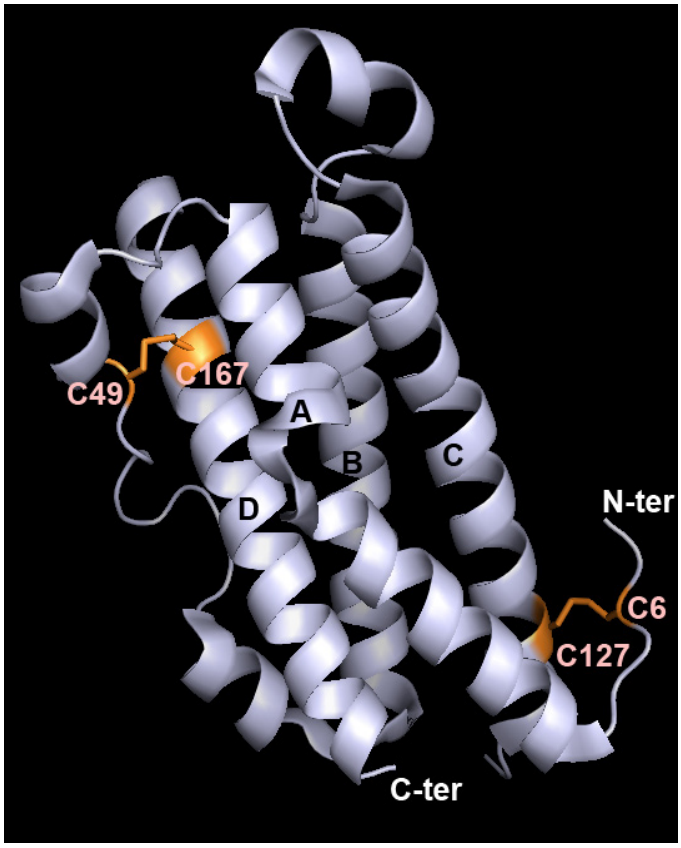


Figure 1.2 Crystal structure of mature human OSM with its N and C terminals indicated.

Helices A, B, C and D are labeled in the picture while the cysteines (C6, C127, C49 and C167) that participate in formation of disulfide bridges are highlighted in orange. (PDB: 1EVS)

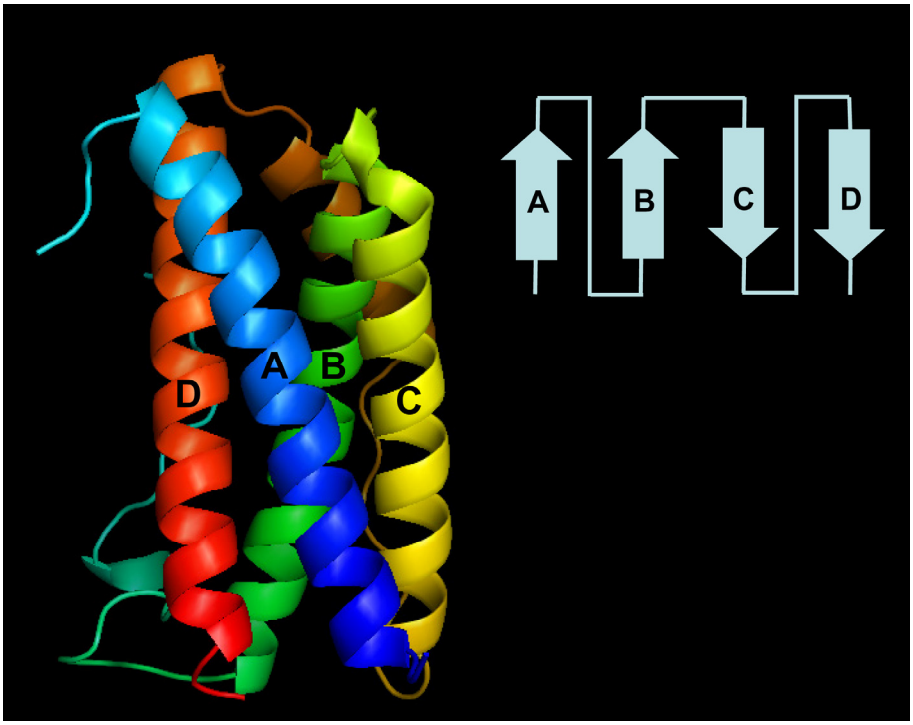


Figure 1.3 Structure of IL-6 with the α-helices A, B, C and D identified
Also shown on top right corner is the "up-up-down-down" topology of the tertiary structure of IL-6. A similar structure and topology are observed for other cytokines. (PDB: 1ALU)

Structural analyses by NMR and X-ray crystallography indicated that the cytokines can be classified into three groups based on the length of their helices (10-12) (Figure 1.4).

1) Short-chain cytokines that have 8–10 residues e.g. IL-2 and IL-4
2) Long-chain cytokines that have 10–20 residues e.g. IL-6 family cytokines, human growth hormone (hGH) and erythropoietin (EPO)
3) Cytokines that have eight-α-helices forming a duplicated version of the 'four-α-helix bundle' structure e.g. IL-5 and interferon (IFN)-γ

The IL-6 family of cytokines, comprising IL-6, IL-11, leukemia inhibitory factor (LIF), OSM, ciliary neurotrophic factor (CNTF), cardiotrophin-1 (CT-1) and cardiotrophin like cytokine (CLC) fall under the category of long chain cytokines (13). With the exception of CNTF and CT-1, all IL-6 family cytokines are classical secretory proteins synthesized with N-terminal signal peptides (14). All these cytokines have 180 – 200 amino acids that collectively exhibit a low sequence homology (~20%). Together, these cytokines execute a broad range, but often overlapping biological activities mediated by the formation a multimeric receptor complex which includes a common receptor gp130. While IL-6 and IL-11 form the signaling complex by homodimerizing gp130s, all other IL-6 family cytokines heterodimerize gp130 with either leukemia inhibitory factor receptor (LIFR) or oncostatin M receptor (OSMR) to form the signaling complex (Figure 1.5).

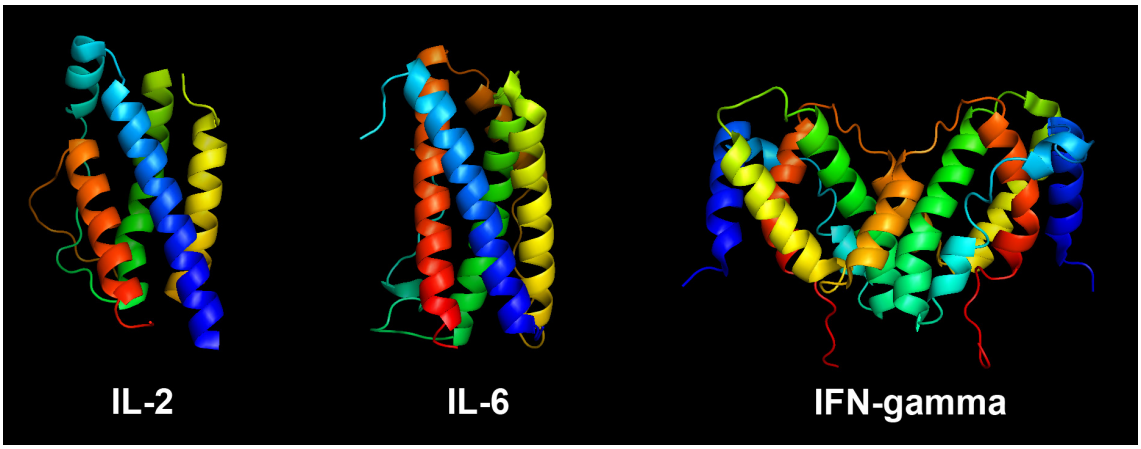


Figure 1.4 Crystal structures of IL-2, IL-6 and IFN-γ.

Clearly, IL-2 and IL-6 display the signature four-α-helix bundle like structure. However, IL-2 is primarily comprised of short-chain α-helices while IL-6 is made up of long-chain α-helices. INF-γ on the other hand exists as a dimer comprised of two four-α-helix bundle like structures. (PDB IDs: IL-2 – 1M47; IL-6 – 1ALU; IFN-γ – 1HIG)

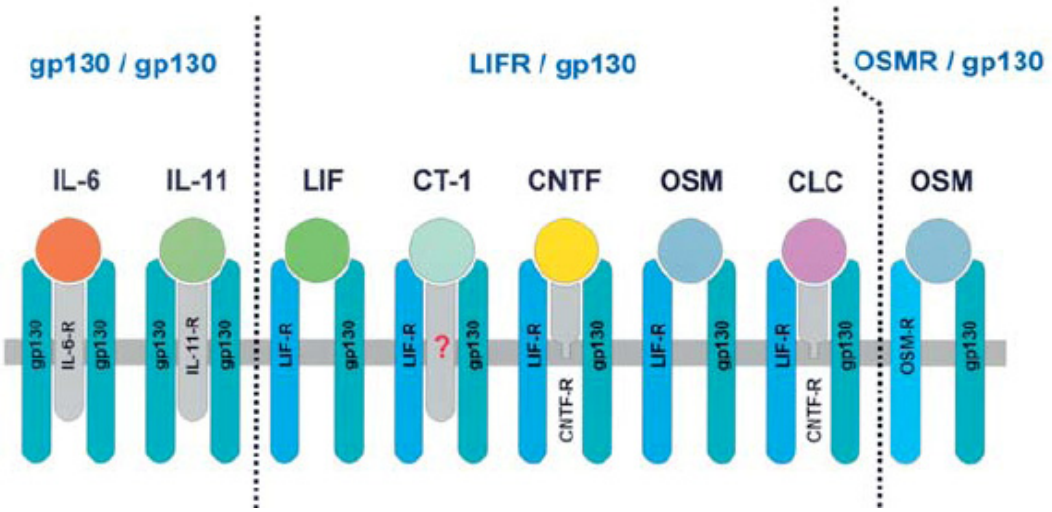


Figure 1.5 Receptor complexes of IL-6 family cytokines

IL-6 type cytokines signal through different combinations of the signaling receptor subunits gp130, LIFR and OSMR with gp130 being used by all the family members. *[Used with permission from Heinrich et al., (14)]*

1.1.2. gp130 family of cytokine receptors

On the basis of common structural features, cytokine receptors are grouped into six major categories:

1. Class I cytokine receptors
2. Class II cytokine receptors
3. Tyrosine kinase receptors
4. TNF receptors
5. IL-1 receptors
6. G-protein coupled receptors

The gp130 family of receptors, comprising gp130, LIFR, OSMR, IL-6Rα, IL-11Rα and CNTFRα fall under the class I cytokine receptors (Figure 1.6) (15). The class I receptors, also known as the hematopoietin receptors, constitute the largest group among the cytokine receptor family (7,16). These receptors have an N-terminal extracellular and C-terminal intracellular orientation. Based on the ability to induce intracellular signaling, the gp130 family of receptors can be further sub-divided into two categories (Figure 1.6) (13,17-29):

1) Signal transducing receptors i.e. gp130, LIFR and OSMR and
2) Non-signal transducing α-receptors i.e. IL-6Rα, IL-11Rα and CNTFRα.

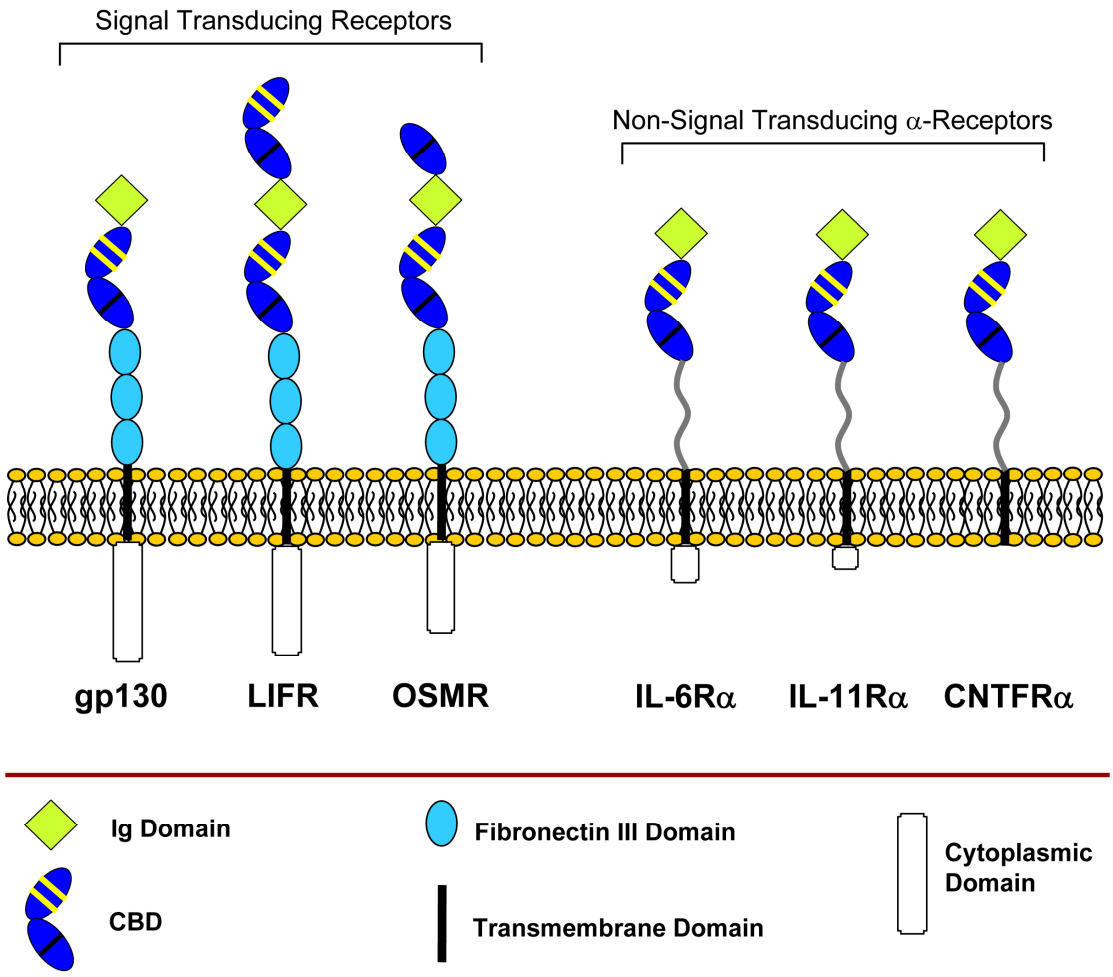


Figure 1.6 Domain composition of receptor subunits involved in IL-6 family cytokine signaling.

The yellow lines in the n-terminal domain of cytokine binding domain (CBD) define the conserved disulfide bonds while the black line in the c-terminal domain defines the conserved WSXWS motif.

In most cases, the signal transducing receptors do not show appreciable affinity for cytokines. But, in the presence of specific α-receptors the cytokines can form high-affinity complexes with the signal transducing receptors that are capable of triggering intracellular signaling. IL-6 and IL-11 associate with their nonsignaling α-receptors IL-6Rα and IL-11Rα before binding to their signal transducing receptor gp130 while CNTFRα binds to the cytokines CNTF, CT-1, and CLC before they can form the signaling complex with gp130 and LIFR (19,28-30). This characteristic co-operative binding effect is used by the receptors as a means of imposing tissue specificity. For example, gp130 is expressed ubiquitously in the human body while IL-6Rα is expressed only on hepatocytes, lymphocytes, neutrophils and macrophages (31). Thus IL-6 can execute its function only on these cells. However, in situations when membrane bound IL-6Rα is shed from the cell surface by proteolytic cleavage, the circulating IL-6Rα binds to IL-6 forming “IL-6 : IL-6Rα” complex which can now activate cells which are otherwise unresponsive to IL-6 (32-36). LIF and OSM are unique in this regard since these two cytokines do not require an α-receptor before they can bind to the signal transducing receptors LIFR or gp130. LIF can directly bind to LIFR and subsequently form a high affinity signal transducing complex with gp130 while OSM can directly bind to gp130 and then form a signal transducing complex with LIFR or OSMR.

An additional characteristic feature of the gp130 family signal transducing receptors is that they are much longer than other cytokine receptors by the virtue

of three additional membrane-proximal fibronectin III like domains. The extracellular part of gp130 is composed of six contiguous β-sandwich domains; a single immunoglobulin (Ig) domain at the top, followed by one cytokine binding domain (CBD), and three fibronectin III-like domains leading to the cell membrane (See Figure 1.6). LIFR has an additional CBD over the Ig domain while OSMR has one extra β-sandwich domain at the N-terminus. The CBD essentially consists of two fibronectin type-III (FNIII) domains connected by a linker, and it represents the signature recognition module for helical cytokines. The upper, N-terminal domain contains four conserved cysteine residues that form interstrand disulfide bonds (37). The lower, C-terminal domain has a conserved WSXWS motif (38,39). Mutagenesis studies have shown an essential structural role for these amino acids in maintaining the tertiary structure of the protein, but they are not involved in cytokine interaction (40). The cytokine-binding site for most CBDs is at the apex of the elbow region, consisting mainly of the interstrand loops connecting the β-strands from both N- and C-terminal domains (39,41). (Figure 1.7) The basic CBD is present in every class I cytokine receptor, and for some receptors such as the human growth hormone receptor (hGHR) (39) and the erythropoietin receptor (EPOR) (42), a single CBD is sufficient to mediate ligand binding and receptor homodimerization. However the gp130 family of receptors require additional domains like the Ig-like domain and membrane-proximal fibronectin domains to function and respond to the IL-6 family cytokines (43).

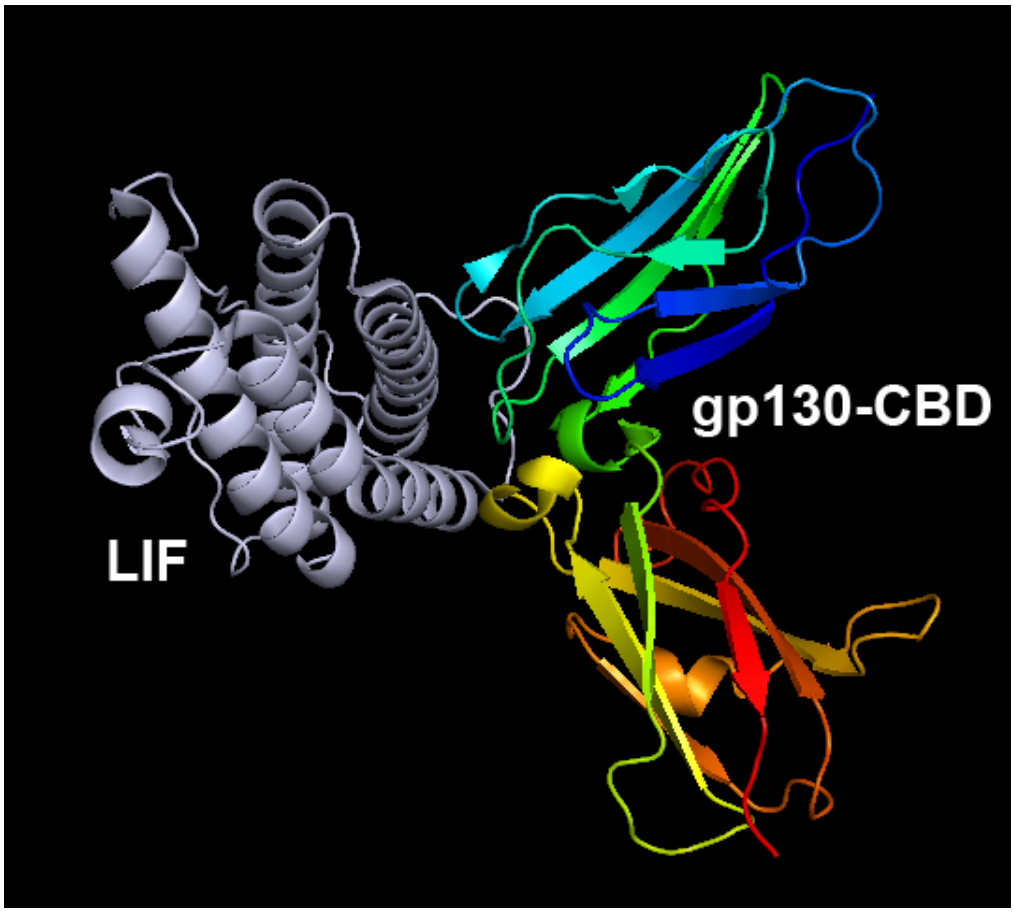


Figure 1.7 Crystal structure of LIF in complex with the cytokine binding domain (CBD) of gp130

As it can be seen in the picture, LIF (shown in gray) binds gp130 (shown in rainbow colors with n-terminus in blue and c-terminus in red) in the apex of the elbow region of gp130. (PDB: 1PVH)

1.1.3. Ligand-Receptor Interaction

Cell signaling induced by secreted cytokines is a central biochemical mechanism for a diverse range of cellular functions and cell-cell communication. The initial step of binding to specific receptor(s) followed by subsequent activation of membrane-proximal and -distal intracellular signaling cascades lead to specific responses that control a diverse range of cellular functions. An issue of fundamental biological significance is the biochemical specificity of this ligand-receptor interaction. This dictates both the identity and the kinetics of resulting signal transduction process and thus the associated biological responses. Important insights into the biochemical specificity of cytokine-receptor interaction have emerged from mutational and structural analysis of the cytokines and their receptors.

The pioneering study of the interaction between human growth hormone (hGH) and the growth hormone receptor (GHR) (39) has provided important initial insights into the structural basis of 'long chain' cytokine-receptor interaction. The structural analysis revealed that a single molecule of hGH forms a homodimeric receptor complex by simultaneously binding two identical receptor subunits. Two discrete regions of the ligand, site I (comprising residues in helix D) and site II (comprising residues from helix A and C), each bind a receptor molecule via interaction with CHR. As a result of this simultaneous interaction with two sites on the ligand, the cytoplasmic domains of the receptor are brought into close proximity (44), triggering a GHR specific intracellular signaling cascade.

Structural and mutational analysis of IL-6 family cytokines revealed an important deviation from the classic 'two-site' model described above for hGH. IL-6 family cytokines instead have three distinct sites of interaction with their respective receptors (26,27,45-48). The first two sites, Site I and Site II are analogous in location to their hGH counterparts: site I is located at the C-terminus of helix D and site II is composed of residues in helices A and C. However, the defining feature of IL-6 family cytokines is the existence of a third binding site (Site III) which is located at the N-terminus of helix D. Matching the interaction epitopes of each cytokine with its respective receptors, reveals a combinatorial pattern of receptor engagement. Site I, if used, is always engaged by a non-signaling α-receptor: IL-6Rα, IL-11Rα or CNTFRα (19,28-30,49). The glycoprotein gp130 always interacts through binding site II and, depending on the cytokine the third binding site (site III) is used for recruitment of LIFR, OSMR or a second gp130 receptor (18,21,23,26,27,50).

This cytokine induced receptor oligomerization leads to the juxtaposition of the intracellular domains of the signal transducing receptors (Figure 1.8). Unlike receptors for many growth factors (e.g., insulin) that have intracellular domains possessing tyrosine kinase activity on the same polypeptide chain, the class I cytokine receptors have no intrinsic enzymatic activity. Rather, the intracellular domains of the class I cytokine receptors are constitutively associated with tyrosine kinases of the Janus kinase (JAK) family (14,51-53).

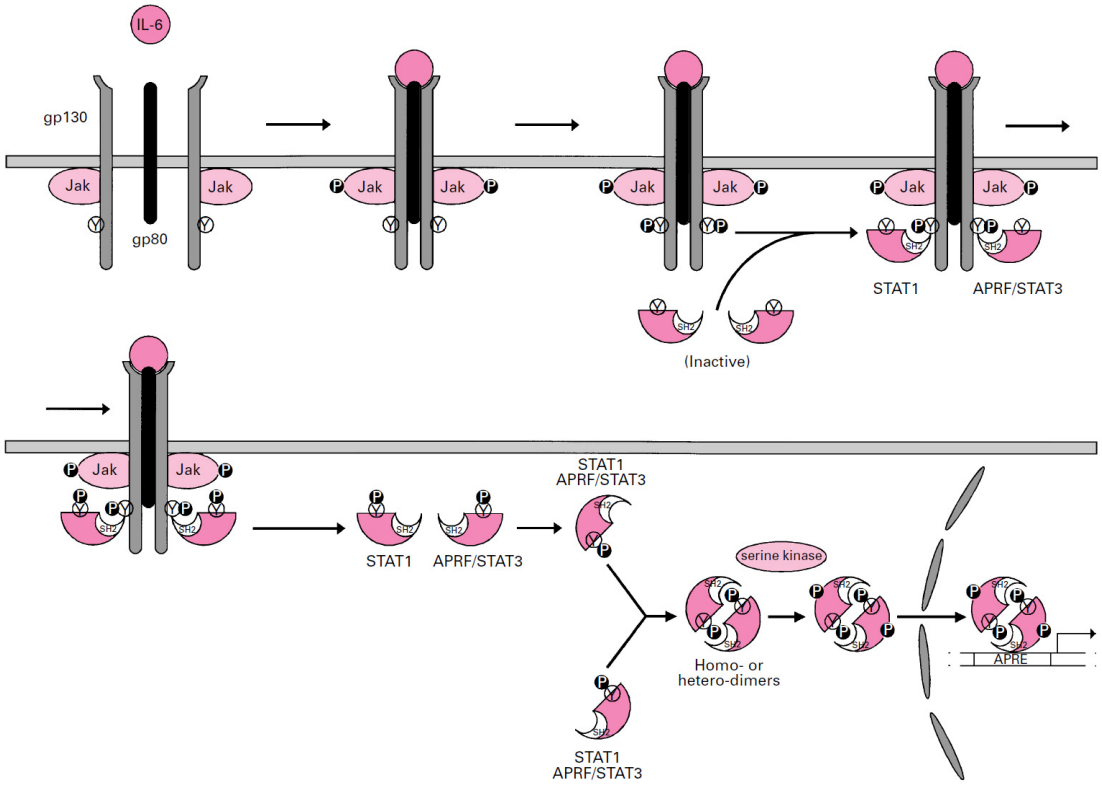


Figure 1.8 IL-6 signaling via the gp130/jak/STAT pathway

IL-6 in presence of IL-6Rα leads to dimerization of two gp130 molecules. Associated Jaks become activated and phosphorylate the cytoplasmic part of gp130, thereby creating a docking site for STAT factors STAT1 and STAT3. Upon association, the Jaks phosphorylate STATs which then dissociate from the receptor and form homo- or hetro-dimers. These dimmers then translocate into the nucleus, where they regulate gene expression. APRF – acute-phase response factor; APRE – acute-phase response element; encircled Y – tyrosine; white P in black circle – phosphate. *[Used with permission from Heinrich et al., (13)]*

After the JAK kinases are activated by ligand-induced receptor oligomerization, they phosphorylate themselves and the tyrosine residues on intracellular domains of the receptors. The phosphorylated tyrosines in the receptors then serve as the docking sites for a second family of proteins, the signal transducer and activator of transcription (STAT) proteins. Binding of STATs to the intracellular domains of the receptors leads to their tyrosine phosphorylation and subsequent dissociation from the receptors. The phosphorylated STATs form dimers and translocate into the nucleus, where they bind to DNA recognition sequences and act as transcription factors (53-55) (Figure 1.8). Besides the major JAK-STAT signaling pathway, the class I cytokine receptors also use other signaling mechanisms such as the RAS-RAF-MAP kinase pathway (56) and PI3 kinase (57,58).

1.1.4. Mapping Binding Sites on the Cytokines

The availability of high resolution structural data combined with functional analysis of receptor activation by mutagenesis studies lead to the definition of the structural features involved in receptor recognition by the IL-6 family of cytokines. These studies revealed that receptor interaction, involves a recognition 'hot spot' that is dominated by a small number of amino acid residues located close together in space. Structural and mutational analysis of LIF (41,48) and OSM (4) have shown that the interaction with gp130 via site II involves a small cluster of residues in the A and C helices (Figure 1.9).

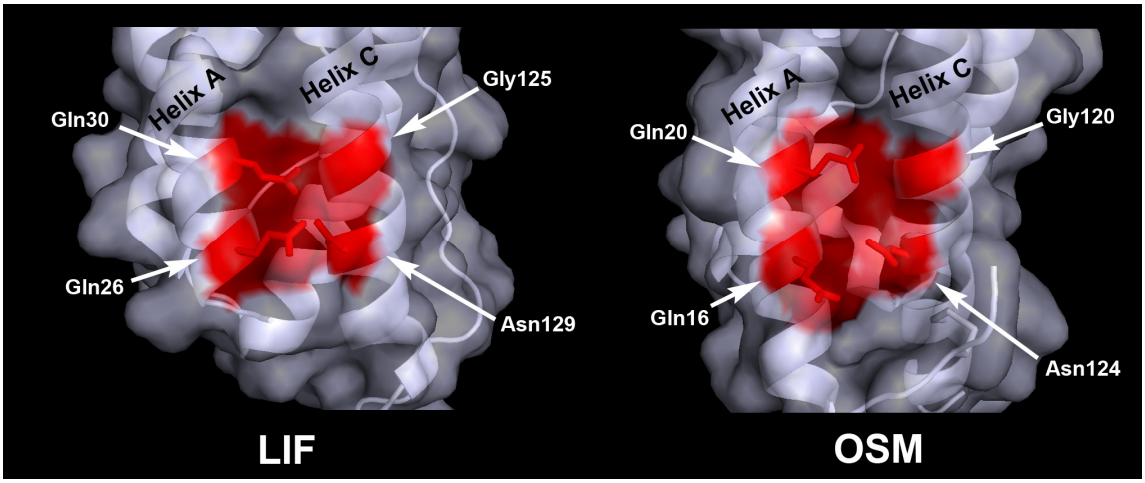


Figure 1.9 Comparison of site II residues on hLIF and hOSM

Both molecules exhibit a remarkable conservation in the identity and structural orientation of the residues that make up the site II responsible for gp130 binding. (PDB IDs: LIF – 1EMR, OSM – 1EVS)

This functional epitope is dominated by a conserved glycine (Gly) residue that, as a consequence of the absence of a side chain, forms a hydrophobic cavity in helix C. The neighboring asparagine (Asn) residue and two glutamine (Gln) residues from helix A further stabilize the interaction with gp130 (4,41) via formation of hydrogen bonds and polar interactions. The crystal structure of gp130 CBD (59) combined with mutagenesis data (60) provides a structural explanation for this interaction. The solvent-exposed hydrophobic residue (Phe169) and an adjacent tyrosine residue (Tyr196) on the CBD surface of gp130 are prominent determinants of this interaction. The exposed Phe169 docks nicely into the hydrophobic cavity on hLIF/hOSM surface formed by the respective Gly125/Gly120 residues on helix C. In this configuration, the hydroxyl group of gp130 Tyr196 can form a hydrogen bond with the exposed amide group of adjacent asparagine (Asn129/Asn124) on helix C (Figure 1.10). Consistent with these observations, mutating Gly120 on hOSM to a bulky tyrosine residue severely disrupts its interaction with gp130 while substitution to alanine, a residue with relatively small non-polar side chain, has a mild effect (4). CNTF has a tyrosine residue on its helix C in the equivalent location of Gly on hOSM. This explains why CNTF interacts with gp130 at a much lower affinity than either hLIF or hOSM (4). The recruitment of an α-receptor, CNTFR, is hypothesized to compensate for this loss of affinity by inducing allosteric changes in CNTF, thereby introducing additional sites for both ligand-receptor and receptor-receptor interaction into the complex (61). Similar to above cytokines, Site II of IL-6 and IL-11 are also dominated by residues in helices A and C. For IL-6, Tyr31, Gly35

from helix A and Ser118, Val121 from helix C are the primary residues involved (62) while for IL-11, Leu45 from helix A and Arg135, Arg139 and Leu142 from helix C are essential for binding to gp130 (63) (Figure 1.11). Both these cytokines again interact with gp130 at its CBD.

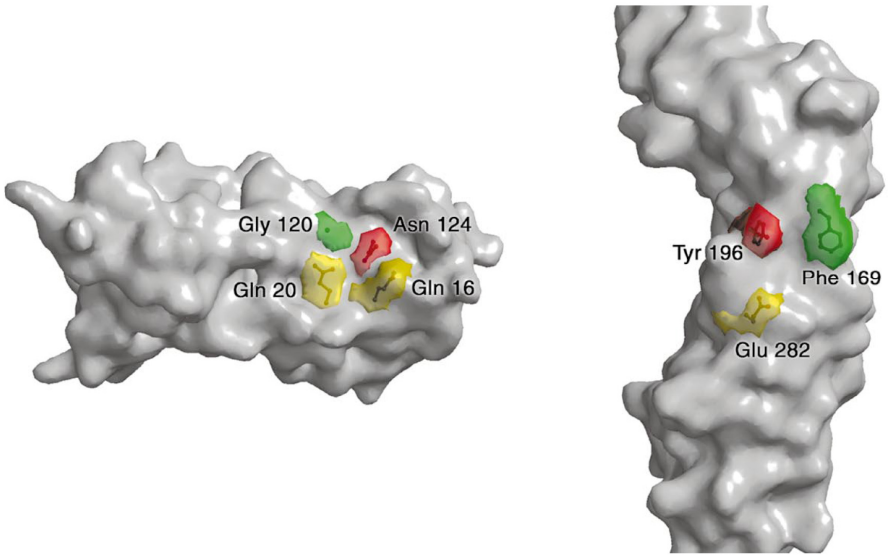


Figure 1.10 Complementarity between the interaction surfaces of hOSM and gp130

The solvent accessible residues that make up the site II on hOSM (left) and the cognate binding site on gp130 (right) are displayed. Residues that complement each other in this binding are color coded accordingly *[Used with permission from Deller et al., (4)]*.

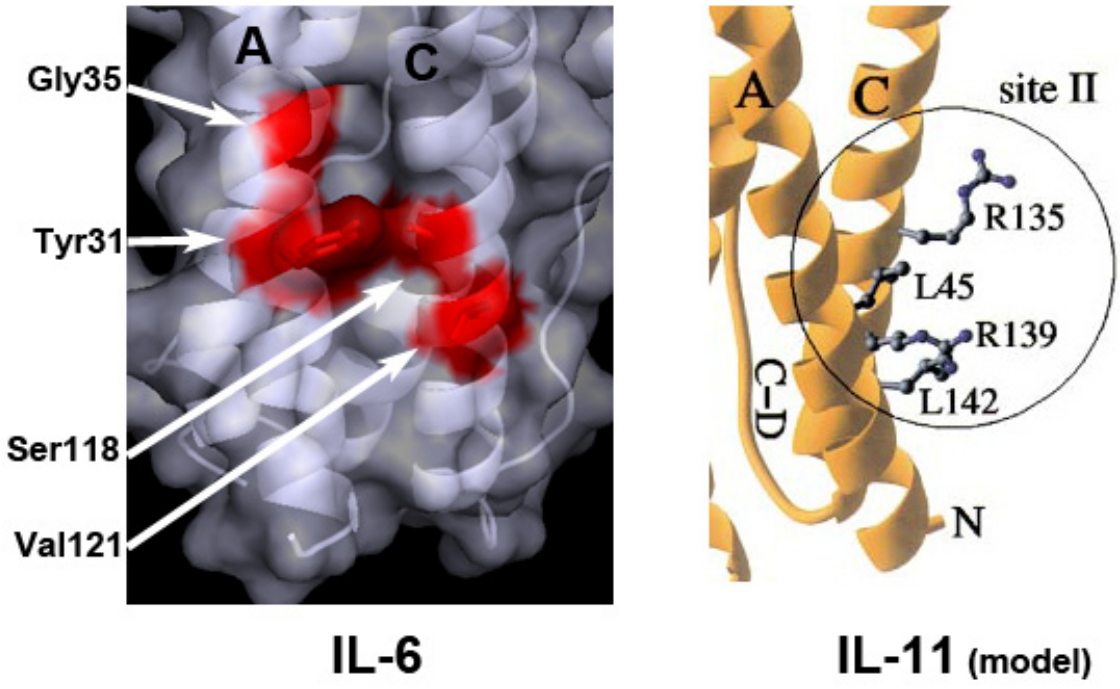


Figure 1.11 Site II residues of IL-6 and IL-11 responsible for gp130 binding. While the structure of IL-6 is based on crystal structure solved (PDB: 1ALU), structure of IL-11 represents model prediction by Tacken et al., (63) (Used with permission from Tacken et al., (63)). Again, as in LIF and OSM, residues in helices A and C play an essential role in binding to gp130.

Among IL-6 family cytokines, there are two sub-classes of cytokines. While both classes of cytokines interact with gp130 at site II, IL-6 and IL-11, interact with a second gp130 at their site III, while the second sub-class, comprising LIF, OSM, CNTF, CT-1 and CLC, interact with LIF-R at their site III. The site III of all LIFR interacting cytokines is dominated by two residues (4,13,47,48); a conserved solvent-exposed phenylalanine (F) and an adjacent lysine (K), commonly termed as the 'FXXK' motif (Table 1.1 and Figure 1.12). Structure of hLIF in complex with mLIFR revealed that the lysine side chain in the FXXK motif forms strong hydrogen bonds with Ser262 and Asn265 in the Ig domain of LIFR (64). In addition, a significant hydrophobic interaction is made by the π-stacking arrangement of the Phe156 of hLIF against the peptide bond of Gly276 in mLIFR. Together, these non-covalent interactions between LIF and LIFR lead to the formation of a tight complex with an equilibrium dissociation constant (K_D) in the nano molar range. Parallel mutagenesis studies of IL-6 and IL-11, which interact with gp130 via site III (46,65) reveal a similar arrangement of a solvent-exposed hydrophobic residue tryptophan (W) and an adjacent acidic residue, aspartate (D) (46,62) (Figure 1.12). Based on these observations, it has been hypothesized that the hydrophobic core of all these cytokine binding sites is utilized to bind the receptor while the polar contacts surrounding the hydrophobic patch determine the specificity of the interaction. Interestingly, OSM which can bind LIFR at its site III can also uniquely bind to a separate receptor called OSMR. The same FXXK motif on OSM is shown to be essential for its interaction (4). This again implies that the difference in receptor specificity between LIF and OSM is a result

of structural differences between these ligands in the vicinity of the core FXXK motif (4). However, to date, residues on OSM that are uniquely responsible for OSM's ability to bind OSMR have not been identified yet.

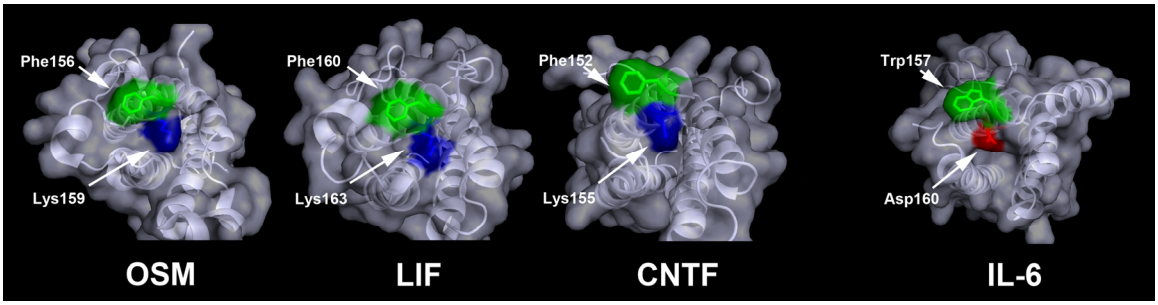


Figure 1.12 Surface representations showing the site III interfaces of OSM, LIF CNTF and IL-6.

The site III of OSM, LIF and CNTF which engages LIFR is defined by a conserved 'FXXK' motif. On the other hand, a tryptophan and an aspartate residue make up the site III for IL-6. These residues participate in engaging a second gp130 receptor onto IL-6. (PDB IDs: OSM – 1EVS; LIF – 1EMR; CNTF – 1CNT; IL-6 – 1ALU)

Table 1.1 Site III amino acid sequences of various IL-6 family cytokines.

The FXXK motif is conserved among the cytokines that engage LIFR while a tryptophan replaces the phenylalanine in IL-6 and IL-11 which engage gp130 at their site III

Cytokine	Site III
hLIF	DV**F**QK**K**KL
hOSM	DA**F**QR**K**LE
hCNTF	GL**F**EK**K**LW
hCT-1	GV**F**PA**K**VL
hCLC	SD**F**LQ**K**MD
hIL-6	NQWLQDMT
hIL-11	SAWGGIRA

By analogy with growth hormone, site I residues are defined as those residues that interact with their respective α-receptors. As described earlier, LIF and OSM do not require binding to an α-receptor before they can bind their signal transducing receptors LIFR and gp130. Thus, site I is not defined for these two cytokines. Based on the clues from hGH, site directed mutagenesis of residues at the C-terminal of the IL-6 family cytokines (IL-6 (66), IL-11(63,67), CNTF (68,69), CT-1 (30) and CLC (70)) yielded several mutants that lack bioactivity as well as the ability to bind to their α-receptors. While some residues directly participate in receptor binding, others are required for maintaining the structural integrity of the cytokine. In most of these cytokines, arginine (Arg) residue located at the end of their D helix was found to be essential for the interaction with the respective α-receptor. Structural analysis of IL-6 in complex with IL-6Rα revealed that this arginine (Arg179) forms polar contacts with Tyr230 and Glu277 in the N-terminal half of the CBD of IL-6Rα (71). Gln175, Arg182 and Phe74 of IL-6 are also shown to be involved in this interaction by providing additional polar and hydrophobic contacts with the receptor (Figure 1.13).

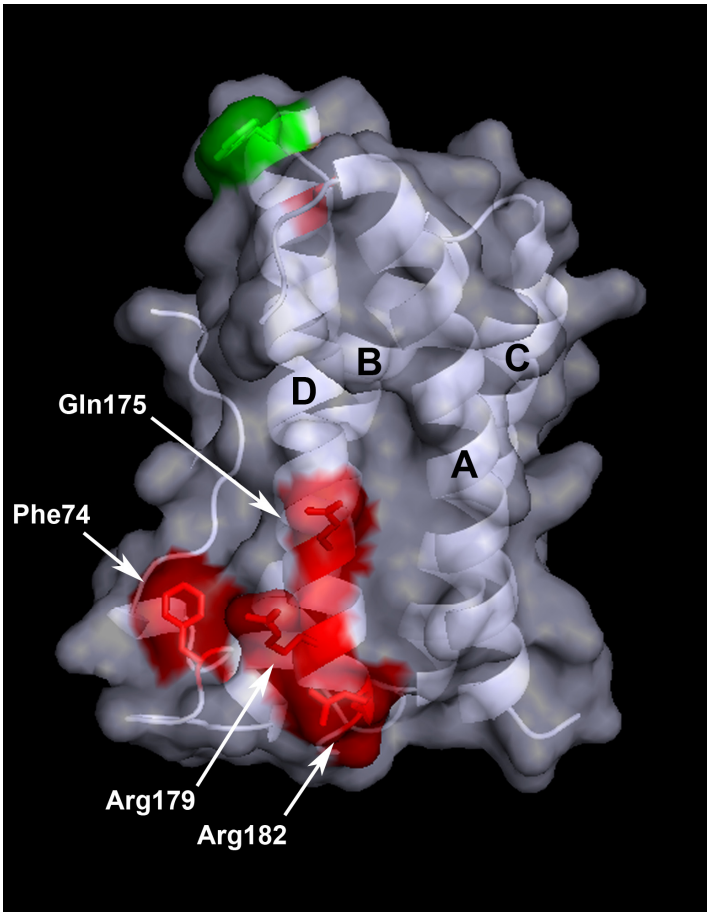


Figure 1.13 Site I residues of IL-6 that participate in IL-6Rα binding.
Arg179 forms the core of this interaction while the surrounding residues Gln175, Phe74 and Arg182 stabilize this interaction by providing additional polar and hydrophobic contacts with the receptor. Helices A, B, C and D are indicated in black letters. Also, shown for reference is the tryptophan residue (green) at the top that makes up the site III which is essential for gp130 binding. (PDB: 1ALU)

Other mutations in this region which affect binding Ser177, Ala180, Leu178 and Leu181 are all buried and may be affecting activity by altering the local conformation of IL-6 (62). Structural analysis of this region also revealed that there is a high density of ordered water molecules which may play a role in binding the receptor by adding entropy to the system as they are displaced (Figure 1.14) (62). Similar to IL-6, IL-11 and CNTF also utilize an arginine residue (Arg190 for IL-11 and Arg177 for CNTF) on the c-terminus of their D helix as the core of site I while the other residues nearby stabilize the interaction with polar and hydrophobic interactions (Figure 1.15).

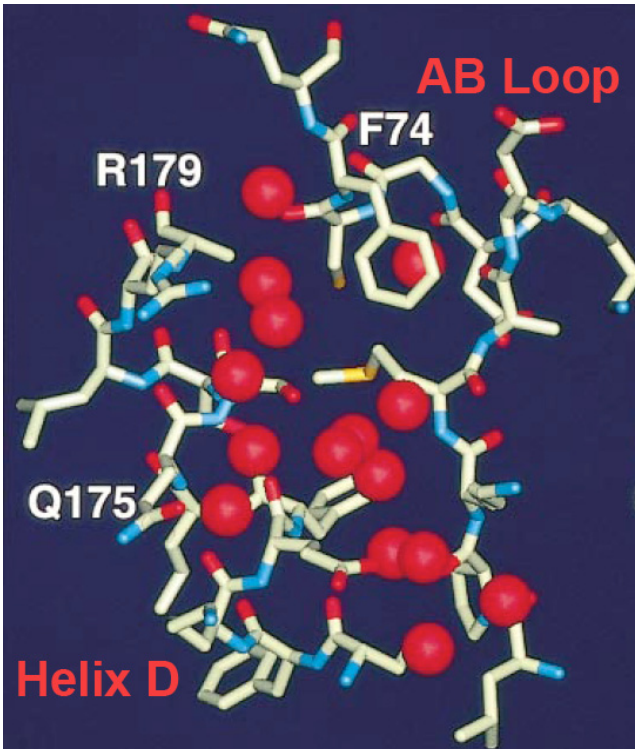


Figure 1.14 Water molecules (red spheres) in the region between the helix D and the A-B loop of IL-6.

[Used with permission from Somers et al., (62)].

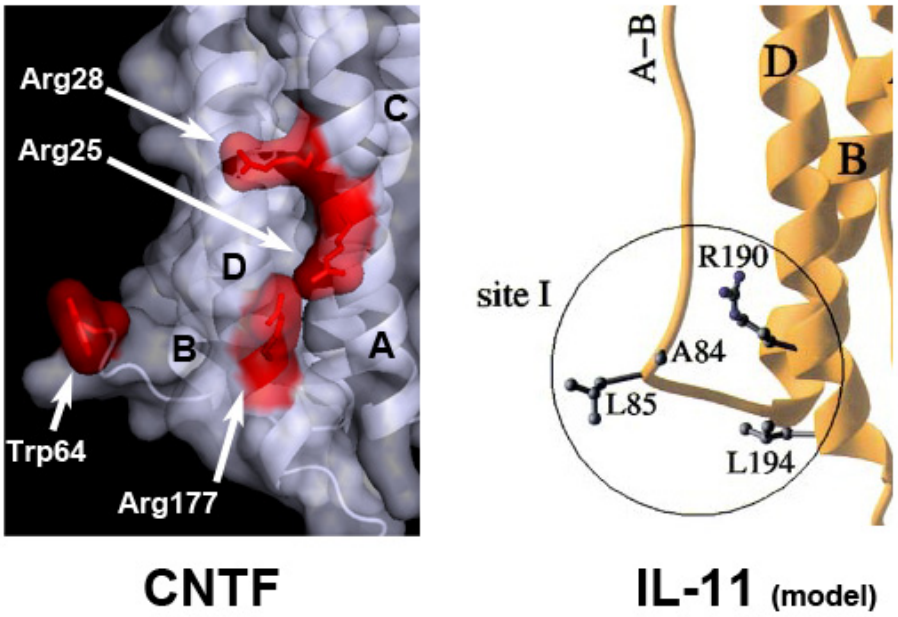


Figure 1.15 Site I residues of CNTF and IL-11 that play a key role in binding CNTFRα and IL-11Rα respectively.

Again, the arginine residues on helix D (Arg177 on CNTF and Arg190 on IL-11) form the core of this interaction while the residues around stabilize the interaction by providing additional contacts. (PDB ID of CNTF: 1CNT). Model structure of IL-11 is adapted from Tacken et al., (63) (Used with permission from Tacken et al., (63)).

1.1.5. Stoichiometry of Signaling Complexes

Based on the structures solved for IL-6 family cytokines in complex with their receptors and mutational analysis conducted on the receptors by deleting domains, it has been identified that 1) the α-receptors always utilize the residues in their CBD to bind site I 2) gp130 always utilizes residues in its CBD to bind site II and 3) receptors that bind at site III, always utilize residues in their IgD (Table 1.2) (61,71).

Table 1.2 Composition of IL-6 family cytokine receptor complexes

Cytokine	Site I (Domain)	Site II (Domain)	Site III (Domain)
hIL-6	IL-6Rα (CBD)	gp130 (CBD)	gp130 (IgD)
hIL-11	IL-11Rα (CBD)	gp130 (CBD)	gp130 (IgD)
hLIF	-	gp130 (CBD)	LIFR (IgD)
hOSM	-	gp130 (CBD)	LIFR/OSMR (IgD)
hCNTF	CNTFRα (CBD)	gp130 (CBD)	LIFR (IgD)
hCT-1	CNTFRα (CBD)	gp130 (CBD)	LIFR (IgD)
hCLC	CNTFRα (CBD)	gp130 (CBD)	LIFR (IgD)

Shown in the table are the receptors and their domains that participate in binding to each of the IL-6 family cytokine. While IL-6 and IL-11 bind gp130 receptor at their site III, all other IL-6 family cytokines engage LIFR at their site III. However, the receptors always use a CBD to engage site I (except for LIF and OSM), a CBD to engage site II and an Ig domain to engage site III.

However, there is a striking contrast between the IL-6/IL-11 systems and the LIF/CNTF/OSM/CT-1/CLC systems of receptor complex formation. IL-6 first engages IL-6Rα CBD through site I to form a binary complex, followed by a low-affinity recruitment of the gp130 CBD through site II to form a non-signaling ternary complex. The final step is a high affinity dimerization of two gp130/IL-6/Il-6Rα heterotrimers via site III where the IgD of gp130 (the CBD of which is already bound to site II of partner IL-6) binds (71). When alone, gp130 IgD does not exhibit any affinity towards IL-6 site III. The dimerization of two trimeric complexes introduces additional contacts between the cytokine and the receptors, stabilizing the weak interaction between IL-6 and gp130 IgD at site III (Figure 1.16). Thus, the formation of a hexameric complex is essential for IL-6 to induce homodimerization of gp130 which can then trigger the activation intracellular signaling cascade. Similar to IL-6 system, CNTF first engages CNTFRα CBD at its site I. And, as in IL-6 system, this pre-complexation with CNTFRα is required for CNTF to engage gp130 CBD at its site II. However, in contrast to the IL-6 system, IgD of gp130 that is bound to site II does not participate in site III interaction. Instead, IgD from a separate receptor (LIFR) occupies this position. Binding studies revealed that pre-complexation of either CNTFRα or the gp130 is not required for CNTF binding to LIFR (61). Similar observation is made in LIF system where pre-complexation with gp130 is not required for LIF binding to LIFR (48).

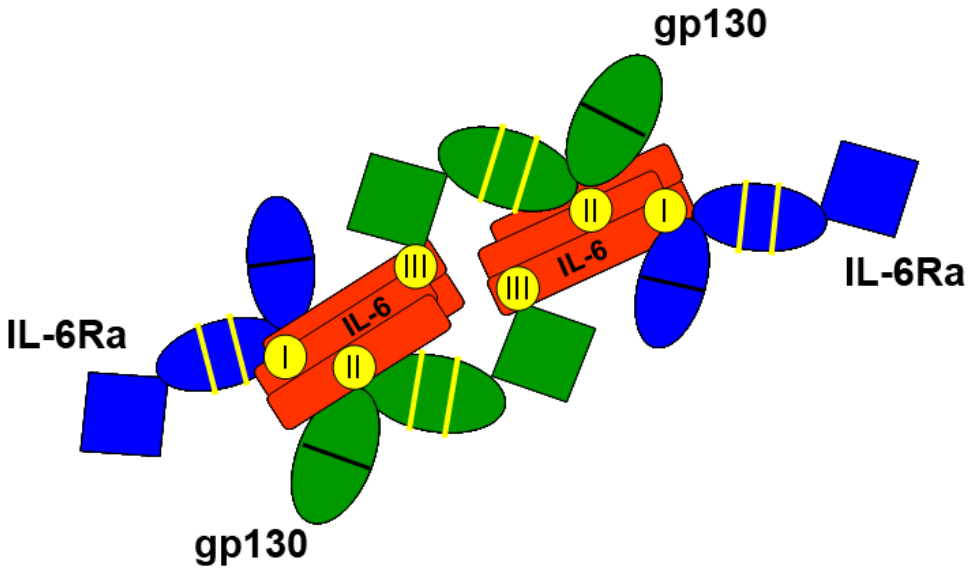


Figure 1.16 Schematic diagram of the hexameric receptor complex assembly for IL-6

The representation for Ig domains and CBDs are as described in figure 1.6. The four-α-helical IL-6 is represented in red while IL-6Rα and gp130 are represented in green respectively. Sites I, II and III are represented in yellow circles. IL-6 first binds IL-6Ra via its site I and then recruits a gp130 at its site II. However, unlike LIF and CNTF, IL-6 does not engage LIFR at its site III. Instead, two IL-6 molecules form two separate IL-6-IL-6Rα-gp130 complexes engage the Ig domain of gp130 from opposite complex to form a hexameric complex. This kind of complex formation stabilizes the weak interaction between gp130 IgD and site III of IL-6.

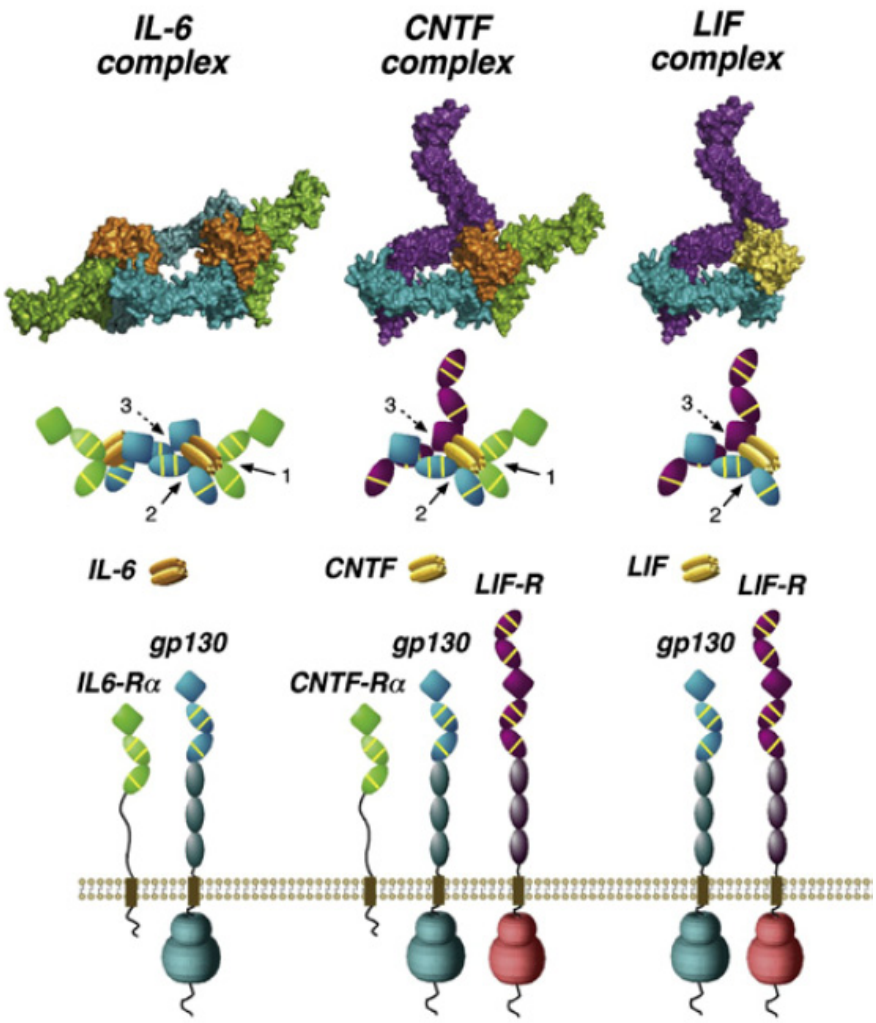


Figure 1.17 Three-dimensional model structures for IL-6 family cytokines in complex with their receptors. *[Used with permission from Skiniotis et al., (61)]* These structures represent the three classes of receptor complex engagement seen in IL-6 family cytokines. 1) Hexameric complex (IL-6, IL-11), 2) quaternary complex (CNTF, CT-1, CLC) and 3) trimeric complex (LIF, OSM). Unlike LIF and CNTF which exhibit a strong interaction with LIFR through their site III, IL-6 requires the formation of a hexameric complex to stabilize its weak interaction with gp130 at its site III. And, unlike other IL-6 family cytokines, LIF and OSM exhibit a direct affinity towards their signal transducing receptors (LIFR or gp130) and do not require an α-receptor for forming the signaling complex.

This implies that, unlike IL-6, CNTF and other cytokines that heterodimerize LIFR/gp130 do not require the hexamer formation to trigger intracellular signaling cascade (Figure 1.17). The high affinity interaction of LIFR with these cytokines via FXXK motif negates the requirement of affinity enhancement through the hexamer formation.

1.2. Biological activities of OSM & other IL-6 family cytokines

IL-6 family cytokines, including OSM, act on a wide variety of cells and elicit diverse overlapping biological responses such as inflammation, neuroprotection, haematopoiesis and development. The functional redundancy of the IL-6 family cytokines can be explained by their shared receptor subunits. However, it has also been recognized that each of these cytokines exhibit unique activities that are not shared by other family members. These unique activities are conferred by their specific receptors and their restricted expression.

1.2.1. Inflammation

Inflammation refers to a complex set of mechanisms by which tissues respond to injury and infection. The initial signs of swelling, pain and heat are characteristics of the initial phase of inflammation, termed as acute inflammatory response (72,73). This is characterized by increased blood flow, increase in permeability of the surrounding capillaries and infiltration of white blood cells, predominantly neutrophils (74-78). In case of severe damage, this reaction is followed by the chronic inflammatory response where the affected tissue is infiltrated by

lymphocytes, macrophages, and mast cells (79). Substantial tissue remodeling can occur during this phase which may lead to complete restoration of normal tissue architecture or a scar formation (80). This complex chain of events is regulated by an array of mediators, which includes cytokines, the extracellular matrix, and adhesion molecules (79,81-83).

Activated T cells and monocytes at the site of injury/infection secrete Oncostatin M (84,85) which in turn stimulates endothelial cells to secrete IL-6 in the blood stream (86). IL-6 then stimulates the liver to secrete acute phase proteins (APPs) into circulation (87). APPs are essential for controlling body homeostasis and regulate the inflammatory response. While other IL-6 family cytokines like LIF, CNTF and IL-11 also stimulate the release of APPs from the liver (87-96), IL-6 was found to be the primary inducer of APPs *in vivo* (87). In addition to the APPs, OSM and IL-6 are shown to modulate the expression of other cytokines and chemokines involved in inflammation e.g., IL-1, IL-8, granulocyte macrophage-colony stimulating factor (GM-CSF), growth related oncogenes α and β (97). Also, OSM induces prolonged expression of P-selectin (98) and E-selectin (97) in endothelial cells which modulate leukocyte adhesion and extravasation. This is an important phenomenon involved in wound healing.

During the repair process, remodeling of extracellular matrix plays an important role in healing the damaged tissue. Matrix metalloproteinases (MMPs) are involved in extracellular matrix breakdown while tissue inhibitors of

metalloproteinases (TIMPs) inhibit the action of MMPs (99-104). OSM plays a crucial role in this process by modulating the expression of TIMP-1 (105) and MMP-1, MMP-3 and MMP-9 in fibroblasts (106) at the wound site.

Besides acute phase reactions, IL-6 family cytokines are also associated with several acute and chronic inflammatory diseases e.g., rheumatoid arthritis, acute pancreatitis, and Alzheimer's disease. In patients suffering from rheumatoid arthritis, elevated levels of IL-6, IL-11, LIF and OSM have been found in the synovial fluids and the serum (107-118) and the levels of these cytokines were shown to correlate with disease severity. Research has shown that these cytokines induce bone remodeling (119-121), stimulate cartilage degradation (122-124) and induce osteoblast proliferation (125,126). Injection of anti-IL-6 receptor monoclonal antibody and LIF antagonists were shown to ameliorate inflammatory reactions in these inflammatory models (127).

1.2.2. Neuroprotection

IL-6 family cytokines LIF, CNTF, OSM and CT-1 all of which signal through heterodimerization of gp130 with LIFR exhibit a wide range of roles in both the developing and mature nervous system. They play a vital role in modulating the differentiation of neuronal cells and promote their survival under stress conditions. While most of these cytokines are expressed in various parts across the body, CNTF is found exclusively in the nervous system.

Initial studies using cytokine knockout models revealed no abnormalities in development (128,129) suggesting that these cytokines are not essential for neuronal development. However, CNTFRα and LIFR knockout mice died within 24 h of birth and had a marked reduction in numbers of spinal motor neurons (128,130,131) indicating that these cytokines in fact play an important role in neuronal survival and the overlapping signals executed by IL-6 family cytokines compensate for the loss of others. Although neurons and astrocytes are known to express LIF, CNTF, and OSM, glial cells are considered to be the major producers of these cytokines (20,132) and this expression is up regulated upon injury or stress by an as yet unknown mechanism. And, *in vivo* the neurons and astrocytes are closely associated with the glial cells thus exposing them to high concentrations of glial-derived neurotrophic factors and cytokines upon ischemic or excitotoxic injuries (133,134).

Excitotoxic pathways initiated after excessive glutamate release have been implicated in traumatic spinal cord injury, stroke and some chronic age-related neurodegenerative diseases like Alzheimer's disease (135). OSM was shown to significantly attenuate the neuronal cell death induced by a similar excitotoxic injury triggered by N-methyl-D-aspartate (NMDA), an analogue of glutamate, both *in vitro* and *in vivo* (136). Similar observations were made for CNTF. Treatment with exogenous CNTF was shown to protect the neurons after a CNS injury induced by both excitotoxic stimulation and by degenerative diseases like multiple sclerosis (MS) and Huntington' disease (137-142). Delivery of LIF, CNTF

and OSM have been demonstrated to be neuroprotective in a number of other *in vitro* and *in vivo* models also (136,143-145). In the eye, studies by La Vail et al., (146-148) have shown that multiple neurotrophic factors including CNTF rescue photoreceptors from damaging effects of constant light and retinal degenerations induced by inherited genetic mutations. Recent work in our lab by Ueki et al., (149) has shown that LIF, another IL-6 family member also protects the photoreceptors from oxidative stress induced by severe bright light. Later, knock out studies by Joly et al., (150) have shown that endogenous LIF extends the life span of retinal photoreceptors in a mouse with degenerating retina induced by genetic mutations. In addition to these, studies by Rattner et al., (134) have shown that the retina responds to severe light stress by up regulating the expression OSMR, suggesting a possible role of neuroprotection by OSM. Together, all these results clearly suggest that IL-6 family cytokines play an important role in protecting the neuronal cells from oxidative stress induced by injury or inherited genetic mutations. Separate studies have shown that preconditioning the eyes with bright cyclic light or with hypoxia also help the photoreceptors survive subsequent doses of severe oxidative stress (151-155). However, the molecules involved in this induced protection remain poorly characterized.

1.2.3. Hematopoiesis

Hematopoiesis can be broadly defined as the regulation of the concentrations of cellular components in blood. In a healthy adult, approximately 10^{11} – 10^{12} new blood cells are produced daily in order to maintain the steady state levels (156). All of these cellular blood components are derived from hematopoietic stem cells (HSCs) which reside mainly in the bone marrow. These stem cells can proliferate and differentiate leading to the production of one or more specific types of blood cells. A number of factors control this process of proliferation and differentiation with great precision and regulate the production of blood cells.

While erythropoietin (Epo) and granulocyte-macrophage colony stimulating factor (GM-CSF) are the primary mediators of this regulation, IL-6 family cytokines also play an important role. mRNA levels for IL-6, IL-11, OSM and LIF are found to be abundant in hematopoietic tissues such as bone marrow, thymus and spleen (13,157). These cytokines, in concert with IL-3 are shown to regulate the proliferation of pluripotent hematopoietic progenitor cells by controlling their entry and exit from the cell cycle (158-160). Also, intravenous administration of LIF, OSM, IL-6 and IL-11 were all shown to result in dramatic increase in megakaryocyte and platelet numbers in the blood (161-166). In addition, IL-6 family members are also shown to inhibit the differentiation of macrophages and several myeloid leukemic cells indicating that these cytokines play an important role in final maturation of the hematopoietic cells (167-169).

1.2.4. Other Functions of Oncostatin M

1.2.4.1 Growth Modulation of Tumor Cells:

Oncostatin M was originally identified by virtue of its ability to suppress tumor cells. It was originally recognized in 1986 by its ability to inhibit the proliferation of A375 melanoma cells (1). Later, it was shown to inhibit the growth of several other types of tumor cells including lung cancer cells, breast cancer cells, glioma cells and solid tissue tumor cells (170-172). LIF, another IL-6 family member closely related to OSM, was not able to display a similar ability in suppressing tumor cells suggesting that OSM executes these functions by recruiting its unique receptor OSMR. In agreement with these observations, more recent studies by Lacreusette et al., (173) have shown that melanoma cell progression towards an OSM resistant metastatic state is accompanied by silencing of the OSMR gene. Thus, in addition to designing novel agonists of OSM, preventing the alteration of promoter region of OSMR can be a potential avenue to suppress the proliferation of tumor cells *in vivo*. Besides tumor cells, OSM also inhibits the proliferation of normal mammary and breast epithelial cells (174). In contrast, OSM stimulates the growth of AIDS related Kaposi's sarcoma cells (175-177) and the normal dermal fibroblasts via mitogen-activated protein kinase (MAPK)-dependent pathway (178).

1.2.4.2 Regulation of Cholesterol Levels:

Increased low density lipoprotein-cholesterol (LDL-c) levels in plasma is a widely recognized risk factor for atherosclerosis and an important underlying cause for a number of cardiovascular diseases (179-183). The LDL receptor (LDLR) plays a pivotal role in the control of plasma cholesterol levels since more than 70% of the LDL-c in circulation is removed by LDLR-mediated endocytosis (184,185). Therefore, the regulation of liver LDLR expression has been considered a key mechanism by which therapeutic agents could interfere with the development of atherosclerosis.

Over the past three decades, statins (e.g., Rosuvastatin (Crestor®), Atorvastatin (Lipitor®), Lovastatin (Mevacor®)) have been extensively studied and applied in the clinical setting to serve as cholesterol depleting agents (179,180,186). They lower cholesterol levels by inhibiting the enzyme HMG-CoA reductase, which is the rate-limiting enzyme involved in cholesterol synthesis (184). Inhibition of this enzyme in the liver not only decreases cholesterol synthesis, but also increases synthesis of LDL receptors, leading to an increase in clearance of LDL-c from the bloodstream. In addition to these, LDLR expression levels were also shown to be regulated by several growth factors and cytokines (187-202). However, among these, OSM was shown to have the most pronounced effect in increasing the levels of LDLR on liver. When administered intraperitoneally, OSM was shown to induce rapid upregulation of LDLR expression in liver and this upregulation was

sustained for 24 hrs (203). In addition, when tested in combination with the commercially available statins, OSM was found to show an additive effect (204). Further investigation showed that OSM regulates the LDLR expression through a separate statin independent mechanism (205). Clinical studies are under way to use OSM as a potential therapeutic agent to regulate cholesterol levels either independently or in combination with the currently available statins.

1.3. Controlled Drug Delivery

Healthcare providers have traditionally been using pills, ointments and injections for delivering drugs into the body. While these modes proved effective in treating a number of disease states, they are inefficient for delivering sensitive drugs that lead to serious toxicity when delivered in large doses and those that have short half-lives. The primary aim of any drug delivery mode is to maintain the drug concentration at therapeutic levels for desired duration. Traditionally, this aim has been achieved by repeated dosages that cyclically alter the *in vivo* concentration of the drug and thus maintain its levels in therapeutic range for longer durations. The drug concentration in blood increases after each administration and as the drug is consumed by the body, the drug concentration decreases until the next dosage is administered (Figure 1.18). However, repeated dosages often result in drug delivered outside the therapeutic region, including drug concentrations beyond the toxic level that can lead to serious side effects (206-209). Therefore, there has been great interest in designing better delivery methods that

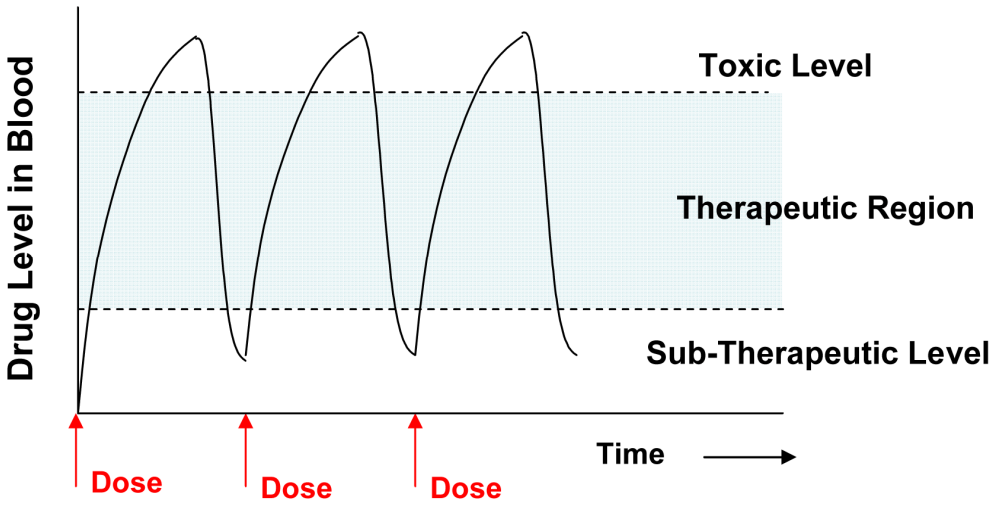


Figure 1.18 Changes in systemic levels of drug concentrations with traditional methods of repeated cyclic administration

Immediately after administration, drug concentrations shoot up beyond the therapeutic ranges possibly leading to toxicity and as the drug is consumed by the body, drug concentrations fall below therapeutic ranges where it is no longer effective.

consistently maintain the drug concentration in the desired therapeutic region (210). These interests are the motivation behind the concept of “Controlled Drug Delivery”. Controlled drug delivery can be broadly defined as a judicious release of drug or any other active agent in a predesigned fashion (211-213). Release rates can be constant over long periods, cyclic or triggered as needed by the environment or other external agents (Figure 1.19). In any case, the purpose is to achieve more effective therapies while eliminating the potential for both under and over dosing. Additional advantages of controlled drug delivery include the need for fewer number of drug administrations, more effective usage of the drug and increased patient compliance. For these advantages to be exploited, choosing a proper drug delivery system is essential. An ideal drug delivery system should be inert, biocompatible, mechanically strong, capable of achieving high drug loading, safe from accidental release and simple to administer and remove.

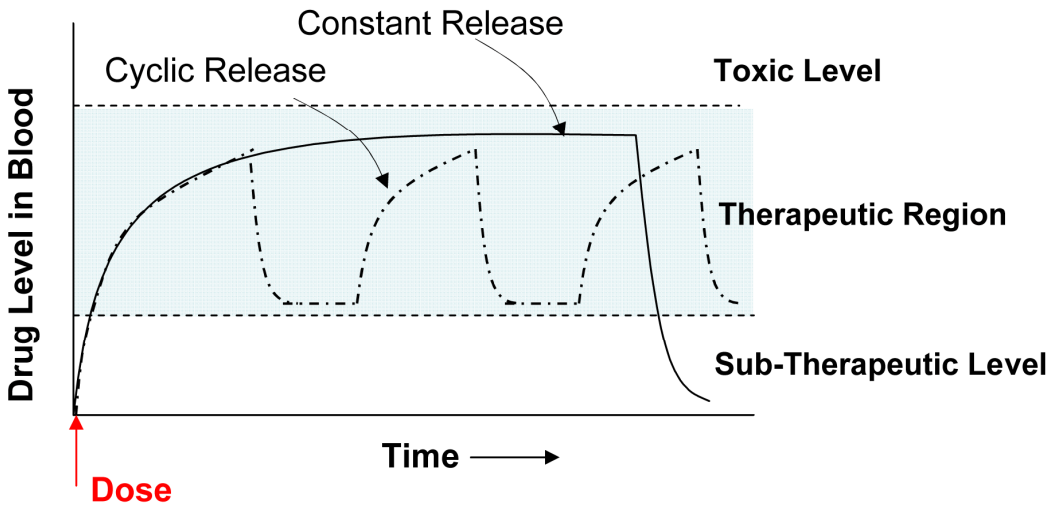


Figure 1.19 Changes in systemic levels of drug concentrations with ideal modes of controlled drug delivery

Shown in solid line is the delivery mode where encapsulated drug is released at a constant rate over long periods of time. Shown in dashed line is the delivery mode where the drug is delivered cyclically in a predetermined fashion. In either case, the drug concentrations stay in therapeutic range for long durations minimizing the effects of under or over doses. Also, the need for fewer administrations to obtain desired therapeutic effect makes these methods more attractive compared to traditional modes.

1.3.1. Hydrogels

Hydrogels are a versatile class of materials that meet most of the criteria required by a controlled release system. They can be generally defined as insoluble, yet water swellable polymer networks. Hydrogels may absorb from 10% to up to 100 times their dry weight in water (214). Hydrogels may be chemically stable or they may degrade and eventually dissolve in aqueous solutions. Since the pioneering work of Wichterle in 1960s (215-217) hydrogels have become materials of great interest to biomaterials scientists. Later, Yannas and co-workers incorporated natural polymers such as collagen and shark cartilage into hydrogels for use as artificial burn dressings (218,219). Hydrogels based on both natural and synthetic polymers have since then been great candidates for encapsulating and delivering various proteins, cells and therapeutic agents (Table 1.3) (220-222). More recently, these hydrogels have become especially attractive to the field of tissue engineering as matrices for repairing and regenerating a wide variety of tissues and organs (223-241).

Table 1.3 Examples of natural and synthetic polymers commonly used in synthesis of hydrogels

Type	Polymer
Natural Polymers	Alginic acid, Chitosan, Polylysine, Collagen, Fibrin, Dextran, Agarose
Synthetic Polymers	Poly(ethylene glycol) (PEG) Poly(lactic acid) (PLA) Poly(glycolic acid) (PGA) Poly(lactic acid-co-glycolic acid) (PLGA) Poly(2-hydroxy ethyl methacrylate) (PHEMA) Poly(N-vinyl pyrrolidone) (PNVP) Poly(methyl methacrylate) (PMMA) Polyacrylamide (PAAM)

1.3.2. Types of Hydrogels

Hydrogels can be broadly divided into two major classes;

1. Physical (reversible)
2. Chemical (permanent)

'Reversible' or 'physical' hydrogels are formed when the polymer networks are held together by molecular entanglements and/or physical forces that include hydrogen bonding, ionic, electrostatic or hydrophobic forces (242,243). 'Permanent' or 'chemical' hydrogels are formed when the polymers/macromers are held together by covalent-crosslinking (244-246) (Figure 1.20). Based on the chemical composition, these hydrogels can be either degradable or non-degradable (213,220-222,244,245,247-249).

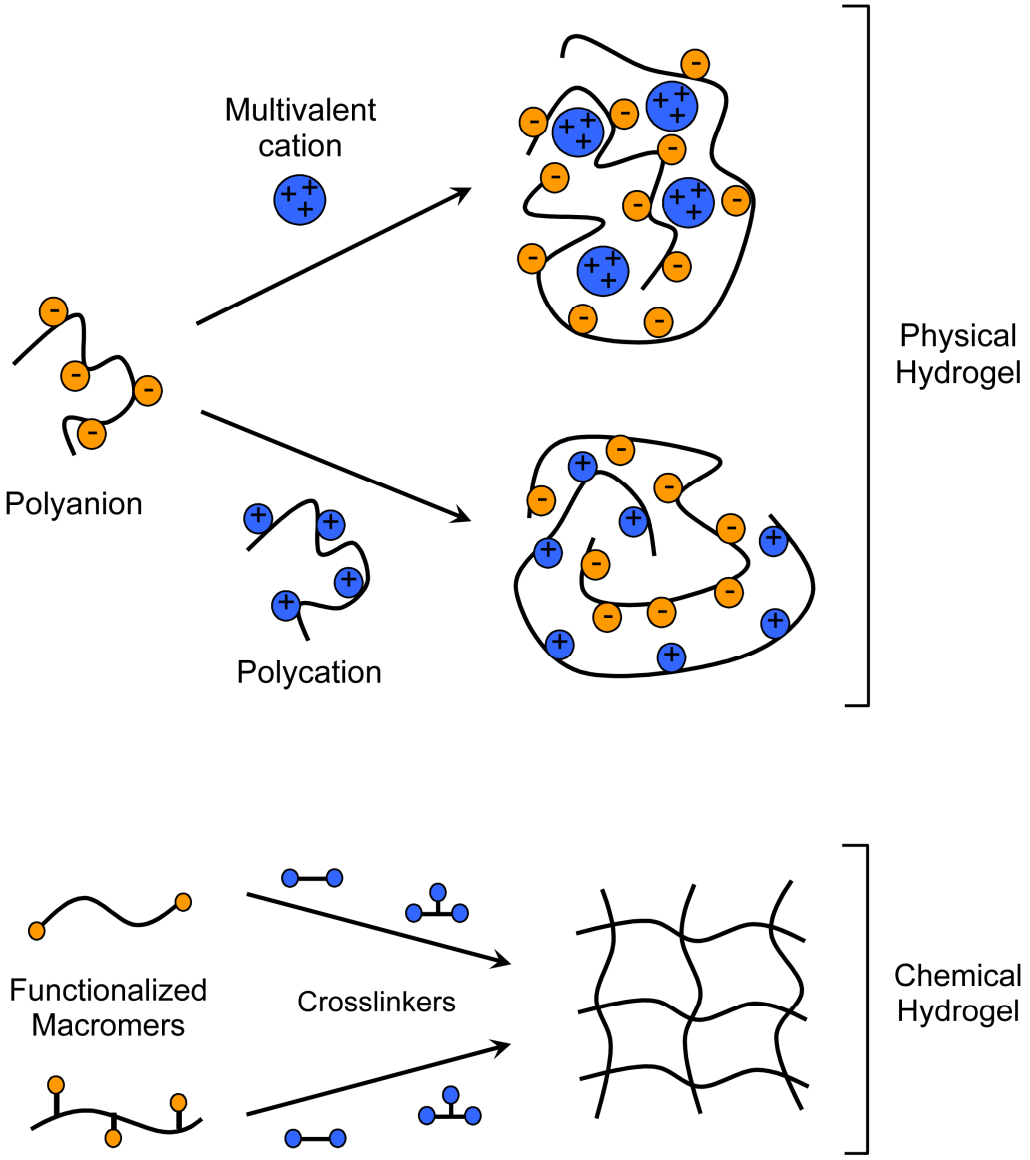


Figure 1.20 Schematic of methods for forming physical and chemical hydrogels Examples of physical hydrogel include alginic acid in complex with Calcium or polylysine. Examples of chemical hydrogel include photopolymerization of diacrylated poly(ethylene glycol) (PEG) using photoinitiators.

In addition, the water inside the hydrogel can exists in two forms (214):

1. Primary bound water (water that hydrates the most polar hydrophilic groups)
2. Secondary bound water (water interacting with the hydrophobic domains that are exposed by swelling of the gel)

Combined, these two forms are often called ‘total bound water’. After the polar and hydrophilic sites have interacted with the water, additional water is imbibed due to the osmotic driving force of the network chains towards infinite dilution. This induces swelling which is opposed by the covalent or physical crosslinks, leading to an elastic network retraction force (250). Thus, the hydrogel will reach an equilibrium swelling level at the point where these two opposing forces are equal. The extent of this swelling level is determined mainly by the nature of the hydrophilic chains and the crosslinking density of the network (250,251). Release of the macromolecular drugs from these hydrogels is primarily controlled by the pore size and the amount of water available for the drug to freely hydrate and diffuse through (244,246,251-253). However, additional parameters like the polymer chemistry, and its strength of interaction with the encapsulated drug may also play an important role in determining the release rates of the drug. In designing a hydrogel matrix for a controlled release application, it is thus essential to match the polymer composition and the crosslink density of the hydrogel matrix with the physical properties of the drug molecule that needs to be delivered.

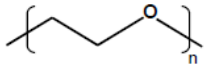
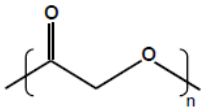
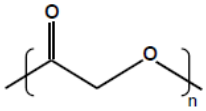
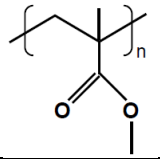
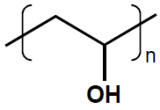
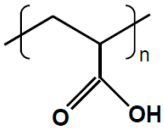
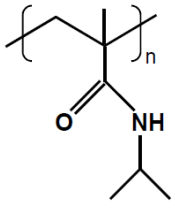
1.3.3. Polymers in Controlled Drug Delivery

A range of polymeric materials are now being employed to control the release of drugs and other active agents, primarily because of their processability and the ability of researchers to readily control their chemical and physical properties via molecular synthesis. Shown in table 1.4 are some of the polymers that are currently being used for synthesizing hydrogels along with their desirable properties.

Early generation of polymers/macromers that made up the hydrogels were usually homopolymers (eg. PEG, PMMA) which displayed specific properties. However, the desire to fabricate materials that possess multiple properties have lead chemists to create co-polymers (eg. PLGA (254,255)) and block co-polymers (eg. PLA-PEG-PLA (244)) that became more attractive for drug delivery applications. For example, PEG is one of the most biocompatible polymers because of its high hydrophilic nature. The tight hydrogen bond formation between PEG and the water molecules around prevent it from adsorbing any protein or biological matter onto its surface. This property has made PEG very attractive for synthesizing hydrogels and as a coating on bio-implants to prevent rejection from the immune system (256). Many research groups have also investigated the attachment of PEG chains onto therapeutic proteins since PEG chains at the surface allow proteins to stay in circulation for longer durations (257-264).

Table 1.4 Chemical structure and desirable properties of some of the common polymers used in synthesis of hydrogels.

PEG – poly(ethylene glycol); PGA – poly(glycolic acid); PLA – poly(lactic acid); PMMA – poly(methyl methacrylate); PVA – poly(vinyl acetate); PAA – poly(acrylic acid); PNIPAAM – poly(N-isopropyl acrylamide).

Polymer	Structure	Desirable Properties
PEG		Very Hydrophilic (265,266)
PGA		Degradable (254,255,267-269)
PLA		Degradable (252,254,255,268)
PMMA		Transparent (270,271)
PVA		Hydrophilic (272-274)
PAA		pH Sensitive (275-278)
PNIPAAM		Temperature sensitive (279-282)

While the non-degradable PEG hydrogels are very inert and trigger minimal to no immune response, its applicability has been limited since it requires surgical procedures to remove the gel once the drug is delivered. Incorporating PLA on one or both sides of the PEG chain allows the formation of block co-polymers PLA-PEG or PLA-PEG-PLA. These block co-polymers are extremely attractive for applications in drug delivery (244,245) since they posses both of the highly desirable properties 1) the hydrophilic surface which prevents protein adsorption and immune rejection and 2) the ability to degrade and dissolve in water.

In addition to these, some polymer materials have allowed the development of a novel concept of 'responsive drug delivery' where the drug is released from the hydrogel in a pulsatile manner only when required by the body (283,284). Much work in this area has the eventual goal of delivering insulin to diabetic patients. Insulin requirements fluctuate throughout the day as patient food intake and activity change blood glucose levels. Current insulin formulations require repeated injections daily and careful control of glucose intake. Responsive drug delivery hopes to revolutionize insulin therapy with the design of systems that release insulin in response to increased blood glucose levels. In general, responsive drug delivery systems have two components: a sensor that detects the environmental parameter that stimulates drug release and a delivery device that releases drug. For diabetes treatment, responsive drug delivery systems have been proposed that use the enzyme glucose oxidase as the sensor (283). When blood sugar levels rise, glucose oxidase converts glucose to gluconic acid

resulting in lowered pH. This pH decrease is then used as the signal for insulin release. Release is achieved by pH-sensitive polymers that either swell or degrade in acidic environments (275).

And finally, depending on the composition and the method of polymerization, hydrogels can be fabricated into many different physical forms that suit a variety of applications. These include (a) soft molded forms (soft contact lens), (b) pressed powder matrices (pills or capsules for oral intake), (c) microparticles (injections, ointments and wound dressings), (d) coatings (on implants and catheters), (e) membranes or sheets (reservoir in a transdermal drug delivery patches), (f) encapsulated solids (osmotic pumps), and (g) liquids (that form gels upon exposure to changes in temperature or pH).

1.3.4. Mechanisms of Drug Delivery

There are two primary mechanisms by which active agents can be released from a delivery system:

1. Diffusion
2. Degradation

One or both of these mechanisms may occur in a given release system. In a diffusion-controlled release system, the diffusion of drug molecule within an aqueous environment is inhibited by the insoluble polymer matrix through which drug molecules must travel to exit the device (285). Polymer chains that form the

cross-linked hydrogel act as diffusion barriers. The swelling of hydrogel in water which creates void space for the polymer to imbibe more water in decreases these diffusion barriers (214,250). Polymers used for diffusion controlled release can be fabricated as either matrices (220-222,248,286) in which the drug is uniformly distributed or as membrane devices that protect a drug reservoir from releasing spontaneously (287-290). While in matrix systems, the drug diffuses through the void spaces between polymer chains out into the environment, diffusion out of reservoir system is determined by the osmotic potential gradients and the drug is transported out of the reservoir, driven by diffusion and convection through the orifices. Shown in figure 1.21 is a comparison of the diffusion mechanisms between the matrix and reservoir systems. Diffusion rates in a matrix system decrease with the release of drug owing to the gradual decrease in concentration gradient of the drug. However, for reservoir systems the delivery rates can remain fairly constant as since drug concentration inside the membrane can stay constant for long durations.

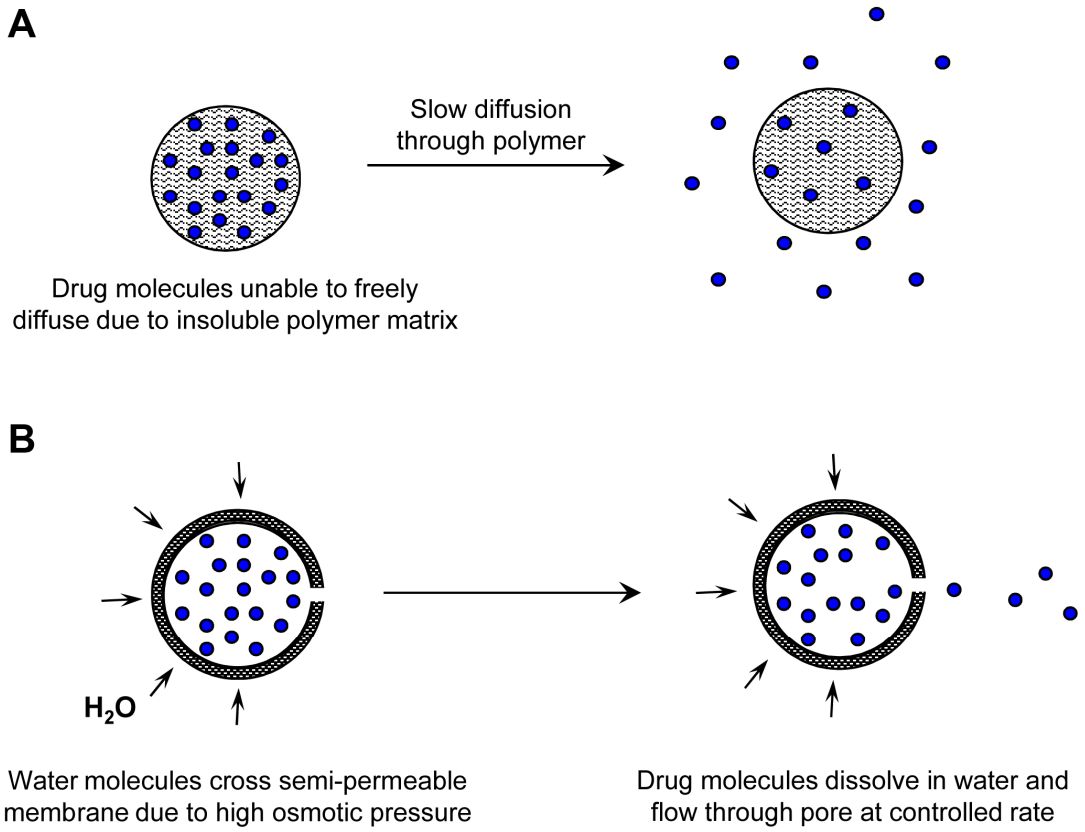


Figure 1.21 Mechanisms of controlled drug delivery from A) matrix and B) reservoir devices

In matrix devices, drug molecule diffusion is limited by the insoluble polymer matrix and the drugs must travel through the tortuous pathways to exit the device. However, in reservoir devices, the drug is trapped in a semi-permeable polymer membrane. High osmotic gradients drive water to diffuse in to the reservoir generating a pressurized chamber inside. This pressure is relieved as the aqueous solution along with the drug flows out of the orifices. The rate of this flow is determined by the size of orifices and the thickness and permeability of the polymer membrane to water.

While the hydrogel systems that are primarily diffusion controlled showed excellent promise for controlled delivery of drugs a great deal of attention and research effort is currently being focused on degradable polymers. These potential drug carriers degrade into biologically acceptable compounds, often through the process of hydrolysis, subsequently releasing the incorporated medications for uptake by living cells. This process eliminates the need to remove the delivery system after release of the active agent is completed.

It is important to note that the term ‘degradation’ specifically refers to bond cleavage, whereas ‘erosion’ refers to depletion of material. Degradation is a chemical process that leads to size reduction of the polymer chains, while erosion is mass loss of polymer matrix by dissolution and diffusion processes.

Two mechanisms of polymer erosion can be identified (Figure 1.22):

1. Surface erosion
2. Bulk erosion

Surface erosion occurs when the rate of degradation exceeds the rate of water permeation, while bulk erosion occurs when water molecules are able to permeate into the bulk of the polymer matrix at a quicker rate than degradation of individual bonds. Homogenous (bulk) erosion where the polymer degrades homogeneously throughout the matrix is a common polymer degradation mechanism (245,267,269).

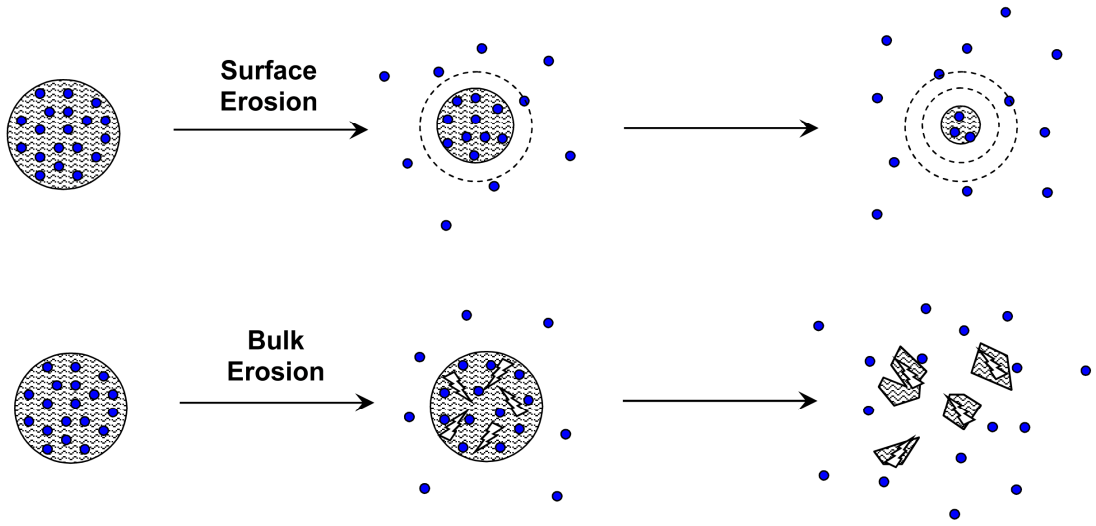


Figure 1.22 Mechanisms of drug delivery from a surface eroding vs. bulk eroding device.

In surface eroding devices, polymer chains degrade at a faster rate than water permeation into the device. However, in bulk eroding devices, water molecules are able to permeate into the bulk of the polymer matrix at a quicker rate than degradation of individual bonds.

The hydrolysis of bulk degrading polymers usually proceeds by first losing molecular weight (i.e. larger chains breaking up into smaller units), followed by a loss of mass in the second stage (i.e. depletion of material from the hydrogel). The bulk degrading polymers commonly used are poly(esters), such as copolymers of PLA and PGA (254,291). However, bulk degradation causes difficulties in the control of drug release, because the release rate may change as the polymer degrades. As the polymer begins to lose mass, the release rate accelerates because it is determined by a combination of diffusion and simultaneous polymer erosion.

In surface eroding systems, the erosion rate depends on the geometry and the surface area of the device rather than the volume of the polymer matrix (249,292,293). Here, the actual erosion process is the rate-limiting step and that the drug release rates depend on the erosion rate of the polymer. However, the surface area decreases as the implant is eroded, with a corresponding decrease in the release rates of drug. Thus, a geometry that does not change its surface area significantly as a function of time helps in attaining more uniform and zero-order release rates.

1.4. Outline

Following introduction, chapter 2 outlines the details of materials and experimental procedures used in this research. In chapter 3, section 3.1, we characterize the role of IL-6 family cytokines in endogenous neuroprotection of retinal photoreceptors. Using quantitative PCR techniques, we provide evidence that in the retina, IL-6 family cytokines LIF, OSM, CT-1 and CLC are strongly upregulated in response to preconditioning with bright cyclic light leading to robust activation of STAT3 in a time-dependent manner. Further, we found that blocking LIFR activation during preconditioning using a LIFR antagonist (LIF05) (48,294) attenuated the induced STAT3 activation and also resulted in reduced preconditioning-induced protection of the retinal photoreceptors. Together, these data demonstrate that LIFR and its ligands play an essential role in endogenous neuroprotective mechanisms triggered by preconditioning-induced stress.

In section 3.2, we present our results on the structural characterization of one of the IL-6 family cytokines, human oncostatin M (hOSM). It has previously been reported that unlike other IL-6 family cytokines, hOSM signals via two different receptor complexes (23,50), LIFR:gp130 (type I and OSMR:gp130 (type II). Also, unlike other LIFR binding cytokines in this family, OSM displays a weak affinity towards LIFR (5,21,50). Based on our structural analysis, we hypothesized that a unique loop structure between the B and C helices of OSM is playing a role in OSM's unique ability to bind OSMR. However, functional evaluation of wild type OSM in comparison with mutant OSMs with truncated BC loops revealed that the

BC loop is not responsible for OSM's unique ability to bind OSMR, but instead acts as a modulator for OSM's affinity towards its receptors. Kinetic and equilibrium binding analysis of the ligand receptor interactions showed that the BC loop on OSM presents a steric hindrance for OSM's strong interaction with both LIFR and OSMR. Removal of the loop resulted in creation of novel cytokines that exhibit improved affinity towards LIFR and OSMR, leading to improved ability in activating LIFR:gp130 and OSMR:gp130 receptor complexes on the cell surface. In section 3.3, we have tested the applicability of poly(ethylene glycol) (PEG) based hydrogels for delivering these cytokines in a controlled manner for therapeutic applications. With *in vitro* and *in vivo* experiments in mice, we show that the macromer content in the hydrogels can be varied to effectively manipulate the physical properties and thus the release rates of the encapsulated drug from these hydrogels. Using PEG 5000 Da macromers, we have shown that one can obtain a sustained release of hOSM for a period of 12 days. And, for transscleral delivery of hOSM to retina, a release rate of at least 0.5 μg/day from the hydrogel is required to cross the scleral barriers and reach the retina to induce STAT3 activation. Finally, in chapter 4, we present our conclusions and recommendations.

2. MATERIALS AND METHODS

2.1. Mutation of human Oncostatin M

A cDNA clone for hOSM was obtained from Invitrogen (Cat # 4548943; Invitrogen, Carlsbad, CA). The gene encoding mature OSM is amplified using PCR (See Table 2.1 for primers). The gene is then cloned into a pGEX-2T vector (Catalog # 27-4801-01, GE Healthcare, Uppsala, Sweden) for protein expression as a GST fusion protein with a thrombin cleavage site between the GST tag and the protein. During the course of purification we observed that the native human OSM contained a cryptic thrombin cleavage site 'AGR' between its C and D helices (Figure 2.1). As expected, when this fusion protein was subjected to thrombin cleavage on a glutathione sepharose 4B column, it resulted in the formation of two new fragments of sizes ~17 kDa and ~6 kDa in addition to the native OSM which is ~23 kDa (Figure 2.2, lane 1). To facilitate recombinant protein purification and to increase protein stability *in vivo*, we induced mutations at DNA level using Quickchange® site directed mutagenesis kit (Stratagene, La Jolla, CA) to replace 'AGR' with 'AGA'. This modification resulted in OSM that was resistant to thrombin cleavage (Figure 2.2, lane 2). The 'AGA' modification did not alter OSM's functional activity on Müller cells (Figure 2.3). Treating human Müller cells with GST fused wild type hOSM (GST-hOSM (WT)) or the OSM modified with AGA (GST-hSOM (modified) resulted in similar levels of STAT3 activation in a dose dependent manner. This was expected since the

modification is located in a flexible loop region, away from the receptor binding sites. We will refer to this 'AGA' modified human OSM as the wild-type* OSM (OSM-WT*). Recombinant proteins with modifications in the BC loop (OSM-M1 and OSM-M2) were made using the 'AGA' modified human OSM as the starting template. Therefore all recombinant OSM proteins we expressed lack the thrombin cleavage site. Mutations and/or deletions of codons in the BC loop region were performed using Quickchange® mutagenesis kit (Stratagene, La Jolla, CA). See table 2.1 for primers used.

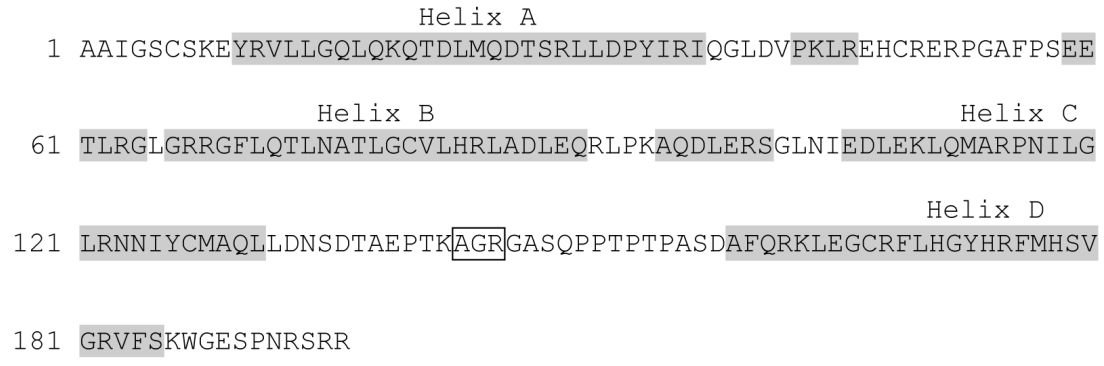


Figure 2.1 Amino acid sequence of human OSM.

All alpha helical regions in OSM are highlighted in gray with the helices A (Y10-I37), B (G66-Q90), C (E106-L131) and D (A159-S185) indicated. The cryptic thrombin cleavage site 'AGR' between helix C and helix D is highlighted in a box.

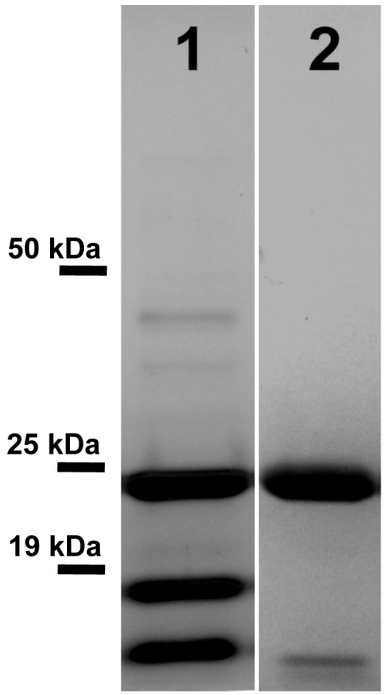


Figure 2.2 SDS-PAGE analysis of OSM with or without the 'AGA' modification after subjection to thrombin cleavage.
Lane 1 – OSM; Lane 2 – OSM with AGA modification.

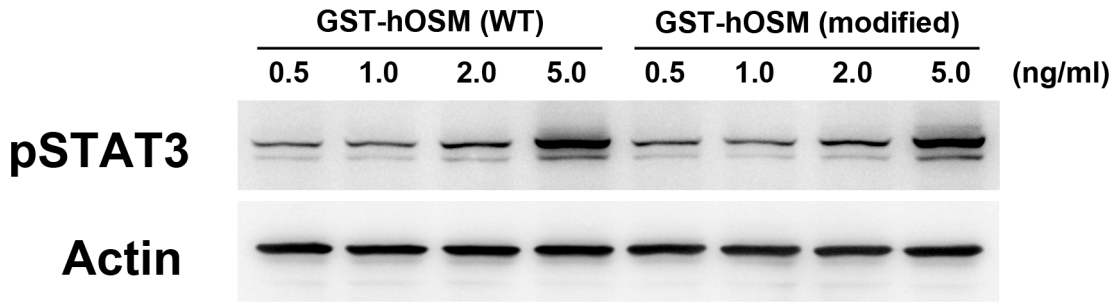


Figure 2.3 STAT3 activation in human Müller cells in response to stimulation with GST fused wild type (GST-hOSM (WT)) or AGA modified human OSM (GST-hSOM (modified).

Table 2.1 Primers used for PCR amplification of hOSM gene and conducting point mutations thereafter.

Gene / Mutation		Sequence (5' to 3')
hOSM	FWD	CTGGTTCCGCGTGGATCCGCGGCTATAGGCAGC
	REV	CAGTCACGATGAATTCGACTATCTCCGGCTCCG
AGR to AGA	FWD	CACGAAGGCTGGCGCGGGGGCCTCTCAG
	REV	CTGAGAGGCCCCCGCGGCAGCCTTCGTG
FXXK to AXXA	FWD	CCCTGCCTCGGATGCTGCTCAGCGCGCGCTGGAGGGCTG
	REV	CAGCCCTCCAGCGCGCGCTGAGCAGCATCCGAGGCAGGG
OSM-M1 (Round 1)	FWD	GACTTAGAGCAGCGCCTCGGCGCGCCCCAGGATTTGGAGAGGT
	REV	ACCTCTCCAAATCCTGGGGCGCGCCGAGGCGCTGCTCTAAGTC
OSM-M1 (Round 2)	FWD	CTCGGCGCGCCCTCTGGGCTGAAC
	REV	GTTCAGCCCAGAGGGCGCGCCGAG
OSM-M2 (Round 1)	FWD	CAGCGCCTCGGCGGGGGCTCTGGGCTGAAC
	REV	GTTCAGCCCAGAGCCCCCGCCGAGGCGCTG
OSM-M2 (Round 2)	FWD	CCTCGGCGGGGGCAACATCGAGGACTT
	REV	AAGTCCTCGATGTTGCCCCCGCCGAGG

2.2. Recombinant protein expression and purification

Expression and purification of hLIF, LIF05, OSM-WT* and its mutants OSM-M1 and OSM-M2 was performed as described previously (Robinson *et al.* 1994a). Briefly, the proteins were expressed as glutathione-S-transferase (GST) fusion proteins in *E. coli* strain JM109. Cultures were grown in LB plus ampicillin (100μg/ml) at 37^{o}C and 300 rpm until they reached midlog phase (A_{600} = 0.6). Isopropyl β-D-1-thyogalactopyranoside (IPTG) was then added to the culture to a final concentration of 0.1 mM and induction was carried out for additional 3 hrs at room temperature. Harvested bacteria are resuspended in lysis buffer (50 mM Tris-HCl (pH 7.5), 150 mM NaCl, 5 mM EDTA, 1% (v/v) NP-40, 5% (v/v) glycerol, and protease inhibitor cocktail (Calbiochem, San Diego, CA) and lysed using sonication at 60 kHz for 10 sec. The lysed solution is then centrifuged at 16000g for 20 min and the fusion protein in supernatant was recovered by affinity binding to a slurry of glutathione-Sepharose 4B beads (GE Healthcare, Uppsala, Sweden). Fusion protein bound beads were washed with 1X PBS three times with each for a duration of 30 min. Isolation of the desired protein was achieved by cleavage of the fusion protein with human thrombin (80 units for 1ml of beads) (Amersham Biosciences, Piscataway, NJ) in 1X PBS (pH 7.3) overnight at room temperature. Following cleavage, elution containing the cytokine was pooled with additional 4 batch washes (1X PBS, pH 7.3). Cleaved cytokines were further purified by fast protein liquid chromatography (FPLC) using a Mono-S (for LIF and LIF05) or MonoQ (for OSM and its mutants) ion exchange column

(Amersham Biosciences, Piscataway, NJ). Elution was carried out with a linear gradient of 0 – 1 M NaCl. Eluted fractions were analyzed using SDS-PAGE and the fractions containing enriched protein were pooled and concentrated by ultrafiltration (Millipore Corporation, Billerica, MA). Identity of the proteins was confirmed by mass spectrometry and concentrations were determined using BCA assay (Thermo Scientific, Rockford IL) using bovine serum albumin (BSA) as the standard.

2.3. Circular Dichroism

CD measurements were performed on a Jasco J-715 spectropolarimeter (Jasco, Easton, MA). Steady state spectra were recorded by scanning in the wavelength region between 200 and 250 nm with 0.1 cm pathlength and a 1 nm bandwidth at 20^{o}C. Spectra of blank buffer solutions acquired under identical conditions were used for background correction. Protein concentrations were maintained at 10 μM in Dulbecco's phosphate buffered saline (PBS) (9.33 mM potassium phosphate, 136 mM NaCl, 2.7 mM KCl, 0.6 mM $MgCl_2$, 0.9 mM $CaCl_2$). Estimation of the α-helical, β-sheet and loop content in the proteins was carried out using SELCON3, CONTINNL and CDSSTR software programs (CD Pro®, Lamar, CO).

2.4. Cell culture and cytokine stimulation

Müller cells and A375 melanoma cells were grown in DMEM-F12 and RPMI 1640 respectively supplemented with fetal bovine serum (10%) (Invitrogen, Carlsbad, CA), penicillin (100 U/ml) and streptomycin (100 μg/ml) (Invitrogen, Carlsbad, CA). Cells were seeded in a 10cm tissue culture dish at a density of 100,000 cells/plate and allowed to grow in a 37^{o}C humidified atmosphere with 5% CO_2. When the cells reached 80% confluency, the culture medium was changed to fresh serum free media (DMEM-F12 or RPMI 1640 supplemented with penicillin (100 U/ml) and streptomycin (50 μg/ml)). Serum starvation was carried out for 30 mins before stimulation with desired doses of the cytokines for a period of 20 mins. Following stimulation, cells were harvested for measurements of STAT3 and ERK1/2 activation by Western blots.

2.5. Cell proliferation

To measure A375 melanoma cell proliferation, ATP activity of the viable cells was quantified using CellTiter-Glo Luminescent cell viability assay (Promega, Madison, WI). A375 melanoma cells were seeded in a 96 well plate at a density of 4000 cells/well in a total volume of 200 μl of RPMI 1640 (Invitrogen, Carlsbad, CA) supplemented with fetal bovine serum (10%), penicillin (100 U/ml) and streptomycin (100 μg/ml). Cells were then treated with different doses of OSM-WT, OSM-M1 or OSM-M2 for desired duration immediately after seeding. Control

cells were treated with carrier solution, 1X PBS. Cell population in the wells was monitored using CellTiter Glo® Luminescent cell viability assay (Promega, Madison, WI) according to the manufacturer's protocol.

2.6. Animals and bright cyclic light preconditioning

[Performed in Collaboration with Dr. Jiangang Wang]

All procedures were approved and performed according to the guidelines provided by Institutional Animal Care and Use Committee (IACUC) of the University of Oklahoma Health Sciences Center. BALB/cJ mice (5-6 weeks of age) were obtained from Jackson laboratories and maintained in 60 lux cyclic light at cage level (12 hr ON: 12 hr OFF) for 7 days. Animals were then maintained in 600 lux cyclic bright light for preconditioning (12 hr ON: 12 hr OFF) for 6 days followed by a 4 day recovery period under normal cage room conditions (i.e., 60 lux: 12 hr ON: 12 hr OFF) (Figure 2.4).

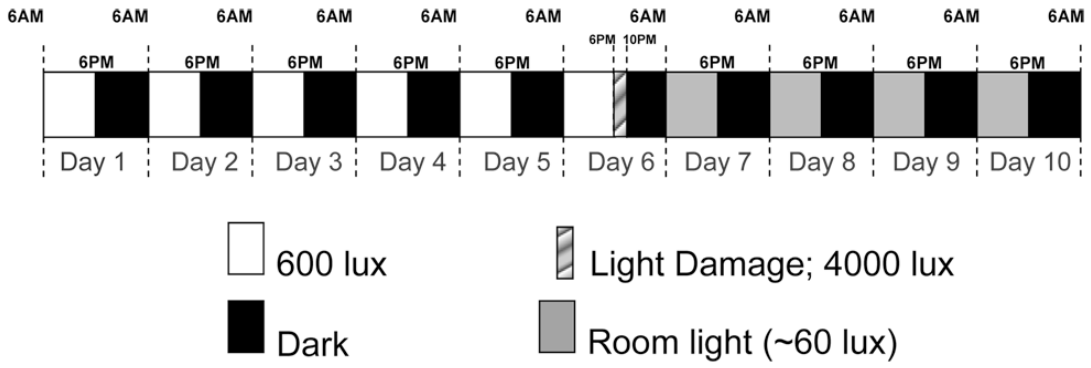


Figure 2.4 Schematic diagram of bright cyclic light preconditioning.

2.7. Bright Light Damage

[Performed in Collaboration with Dr. Jiangang Wang]

For bright light damage, unanesthetized mice were exposed to diffuse white fluorescent light maintained at 4000 lux at cage level for 4 hrs immediately after the bright light exposure (600 lux) on the 6th day of preconditioning (Figure 2.3). Control mice were maintained in normal cage room light condition (60 lux) prior to exposure to 4000 lux damaging light. After light exposure, all mice were allowed to recover for 8 hours in the dark and then kept in normal cage room lighting for 4 days before analysis by ERG and histology.

2.8. Real-time RT-PCR

[Performed by Dr. Jiangang Wang]

mRNA levels of selected genes were measured using real-time PCR with cDNA extracted from retinas as templates. Primers (Table 2.2) were designed using PrimerQuest software (Integrated DNA Technologies, Coralville, IA, USA) spanning the intron–exon boundary to amplify the corresponding mRNAs without amplifying potentially contaminating genomic DNA. Real-time PCR was carried out with the SYBR green PCR master mix (Bio-Rad Lab., Hercules, CA, USA) using the MyiQ Single-Color Real-Time PCR detection system (Bio-Rad Lab., Hercules, CA, USA) following the manufacturer's instructions. Electrophoresis of PCR products was performed to identify that a single band of the correct size had been amplified (data not shown).

Table 2.2 Forward and reverse primers used in RT-PCR analysis. (F – Forward, R – Reverse, bp – base pairs)

Name		Sequences (5' to 3')	Product size (bp)
RPL19	F	TCACAGCCTGTACCTGAAGG	151
	R	TCGTGCTTCCTTGGTCTTAG	
LIF	F	TGAGATGCAGGGATTGTGCCCTTA	187
	R	AAATGAAGAGAGCATTGGCGCTGC	
OSM	F	TTTGACCCTCAGTCTCCTCATCCT	134
	R	AGGGCTCCAAGAGTGATTCTGTGT	
CT1	F	AAGACCACCAGACTGACTCCTCAA	126
	R	GCTGCACGTATTCCTCCAGAAGTT	
CLC	F	ACGAGCCTGACTTCAATCCTCCT	147
	R	ACGCAAGTAACACAGGAGGTGACT	
CNTF	F	AGAGCAATCACCTCTGACCCTTCA	189
	R	ATCTCACTCCAGCGATCAGTGCTT	
BDNF	F	AGAAGGTTCGGCCCAACGAAGAAA	145
	R	GACATGTTTGCGGCATCCAGGTAA	

2.9. Electroretinograms (ERGs)

[Performed in Collaboration with Dr. Jiangang Wang]

ERGs were recorded using a Colordome ERG instrument (Diagnosys, Littleton, MA) to measure the function of surviving photoreceptors. Analysis was carried out as described previously by Ueki et al. (149). Briefly, after an 8 hr dark adaptation, mice were deeply anesthetized with a single intraperitoneal injection of xylazine (7 mg/kg) and ketamine (40 mg/kg). Mice were then placed on a 37°C heating pad throughout the experiment. Pupils were dilated with tropicamide and phenylephrine. Full-field ERGs were recorded from both eyes using gold wire electrodes placed centrally on the cornea. A platinum reference electrode was attached in the mouth, and a platinum needle electrode in the tail served as a ground. Electrode positioning was monitored throughout the measurements using an infrared camera. A series of increasing flash intensities over a range of 6 logarithmic units of intensity (0.001, 0.01, 1, 100, 200 and 400 cd.s/m^2) were used (A light intensity of 1cd produces an illumination of 1 lux at a distance of 1 meter from the light source). The amplitude of the a-wave was measured from the baseline to the trough of a-wave. After the ERG recording, retinas were harvested for histological analysis.

2.10. Intravitreal Injections

[Performed in Collaboration with Dr. Jiangang Wang]

Normal BALB/cJ mice were deeply anesthetized with a single intraperitoneal injection of xylazine (7 mg/kg) and ketamine (40 mg/kg). One micro liter of the cytokines or PBS (vehicle control) was injected into the vitreous chamber of the eye using a 36 gauge needle (World Precision Instruments, Sarasota, FL) through the temporal lymbus of the eye. For inhibition studies during bright cyclic light preconditioning, 8 μg of LIF05 were injected into the right eye of BALB/cJ mice in a volume of 1 μl PBS after 2 days of bright cyclic light preconditioning. 1 μl of PBS was injected into the right eye which served as control. Following injection, the mice were returned to their cages for 4 more days of bright cyclic light preconditioning. After a total of 6 days of preconditioning, mice were euthanized and the eyes were enucleated and subjected to western blot analysis.

2.11. Histological analysis

[Eyes were processed by Dean A. McGee Eye Institute histological core facility and counting were done by Jiangang Wang and Srinivas Chollangi]

Mice were euthanized with CO_2 and the eyes were enucleated and marked with a green dye on dorsal surface to mark the superior hemisphere. Eyes were then fixed in PERFIX (20% isopropanol, 2% trichloroacetic acid, 4% paraformaldehyde, and 2% zinc chloride) overnight and placed in 70% ethanol at room temperature for 4 days followed by embedding in paraffin. Sagittal sections

through the center of the eye, including the optic disc, were cut at 5 μm thickness. After hematoxylin and eosin (H&E) staining, rows of photoreceptor nuclei were counted using light microscopy at nine equidistant points beginning at the optic nerve head toward both the inferior and superior retinal hemispheres.

2.12. Western Blots

For *in vivo* studies, retinas were harvested immediately after animals were euthanized while for cell culture studies, the cells were scraped off tissue culture plate in ice-cold PBS and centrifuged to get rid of the PBS. The retina or pelleted cells are then homogenized in a lysis buffer [50 mM Tris-HCl (pH 7.5), 150 mM NaCl, 5 mM EDTA, 1% (v/v) NP-40, 5% (v/v) glycerol, and protease inhibitor cocktail (Calbiochem, San Diego, CA)]. Protein content was measured using BCA protein assay (Pierce, Rutherford, IL). Total protein from each sample (15 μg) was electrophoresed on 4-20% gradient SDS-polyacrylamide gels (Invitrogen, Carlsbad, CA), and transferred to nitrocellulose membranes (Bio-Rad, Hercules, CA). The membranes were incubated in blocking buffer [5% BSA in TBST (20 mM Tris-HCl , pH 7.5, 100 mM NaCl, and 0.1% Tween-20)] for 1 h at room temperature, and then incubated overnight at 4˚C with rabbit polyclonal anti-phospho-STAT3 antibody or anti-phospho-ERK1/2 antibody (Cell Signaling Technology, Beverly, MA), in blocking buffer, followed by 1h incubation at room temperature with HRP-conjugated goat anti-rabbit secondary antibody (Amersham Biosciences, Piscataway, NJ). Signals were visualized using SuperSignal West Dura extended duration substrate (Pierce, Rutherford, IL) and

quantified by conventional digital image analysis using an ImageStation 4000R (Software: Kodak MI; Eastman Kodak, Rochester, NY). Blots were stripped and reprobed with anti-βactin (Abcam, Cambridge, MA) followed by appropriate secondary antibodies. Band intensities of pSTAT3 and pERK1/2 were normalized against the intensity of β-actin to account for loading variability.

2.13. Surface Plasmon Resonance (SPR)

[Experiments were performed by Srinivas Chollangi with guidance from ICX Technologies, Oklahoma City, OK]

Kinetic parameters of the interactions between receptor domains and the cytokines LIF, OSMWT*, OSM-M1 or OSM-M2 were analyzed by surface plasmon resonance (SPR) using the SensiQ system (ICX Technologies, Oklahoma City, OK) as described by the manufacturer protocol. Briefly, a carboxyl sensor with two channels, was installed in SensiQ and allowed to thermally equilibrate for about 15 min. The channels were initially cleaned with a 3 min injection of 0.1 M HCl. An activation solution of 2 mM 1–Ethyl–3-[3–dimethylaminopropyl] carbodi- imide hydrochloride (EDC) and 0.5 mM N-hydroxysulfosuccinimide (NHS) was prepared in deionized water immediately before injection. Activation solution was injected over both channels for approximately 3 min followed by a 10 min injection of 50 μg/mL cytokine (LIF, OSM-WT*, OSM-M1 or OSM-M2) in 10 mM acetate buffer pH 5.0 over channel 1. Channel 2 did not receive any cytokines and thus served as a reference for

non-specific binding. Unreacted NHS esters were capped with a 3 min injection of 1 M ethanolamine, pH 8.0 over both channels. A concentration series of soluble LIFR, OSMR or gp130 (R&D Systems, Minneapolis, MN) in running buffer (10 mM HEPES pH 7.4, 150 mM NaCl, 3.4 mM EDTA, 0.005% Tween-20) were injected over both channels at a flow rate of 25 μl/min. Following a dissociation period of 3 min, the surfaces were regenerated by injecting 10 mM NaOH for 30 seconds. Rate constants for association (k_a) and dissociation (k_d) rates are derived by global analysis of the response curves fit to a 1:1 kinetic model (Equations 1 and 2) using QDat software (BioLogic Software, Ltd. Knoxville TN and Nomadics, Inc. Stillwater, OK) using 1:1 stoichiometry.

$$RU = RU_{max} e^{-k_d t} \qquad \text{Eqn 1}$$

$$RU = RU_{max} \left(1 - e^{-(k_a[C_o]+k_d)t}\right) \qquad \text{Eqn 2}$$

Where, RU – real time response units as measured by the SensiQ instrument; RU_{max} –the maximum response obtainable for a given concentration of the soluble receptor, t – time and C_o – Concentration of the soluble receptor analyte in solution.

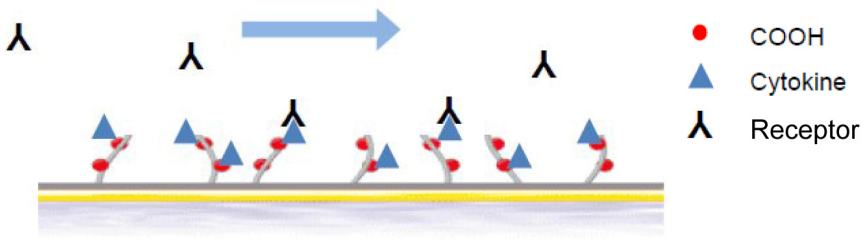


Figure 2.5 Schematic representation of cytokine – receptor interaction on SPR chip

2.14. Enzyme-linked immunosorbent assay (ELISA)

ELISA was used to evaluate the equilibrium binding strength of the interaction between the cytokines and their receptors. This technique has traditionally been used as a sensitive method to quantify the binding affinites between two interacting proteins. However, unlike in SPR, ELISA involves immobilization of the proteins on a flat plastic surface driven by hydrophobic and ionic interactions. This might cause some distortion in the 3 dimensional structure of immobilized protein which leads to inaccuracies in the estimation of dissociation constants. It is thus important to bear in mind that the values estimated using this technique are to be used only for comparison between species but not as true equilibrium binding constants. The results obtained using this techinique will thus be presented as apparent equilibrium dissociation constants ($K_{D,App}$). For direct interaction studies, cytokines (LIF, OSM-WT, OSM-M1 or OSM-M2) were immobilized on the 96 well ELISA plate by incubating the wells with 200 μl of 5 nM cytokine solution in PBS, pH 7.4 overnight at 4^{o}C. The wells were then blocked with blocking buffer (4% BSA in PBS) for 1 hour at room temperature. After washing with 250 μl of washing buffer (0.05% Tween-20 in PBS) 3 times, the cytokines were treated with a series of concentrations of soluble human LIFR (Catalog # 249-LR-050/CF, R&D Systems, Minneapolis, MN) or OSMR (Catalog # 4389-OR-050, R&D Systems, Minneapolis, MN) in 150μl of blocking buffer for 2 hours. The wells were then incubated with 150 μl of polyclonal anti-hLIFR (Catalog # AF249-NA, R&D Systems, Minneapolis, MN) or anti-hOSMR (Catalog # AF662, R&D Systems, Minneapolis, MN) in blocking buffer for 1 hour followed

by incubation with 150 μl of HRP conjugated anti-mouse antibody (GE Healthcare, Uppsala, Sweden) in blocking buffer for 30 min. The wells were then washed 3 times with washing buffer and treated with 100 μl of chromogenic Slow-TMB® HRP substrate (Catalog # 34024, Thermo Scientific Fisher, Rockford, IL) for 15 min. The reaction was then stopped by adding 100 μl of 2M H_2SO_4 and the absorbance of each well at 450nm was read immediately using a UV detector (iMark® Microplate Reader, Biorad, Hercules, CA). For interactions of higher order, soluble human gp130 (Catalog # 671-GP-100, R&D Systems, Minneapolis, MN) was immobilized on 96 well ELISA microplates by incubating the wells with 200 μl of 1 nM gp130 solution (in PBS, pH 7.4) overnight at 4^{o}C. The wells were then blocked with 150 μl of blocking buffer (4% BSA in PBS) for 1 hour at room temperature. After washing with 250μl of washing buffer 3 times, gp130 was treated with saturating amounts of the cytokines (500 nM hLIF, 200 nM OSM-WT*, 200 nM OSM-M1 or 200 nM OSM-M2) in a volume of 150 μl of blocking buffer for a period of 2 hours. The cytokine solution was discarded and a series of concentrations of soluble human LIFR or OSMR in a final volume of 150 μl blocking buffer were then added to the wells and the incubation was continued for another 1 hour. After washing with 250 μl of washing buffer 3 times the wells were then incubated with 150 μl of polyclonal anti-hLIFR or anti-hOSMR in blocking buffer for 1 hour. After 3 washes with 250 μl of washing buffer, the wells were then incubated with 150 μl of HRP conjugated anti-mouse antibody in blocking buffer for 30 min. The wells were then washed again 3 times with

washing buffer and treated with 100 μl of chromogenic Slow-TMB® HRP substrate for 30 min. The reaction was then stopped by adding 100 μl of 2M H_2SO_4 and the absorbance of each well at 450 nm was read using a UV detector. Equilibrium dissociation constants (K_D) are estimated by non-linear curve fitting to the optical density (OD) values plotted against the concentrations of soluble receptor using GraphPad Prism software (GraphPad Software, La Jolla, CA).

2.15. Synthesis of PEG hydrogels

Diacrylated poly(ethylene glycol) (PEG) macromer with a molecular weight of 5000Da was purchased from Laysan Bio, Inc (Catalog # ACRL-PEG-ACRL-5000, Laysan Bio, Inc. Arab, AL) (Figure 2.6). For hydrogel preparation, the PEG macromer was allowed to equilibrate to room temperature and then dissolved in 50 mM phosphate buffer solution (PBS) (pH 7.4) to a final macromer weight percentage of 10%, 20%, 30%, 40% or 50%. 10μg of desired protein (hOSM or BSA) and photoinitiator, Irgacure 2959 (final concentration of 0.1 wt%) (Catalog # 410896, Sigma, St. Louis MO) were also added to the macromer solution and the mixture was agitated well until all the components were dispersed homogeneously in the solution. 10 μl of the final solution is transferred into a transparent disc shaped mould and exposed to UV light at a wavelength of 365 nm (Kodak GL100, Eastman Kodak, Rochester, NY) for approximately 7 minutes to ensure complete polymerization of the functionalized macromer (Figure 2.7). After polymerization, solidified gel was carefully removed from the mold and used

for swelling and drug release studies. Hydrogels made with no protein inside served as controls.

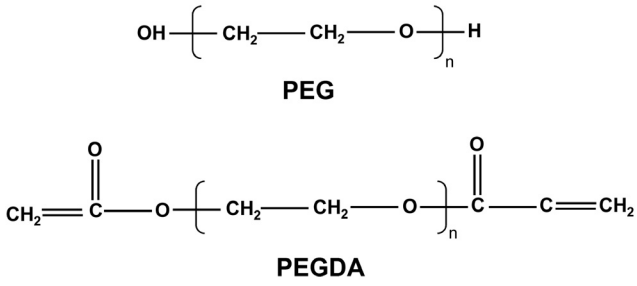


Figure 2.6 Chemical structures of poly(ethylene glycol) (PEG) and poly(ethylene glycol) diacrylate (PEGDA) macromers

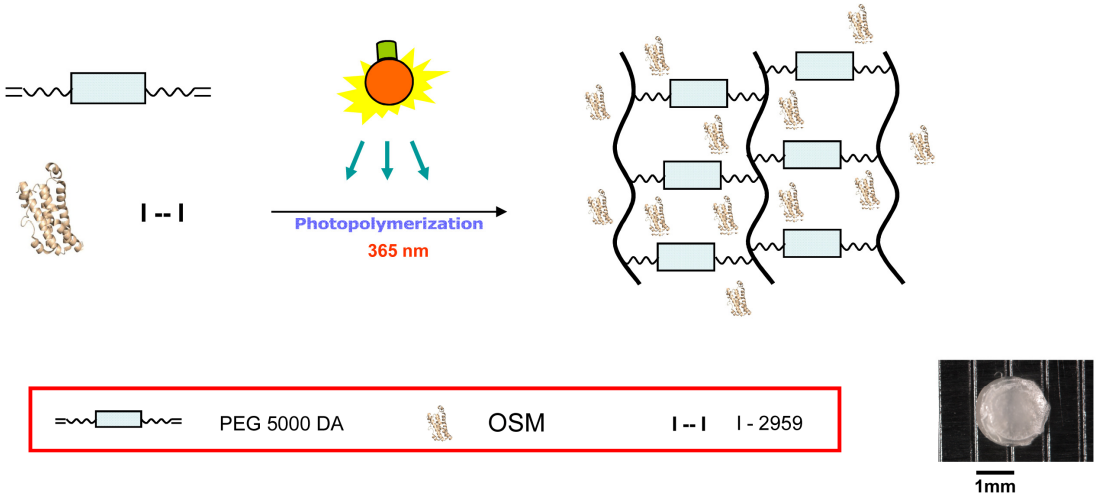


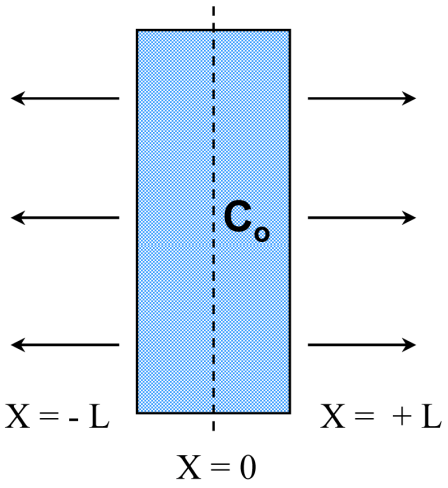
Figure 2.7 Schematic representation of photopolymerization.
(PEG 5000 DA – Diacrylated PEG with an average molecular weight of 5000 Da; OSM –Oncostatin M; I--I 2959 – commercial photoinitiator used to trigger the polymerization reaction). Also shown in the inset at right hand corner is the picture of a hydrogel obtained after polymerization and drying under vacuum overnight.

2.16. Theoretical Estimation of Drug Release

A disc shaped non-degradable hydrogel with high aspect ratio was considered for all the experiments and the drug was assumed to be dispersed homogeneously throughout the gel (Figure 2.8). Three boundary conditions were used to solve the model: (i) concentration of diffusible species (i.e. free drug) at the gel boundary (x = $\pm$ L) is zero (ii) concentration of the diffusible species inside the hydrogel is homogenous and constant C_o at time t = 0 and (iii) diffusion is symmetric about the center of the gel (x = 0). A high aspect ratio leads to the valid assumption of unsteady state one-dimensional diffusion from either face of the gel according to Fick's second law as given by the equation:

$$\frac{\partial C}{\partial t} = D_g \frac{\partial^2 C}{\partial x^2}$$

C is the concentration of drug inside the gel at time t and position x, and D_g is the diffusion coefficient of the drug inside the swollen hydrogel. The hydrogel is non-degradable and thus the structural properties of the hydrogel and thus diffusion coefficient of the drug will stay constant throughout the release process. However, if the network were to be degradable, both the mesh size (ξ) and the diffusivity of the drug in hydrogel (D_g) change with respect to time. Applying the above boundary conditions, one can solve the equation to obtain the concentration distribution of drug inside the hydrogel with respect time (t) and position (x). Also, using this information, the percent release of drug from the hydrogel with respect to time and the release rates were estimated.



Boundary Conditions

$C(\pm L, t)$	$= 0$		BC1
$C(x, 0)$	$= C_o$	$(-L < x < +L)$	BC2
$\left.\frac{\partial C}{\partial x}\right\|_{x=0}$	$= 0$		BC3

Figure 2.8 Schematic representation of a lateral section of circular disc uniformly dispersed with drug (shown in blue color) at a concentration C_o.

Boundary conditions are as described on the right side panel. Diffusion is symmetric about the central plane of the hydrogel i.e. x=0

2.17. Evaluation of Drug Release – *In vitro*

Immediately after photopolymerization, drug encapsulated hydrogels were weighed and then transferred to a 1 ml sink of 50 mM phosphate buffered saline. The saline along with hydrogel is continuously shaken throughout the experiment to maintain the boundary conditions. 10 μl samples of the supernatant solution were taken out at regular intervals and replaced with 10 μl of fresh PBS. Samples taken out were assayed for protein concentration using BCA assay and the resulting values were used to calculate the total amount of drug released from the hydrogel until that time point.

2.18. Evaluation of Drug Release – *In Vivo*

After polymerization, the drug encapsulated hydrogels are maintained under vacuum over night until they are completely dry and solid. Normal BALB/cJ mice were deeply anesthetized with a single intraperitoneal injection of xylazine (7 mg/kg) and ketamine (40 mg/kg). A small 2 – 3 mm width incision is then made on the superior side of the conjunctival membrane. The dried hydrogel is then implanted sub-conjunctivally and slid to the posterior side of the eye (Figure 2.9). The mice were then placed back into their cages and maintained under normal cage room light conditions. At desired time points, the mice were euthanized with CO_2 and the eyes were enucleated immediately. Retinas were then harvested for analysis of STAT3 activation using Western blots.

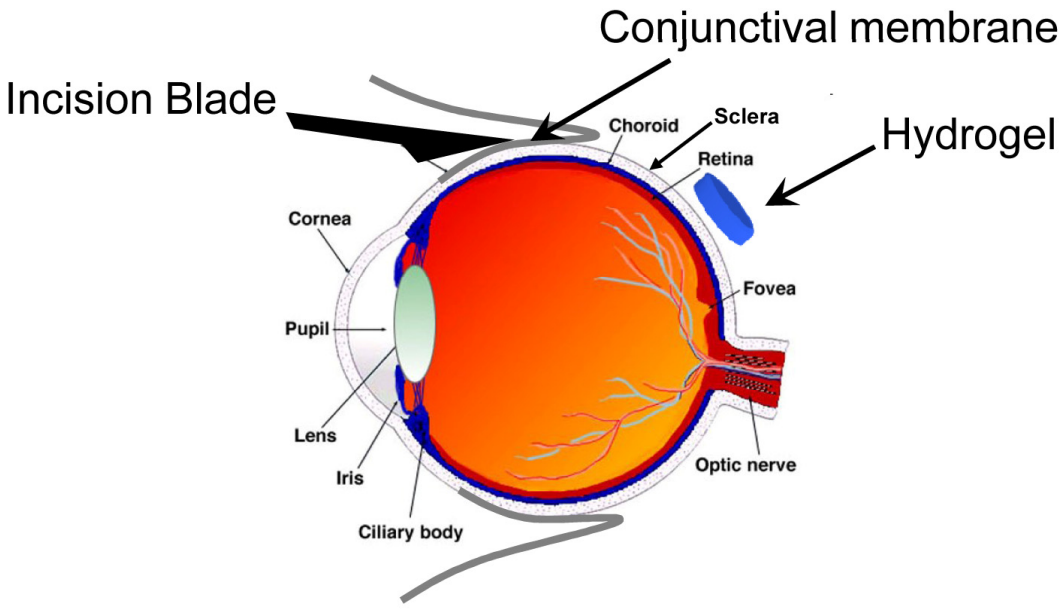


Figure 2.9 Schematic representation of sub-conjunctival hydrogel implantation in a mouse eye

[Modified and used with permission from: http://webvision.med.utah.edu/sretina.html]

2.19. Statistical Analysis

All statistical analyses are done using SigmaStat 3.10 (Systat Software, Inc. Richmond, CA). Results are expressed as mean ± standard deviation (SD). Differences between two groups were assessed using either paired or unpaired t-tests while differences between more than two groups were assessed using Analysis of Variance (ANOVA) followed by Holm-Sidak post hoc test. A p-value less than 0.05 was considered significant.

3. RESULTS AND DISCUSSION

3.1. Preconditioning-Induced Protection from Oxidative Injury is Mediated by Leukemia Inhibitory Factor Receptor (LIFR) and its Ligands in the Retina

3.1.1. Introduction

Photoreceptor cells are the sensory neurons in the eye that absorb light to initiate vision (See figure 3.1 for schematic representation of cells in retina). Since these cells are postmitotic, loss of photoreceptors results in permanent blindness. Insults that can kill photoreceptors include genetic mutations, mechanical injury and oxidative damage (146,295-297). Prolonged bright light exposure can also induce oxidative damage which, when severe, kills photoreceptors (298,299). However, under such unfavorable conditions, retinal cells initiate a response to rescue photoreceptors by recruiting or secreting a variety of antioxidants, cytokines and/or neurotrophic factors (153,298,300-303). This has been clearly demonstrated in models where exposure to subtoxic levels of stress (e.g., bright cyclic light) induced changes in retinal tissue that protect photoreceptors from a subsequent dose of lethal stress (151-153,298).

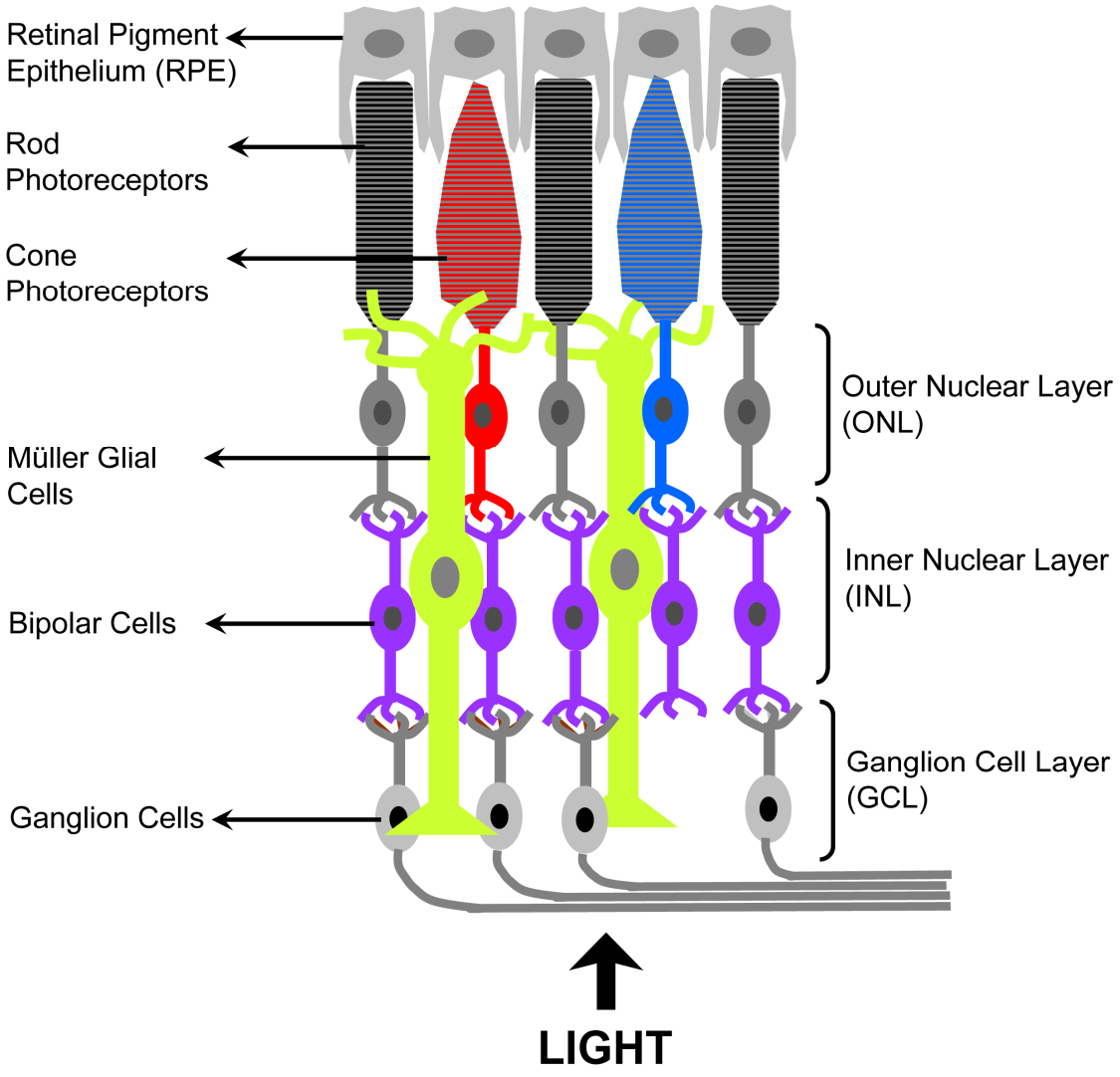


Figure 3.1 Schematic representation of cellular architecture in the retina

Factors that were shown to be upregulated under oxidative stress include basic fibroblast growth factor (bFGF), CNTF, brain derived neurotrophic factor (BDNF), LIF, and CLC (134,296,300,304). While these are hypothesized to play a role in preconditioning-induced endogenous neuroprotection, it has not yet been demonstrated which factors or receptors are essential for the protection. Intriguingly, among the upregulated molecules LIF, CNTF, and CLC belong to the same family and signal through heterodimerization of leukemia inhibitory factor receptor (LIFR) and glycoprotein 130 (gp130). Since these ligands and receptors are functional in the retina (149,302,305), our hypothesis is that activation of LIFR:gp130 complex plays an essential role in preconditioning-induced endogenous protection of retinal photoreceptors. This hypothesis predicts that inhibiting the activation of these receptors during stress would make the photoreceptor cells more susceptible to oxidative damage. LIF05, a mutant LIF molecule, antagonizes LIF, CNTF, CT-1 and CLC activities by competitively binding and blocking the LIFR dimerization with gp130 (48,294). In this study, we tested our hypothesis by delivering LIF05 during preconditioning. The data show that inhibiting LIFR activation blocks the protective effects of preconditioning, resulting in increased photoreceptor sensitivity to oxidative stress.

3.1.2. Results

3.1.2.1. Preconditioning-Induced Protection

Functional and morphological evaluation of photoreceptor cell protection by bright cyclic light preconditioning was carried out using ERG and quantitative histological analysis. BALB/cJ mice, with or without prior bright cyclic light preconditioning were subjected to severe light stress before returning them to room light conditions for 4 days of recovery followed by ERG and histological analysis. Figures. 3.2A and 3.2B show amplitudes of ERG a-waves in response to different intensities of light flashes. a-waves represent the electric response generated in photoreceptors and thus serve as a measure of photoreceptor function in response to light. As expected, mice that were exposed to severe light stress without preconditioning exhibited almost complete loss of photoreceptor function. However, mice that were preconditioned with bright cyclic light (600 lux; 6 AM to 6 PM for 6 days) prior to the severe light stress were able to retain almost 83% of their retinal function. Figures 3.2C and 3.2D show representative sections of the superior retina and quantitative analysis of photoreceptor numbers in the outer nuclear layer (ONL), respectively. As reflected in the ERG analysis, animals that were subjected to light stress without preconditioning exhibited severe photoreceptor degeneration. Compared to normal, undamaged retina that contain 10–11 rows of photoreceptor nuclei in the ONL, these animals retained only 1–2 rows of photoreceptor nuclei following bright light exposure.

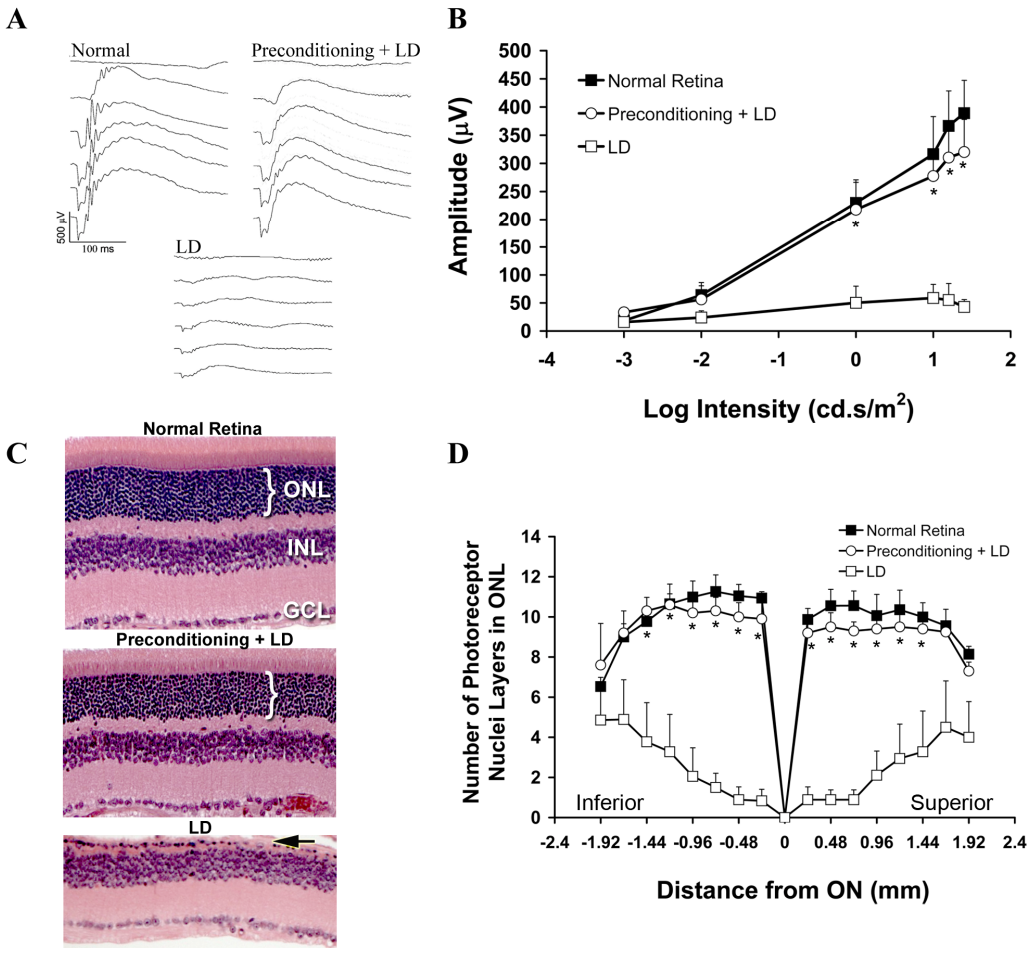


Figure 3.2 Functional and morphological evaluation of preconditioning-induced protection of retinal photoreceptors

A) Representative ERG traces and B) a-wave amplitudes of BALB/cJ mice that have been light damaged (LD) (4000 lux for 4 h) with (○) or without (□) prior bright cyclic light preconditioning (600 lux; 6 AM to 6 PM) for 6 days. Control eyes are represented in solid squares (■). n=6; value = mean ± SD. (*p<0.001, vs. LD eyes, paired t-test). C) Representative sections and D) quantification of number of rows of photoreceptor nuclei in the outer nuclear layer (ONL) along the vertical meridian of the retina. n=6; value = mean ± SD (*p<0.001, vs. LD eyes, paired t-test). ONL – Outer nuclear layer; INL – Inner nuclear layer; GCL – Ganglion cell layer; ON – Optic nerve. *[Experiments were performed in collaboration with Dr. Jiangang Wang]*

However, in animals that were subjected to bright cyclic light preconditioning, the degeneration was modest, as mice retained 9–10 rows of photoreceptor nuclei in spite of the severe light stress. These data demonstrate that preconditioning with sub-toxic light stress protects the retina from a subsequent dose of lethal light damage.

3.1.2.2. Expression of neuroprotective factors during preconditioning

Previous reports have shown that injury or stress in the retina can induce expression of neuroprotective factors (150,296,303,304,306,307). To determine which factors could be responsible for preconditioning-induced protection in our model, we measured gene expression changes of neuroprotective factors that include LIF, CNTF, OSM, CT-1, CLC and BDNF. Ribosomal protein RPL19 was used as control. Results show that LIF, OSM, CT-1 and CLC exhibit a strong upregulation (166, 74, 21 and 47-fold respectively) with bright cyclic light preconditioning in a time-dependent manner (Figure 3.3A). Surprisingly, unlike reported results in rats (153) we did not observe any upregulation of CNTF. BDNF, another neuroprotective factor, exhibited an 11-fold increase in its levels by the end of the 6th day of preconditioning. We then tested whether this strong upregulation of LIF, OSM, CT-1, CLC and BDNF is reflected at a functional level by measuring activation of a common downstream signaling molecule, STAT3. Results show a robust time-dependent activation of STAT3 with bright cyclic light preconditioning (Figures 3.3B and 3.3C). STAT3 reached peak activation by the

end of 4 days of preconditioning and remained elevated with 6 days of preconditioning. Activation of STAT3 could be mediated by LIFR:gp130 heterodimer (triggered by LIF, CT-1, CLC (21,22,308)), OSMR:gp130 heterodimer (triggered by OSM (309)) or the TrkB receptor (triggered by BDNF (310)). Therefore, we tested whether LIFR:gp130 activation is essential for preconditioning-induced STAT3 activation and protection.

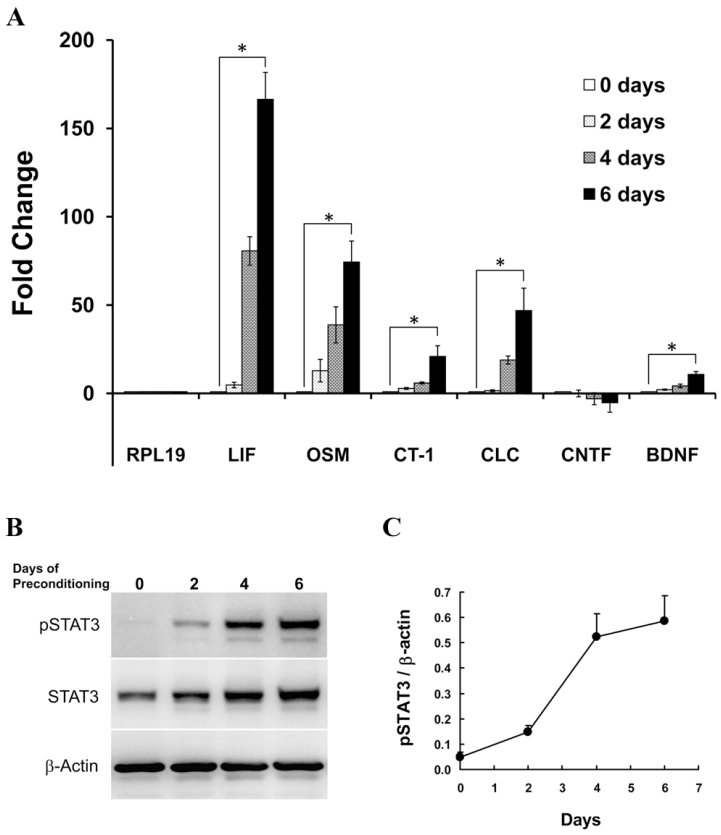


Figure 3.3 Preconditioning with bright cyclic light leads to strong upregulation of neuroprotective factors.

A) Time-dependent quantitative evaluation of cytokine mRNA upregulation using real time RT-PCR in response to bright cyclic light preconditioning (600lux; 6AM to 6PM). Members of IL-6 family cytokines (LIF, OSM, CT-1 and CLC) are upregulated 166, 74, 21 and 47 fold in response to bright cyclic light preconditioning. While CNTF did not exhibit a similar upregulation, BDNF exhibited an 11-fold increase in its mRNA levels by the end of the 6th day of preconditioning. Ribosomal protein RPL19 served as a control. n=4; value = mean ± SD. (*$p<0.01$, paired t-test). B) Representative Western blots and C) quantification of STAT3 activation. n=3; value = mean ± SD. We observed a robust preconditioning-dependent STAT3 activation which reached peak activation by the end of 4 days of preconditioning and remained elevated throughout the preconditioning exposure. *[Experiments were performed in collaboration with Dr. Jiangang Wang]*

3.1.2.3. Antagonism of LIFR attenuates preconditioning-induced STAT3 activation

hLIF has two active sites, site II and site III that bind to gp130 and LIFR respectively (21,22,48,64,311,312). LIF first binds LIFR and then recruits gp130 forming a high affinity heterodimer complex (21,23). This heterodimerization leads to the activation of Jak mediated STAT3 pathway (13,14,313,314). Hudson et al. (48,294) have mutated the gp130 binding sites on hLIF generating the antagonist LIF05, which binds LIFR but can no longer bind gp130 to activate the STAT3 pathway. It thus acts as a competitive inhibitor for all cytokines that recruit LIFR. If injected *in vivo*, LIF05 is predicted to block the activities of LIFR activating cytokines LIF, CNTF, CT-1 and CLC. Unlike in humans, mOSM can signal only through OSMR:gp130 (type II receptor complex) but not LIFR:gp130 (type I receptor complex) (23,309). Thus, LIF05 cannot antagonize OSM activities in mice. To determine whether LIFR activation was responsible for preconditioning-induced STAT3 activation we injected 2, 5 or 8 µg of LIF05 into the right eyes of mice after 2 days of preconditioning while left eyes were injected with PBS to serve as controls. Following injection, mice were preconditioned 4 additional days in bright cyclic light. After a total of 6 days of preconditioning, STAT3 activation was measured using Western blot analysis. Figure 3.4 shows that 2 µg of LIF05 was able to inhibit 45% of the preconditioning-induced STAT3 activation while 5 µg and 8 µg of LIF05 were able to block the activation by about 60% and 70%, respectively. This clearly demonstrates that LIF05 is able to inhibit the preconditioning-induced STAT3 activation in a dose-dependent manner by

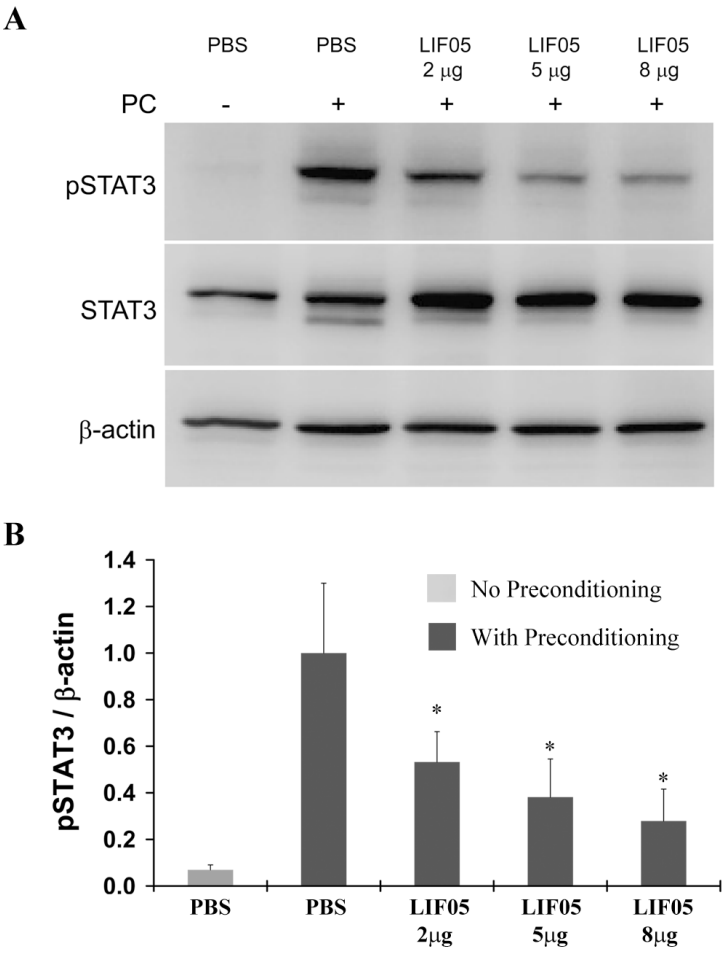


Figure 3.4 LIF05 inhibited preconditioning-induced STAT3 activation.

A) After 2 days of bright cyclic light preconditioning (600lux; 6Am to 6PM), mice were injected with PBS in the left eye (control) and LIF05 (2μg, 5μg or 8μg) in the right eye and returned to their cages for additional bright cyclic light preconditioning. After the 6th day of preconditioning, retinas were harvested and STAT3 activation was analyzed using Western blotting. PBS injected eyes without preconditioning served as controls for basal levels of STAT3 activation. PC – Preconditioning. B) Bands were quantified by conventional digital image analysis using a KODAK Image Station 4000R. n=3; value = mean ± SD. (*$p<0.05$, vs. PBS injected eyes with preconditioning, one way ANOVA and *post hoc* Holm-Sidak test for multiple comparisons) *[Experiments were performed in collaboration with Dr. Jiangang Wang]*

antagonizing LIFR activation. Injection of 12 µg LIF05 did not further decrease the STAT3 activation compared to 8 µg LIF05. This residual activation could be due to other factors including OSM and BDNF which LIF05 cannot antagonize. Clearly LIFR activation is playing an essential role in preconditioning-induced STAT3 phosphorylation. Surprisingly, preconditioning also induced a 2-fold increase in total STAT3 levels (Figure 3.3B). This increase was not reduced by LIF05 (Figure 3.4) suggesting that the increase in total STAT3 is a result of activation of pathways independent of LIFR such as OSMR or TrkB.

3.1.2.4. Antagonism of LIFR blocks preconditioning-induced protection

In order to assess the role of LIFR in preconditioning-induced protection, we injected LIF05 during bright cyclic light preconditioning and determined whether blocking LIFR abolishes the preconditioning-induced protection. After 2 days of preconditioning, PBS or LIF05 (8 µg) were injected intravitreally and the mice were returned to their cages for additional bright cyclic light preconditioning. After the 6th day of preconditioning (i.e., 4 days after injection), animals were subjected to severe light stress (4000 lux for 4 h; 6 PM to 10 PM) immediately after the bright light adaptation and allowed to recover from the stress for 4 days under normal cage room light conditions (60 lux; 6 AM to 6 PM). Following recovery, animals were subjected to functional analysis using ERG and the eyes were harvested immediately for quantitative histological analysis. Figures 3.5A and 3.5B show that LIF05 injection reduced preconditioning-induced preservation

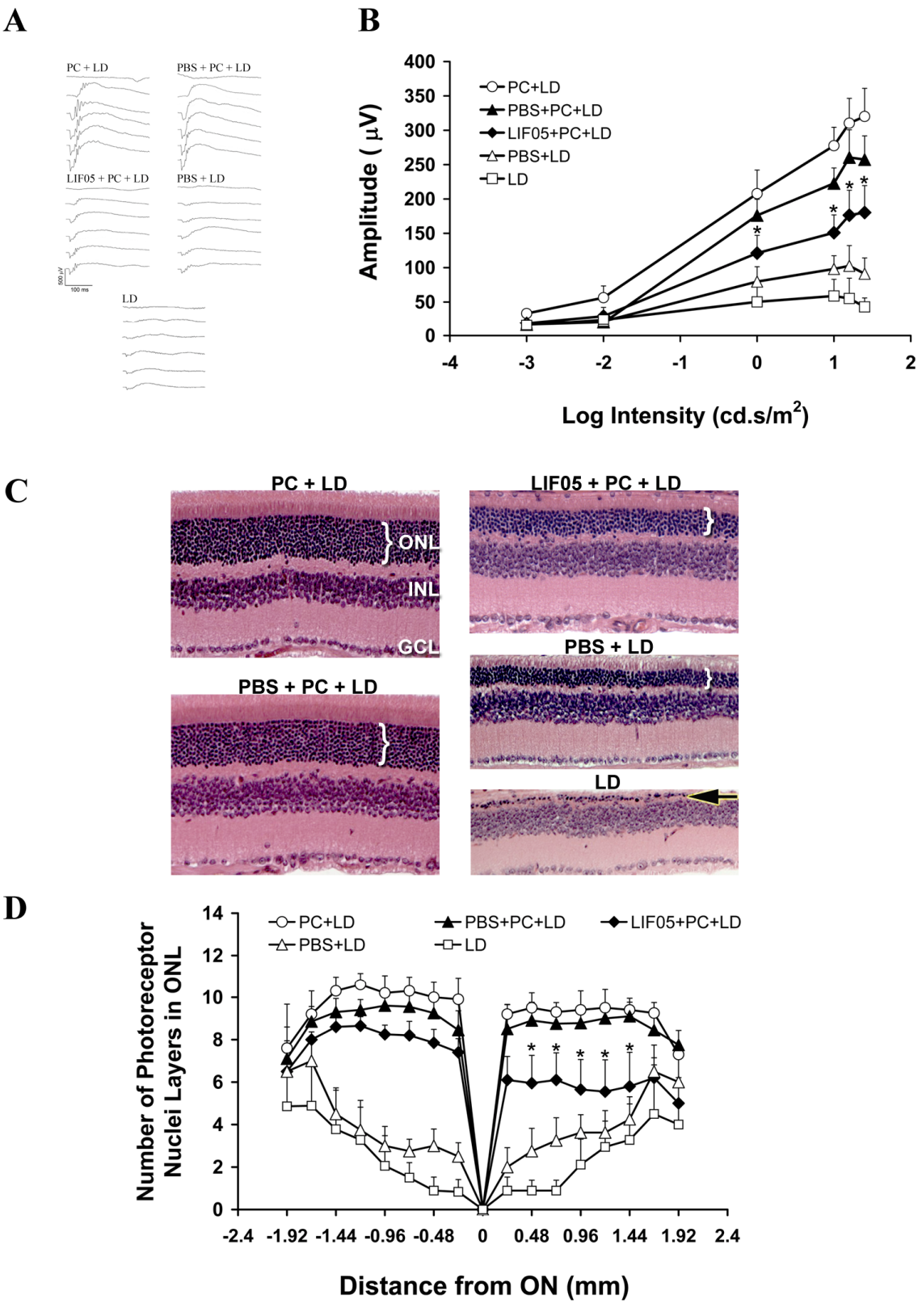

A
PC + LD
PBS + PC + LD
LIF05 + PC + LD
PBS + LD
LD
B
Amplitude (μV)
Log Intensity (cd.s/m2)
PC+LD
PBS+PC+LD
LIF05+PC+LD
PBS+LD
LD
C
PC + LD
ONL
INL
GCL
LIF05 + PC + LD
PBS + LD
PBS + PC + LD
LD
D
Number of Photoreceptor Nuclei Layers in ONL
Distance from ON (mm)

Figure 3.5 LIF05 inhibited preconditioning-induced protection of retinal photoreceptors.

A) Representative ERG traces and B) quantification of a-wave amplitudes of BALB/cJ mice that are light damaged (LD) (4000lux for 4h) with (○,▲,♦) or without (Δ, □) prior bright cyclic light preconditioning (600lux; 6AM to 6PM for 6 days). Compared to uninjected eyes with preconditioning (○), LIF05 injected eyes lost 44% at the brightest flash intensity. n=6; value = mean ± SD (*p<0.05, vs. PC+LD eyes, paired t-test). C) Representative sections from superior retina and D) quantification of the number of rows of photoreceptor nuclei in the outer nuclear layer (ONL) along the vertical meridian of the retina. n=6; value = mean ± SD (*p<0.05, vs. PC+LD eyes, paired t-test). ONL – Outer nuclear layer; INL – Inner nuclear layer; GCL – Ganglion cell layer; ON – Optic nerve. *[Experiments were performed in collaboration with Dr. Jiangang Wang]*

of the retinal function by 44% (compared at the brightest flash intensity, LIF05+PC+LD vs. PC+LD). This decrease in retinal function is caused by reduced protection of photoreceptors in the presence of LIF05 since we observe a significant increase in photoreceptor cell loss following light stress in LIF05 injected eyes (Figures 3.5C and 3.5D, 10 layers in PC+LD vs. 6 layers in LIF05+PC+LD). While PBS injection caused a slight decrease in the retinal function (Figures 3.5A and 3.5B), it did not lead to a significant decrease in photoreceptor survival (Figures 3.5C and 3.5D). The mechanism for the loss of function in PBS injected eyes without a loss in photoreceptor cells is currently unknown, but similar results have been observed in the absence of light stress where PBS injection causes a transient reduction in retinal function without causing any cell death. As expected, PBS injected control eyes that were subjected to light damage without preconditioning (PBS+LD), exhibited dramatic loss in retinal function and the photoreceptors, but was slightly protective compared to non-injected light damaged eyes (LD). Together, these results clearly suggest that blocking LIFR activation during preconditioning attenuates the endogenous protective mechanism triggered by bright cyclic light preconditioning.

3.1.2.5. Effect of LIF05 on normal retinal function

In order to rule out the possibility that injection of LIF05 itself kills photoreceptors, we injected 8 µg of LIF05 intravitreally into a normal BALB/cJ mice and

measured the retinal function and morphology using ERG and histological analysis 8 days after injection. LIF05 did not induce any change in retinal function or morphology compared to PBS control (Figures 3.6A and 3.6B). This suggests that LIF05 had no toxic effects on retinal function and morphology up to dosages of 8 μg.

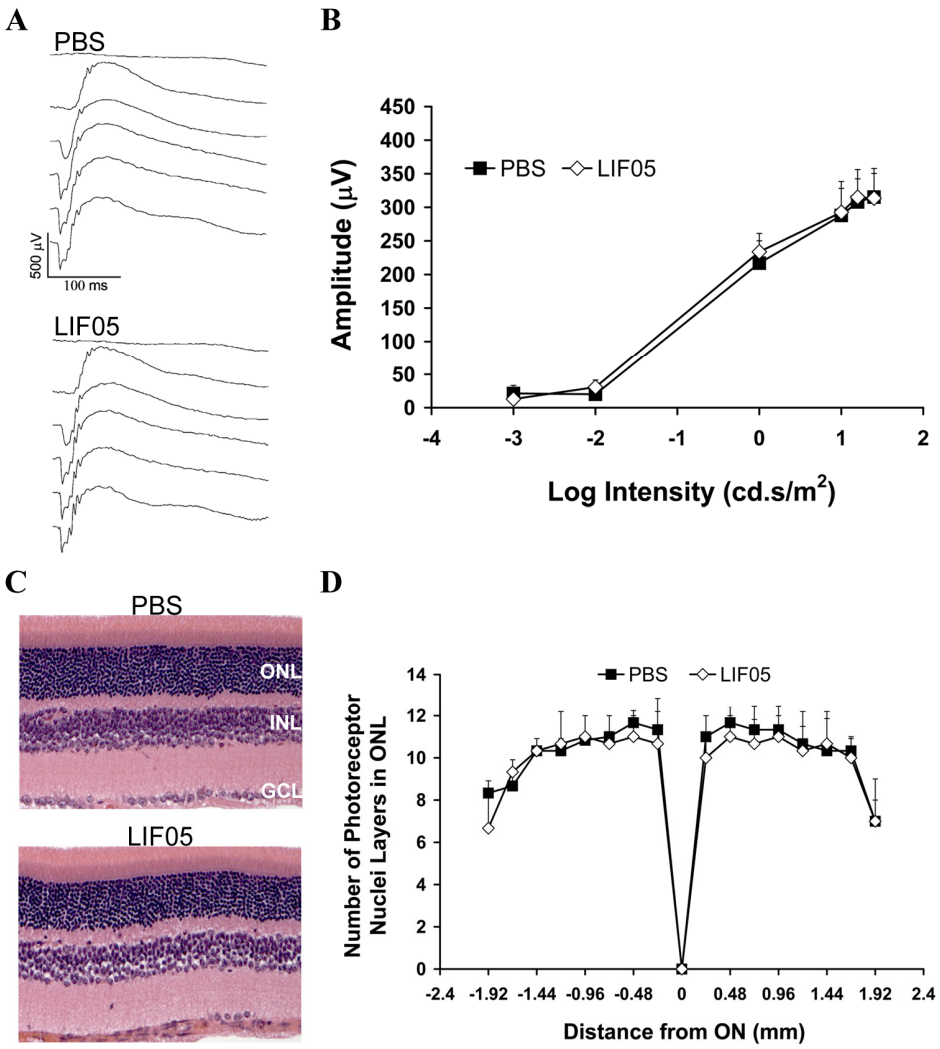


Figure 3.6 Evaluation of LIF05 toxicity towards retinal function and morphology A) Representative ERG traces and B) quantification of a-wave amplitudes of BALB/cJ mice 8 days after injection with PBS (■) or LIF05 (◊). C) Representative sections from superior retina and D) quantification of the number of rows of photoreceptor nuclei in the outer nuclear layer (ONL). n=3, value = mean ± SD. ONL – Outer nuclear layer; INL – Inner nuclear layer; GCL – Ganglion cell layer; ON – Optic nerve. *[Experiments were performed in collaboration with Dr. Jiangang Wang]*

3.1.2.6. LIF05 inhibits LIF induced STAT3 activation

To demonstrate that LIF05 functions as an antagonist specifically against LIFR ligands, we intravitreally injected 0.1 µg of LIF, a quantity that was previously shown to activate STAT3 in the retina (149), with or without the antagonist LIF05. PBS injected eyes served as negative controls. Two days after injection, we measured the levels of STAT3 activation using Western blot analysis. While 2 µg of LIF05 was able to inhibit 50% of the LIF induced STAT3 activation 5 µg and 8 µg of LIF05 were able to inhibit STAT3 activation by 60% and 90% respectively (Figure 3.7). This clearly demonstrated that LIF05 inhibits LIFR activation by agonists in vivo in a dose-dependent manner. However, significantly larger amounts of LIF05 were needed (8µg) to effectively antagonize smaller doses of LIF (0.1 µg). To determine why such large quantities of antagonist are needed, we performed receptor binding assays using surface plasmon resonance (SPR).

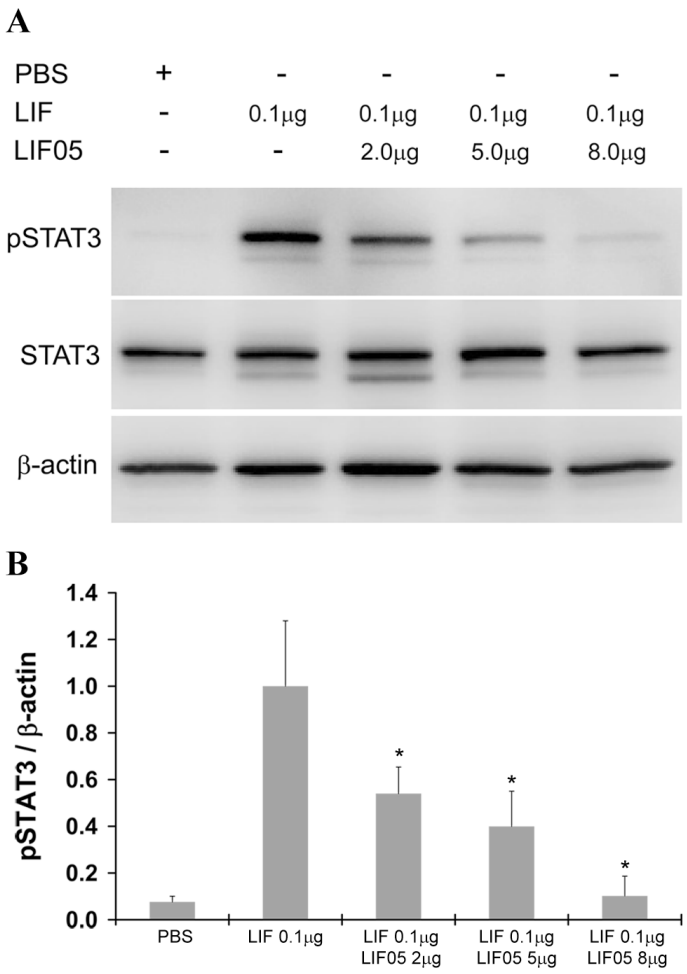


Figure 3.7 LIF05 inhibits LIF stimulated STAT3 activation *in vivo*.

A) 0.1 μg of LIF was injected intravitreally with 0, 2, 5, or 8 μg of the antagonist LIF05. After 2 days of injection, retinas were harvested and STAT3 activation levels were analyzed using Western blot analysis. Staining for total STAT3 and β-actin served as loading controls. A) Bands were quantified by conventional digital image analysis using a KODAK Image Station 4000R. n=3; value = mean ± SD (*$p<0.05$, vs. LIF only injected eyes (LIF 0.1 μg), one way ANOVA and *post hoc* Holm-Sidak test for multiple comparisons). *[Experiments were performed in collaboration with Dr. Jiangang Wang].*

3.1.2.7. LIF forms a high affinity stable complex with LIFR and gp130

Figures 3.8A and 3.8B show the SPR analysis of LIFR interaction towards LIF and LIF05. Recombinant soluble LIFR and gp130 were injected over immobilized GST-LIF or GST-LIF05 to determine the kinetic rate constants for association and dissociation. Results show that both LIF and LIF05 display high affinity towards LIFR, exhibiting fast association and dissociation rates yielding an equilibrium dissociation constant (K_D) of 2.93nM and 4.72nM respectively (See Table 3.1). Also, LIF displays a weaker affinity towards gp130 exhibiting a slow association and fast dissociation from gp130 compared to LIFR yielding an equilibrium dissociation constant of 74.57nM (See Table 3.1). Because of its mutations, as expected, LIF05 did not exhibit any affinity towards gp130 (Figure 3.8D; Table 3.1).

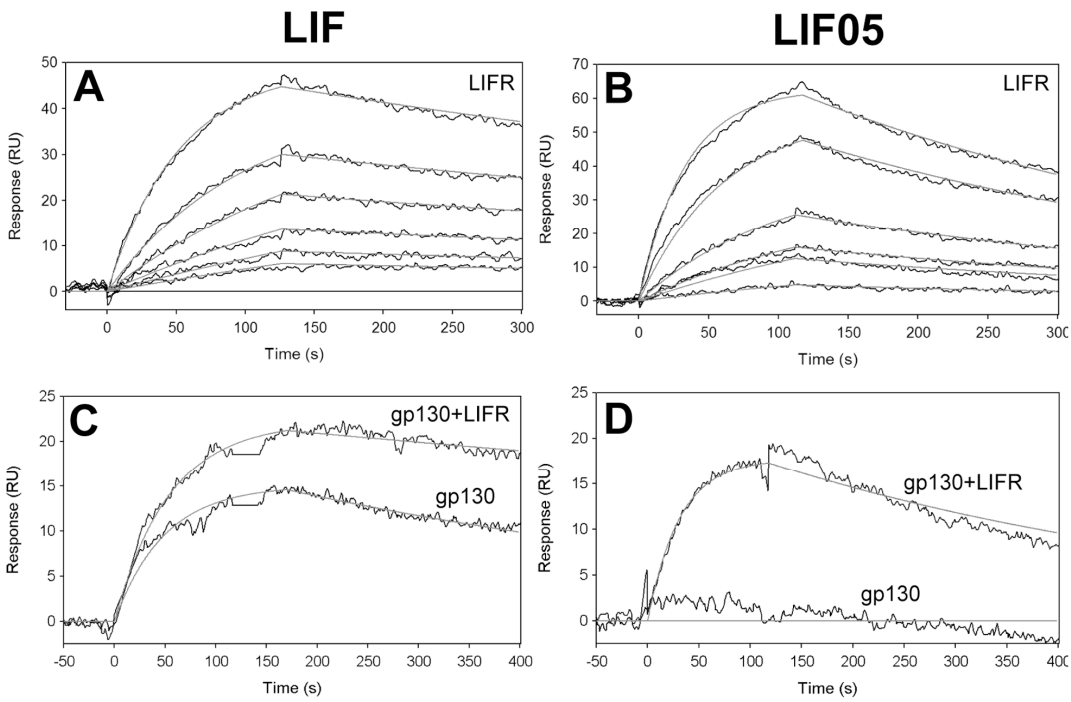


Figure 3.8 Kinetic analysis of LIFR and gp130 interaction towards LIF and LIF05 Soluble LIFR at concentrations of 1.5 nM, 3 nM, 6.25 nM, 12.5 nM, 25 nM or 50 nM were injected over an SPR sensor chip with anti-GST immobilized A) GST-LIF or B) GST-LIF05 at flow rates of 25 μl/min. Responses obtained were corrected for background signal using a control flow cell. Association and dissociation rates are derived by global analysis of the response curves fit to a 1:1 kinetic model using QDat software (BioLogic Software, Ltd. Knoxville TN and Nomadics, Inc. Stillwater, OK) using 1:1 stoichiometry. Models are indicated in smooth gray line overlaid over response curve traces. Soluble gp130 (100 nM) was injected over C) GST-LIF or D) GST-LIF05 either as a mixture with soluble LIFR (10 nM) or separately at flow rates of 25 μl/min. *[Experiments were performed with assistance from ICX Technologies, Oklahoma City, OK]*

Table 3.1 Comparison of association (k_a), dissociation (k_d) and estimated equilibrium dissociation (K_D) constants for LIFR and gp130 binding to LIF and LIF05.

	LIFR (analyte)			gp130 (analyte)		
	k_a ($M^{-1}s^{-1}$)	k_d (s^{-1})	K_D (nM)	k_a ($M^{-1}s^{-1}$)	k_d (s^{-1})	K_D (nM)
LIF	3.66×10^5	1.07×10^{-3}	2.93	0.72×10^5	5.37×10^{-3}	74.57
LIF05	5.62×10^5	2.65×10^{-3}	4.72	ND	ND	ND

3.1.3. Discussion

Previous work and our results show that preconditioning with moderate light stress protects retinal photoreceptors from a subsequent exposure to damaging light (151-153,298). However, the mechanism for this inducible protection is far from fully understood. Previous studies have shown that exposure to light stress results in a strong upregulation of CNTF, bFGF (in rats), LIF and CLC (in mice) (153,304). Separate studies have also shown that injection of these factors (CNTF, LIF or bFGF) in the absence of preconditioning can also protect photoreceptors from light damage (148,149,296) suggesting that their upregulation during stress is functionally connected to protection. In addition, other reports in rats have shown that photoreceptors near sites of mechanical injury are protected from a subsequent light stress. This protection was again accompanied by increases in the levels of bFGF and CNTF at the site of injury (301,303,306). These findings clearly indicate that the retina has a self defense mechanism that helps it cope with unfavorable changes in the retinal tissue environment. However, the multiple factors that are upregulated can activate a variety of receptors and signaling pathways. It is thus far not clear, which of these pathways are primarily involved in the endogenous protective mechanism.

In our experiments with the bright cyclic light preconditioning model, we observed a strong upregulation of neuroprotective factors LIF, OSM, CT-1 and CLC which recruit either LIFR:gp130 or OSMR:gp130 complex for signaling. However, unlike

in rats, we did not notice any similar upregulation of CNTF in mice in response to bright cyclic light preconditioning. A similar observation was made by Samardzija et al. (304). This difference in the type of neuroprotective factors that regulate endogenous protection is probably attributed to species differences. Intriguingly LIF, CNTF, OSM, CT-1, and CLC, all belong to the same IL-6 family of cytokines that utilize gp130 receptor complexes to elicit similar and overlapping physiological responses mediated by STAT3 activation (13,14). So, the final neuroprotective responses in both mice and rats could be very similar. Also, we observed a modest increase in another neuroprotective factor, BDNF which signals via TrkB receptors. The robust activation of STAT3 in a preconditioning-dependent manner suggests that these expressed cytokines (LIF, OSM, CT-1 and CLC) are functional and activating the signal transducing receptor gp130 leading to STAT3 phosphorylation. We thus hypothesized that activation of LIFR:gp130 complex plays an essential role in preconditioning-induced protection of retinal photoreceptors.

In mice LIF, CNTF, CT-1 and CLC bind to LIFR and gp130 to induce signaling while OSM utilizes OSMR and gp130. Blocking LIFR activation during preconditioning significantly attenuated induced STAT3 activation and protection of photoreceptor cells in the retina. These results confirm that LIFR is a vital part and plays an essential role in the endogenous protective mechanism inside the retina leading to photoreceptor survival and that the protection is likely mediated by its ligands LIF, CT-1 or CLC. In agreement with our observations, Joly et al.,

(150) have recently shown that LIF knockout mice have accelerated photoreceptor degeneration in a mouse model of inherited autosomal dominant retinitis pigmentosa. Together, these results demonstrate an important role for LIFR in an endogenous protective mechanism. Our previous observations that intravitreal LIF injections can lead to signal transduction in photoreceptors demonstrates that LIF can penetrate retinal cell layers to directly activate LIFR/gp130 complexes on photoreceptors (149). The formation of a stable complex between LIF, LIFR and gp130, and persistent robust signal transduction suggests that this would make an effective ligand–receptor system for induction of long-term protection from a chronic stress.

Finally, the observation that LIF05 did not induce photoreceptor cell death under normal conditions (Figure 3.6) together with the evidence that there is no STAT3 activation at such conditions (Figures 3.3B and 3.3C, 0 days) suggests that LIFR is not active and its activation is not required for the survival of photoreceptors at physiological conditions. It is only under stressed conditions that this receptor is activated and leads to photoreceptor survival via STAT3 mediated survival pathways (315). Endogenous inducibility, cooperative binding and prolonged signaling of the LIF receptor system thus makes it ideally suited for long-term protection.

3.2. A Unique Loop Structure in Oncostatin M Reduces Binding Affinity Towards Oncostatin M Receptor and Leukemia Inhibitory Factor Receptor

3.2.1. Introduction

IL-6 family cytokines (IL-6, IL-11, LIF, OSM, CNTF, CT-1 and CLC) possess a typical "four-α-helix bundle" like structure and act on their target cells by forming a multimeric receptor complex which includes the common receptor gp130 (13). Extensive mutagenesis studies revealed that these cytokines interact with the receptor-chains through three distinct binding sites referred to as sites I, II and III (316,317). Cytokines requiring a co-receptor chain (IL-6, IL-11, CNTF, and CT-1) first bind to the co-receptor (IL-6R, IL-11R, or CNTFR) through the binding site I (19,28-30,49). The glycoprotein gp130 always interacts through binding site II and, depending on the cytokine, the third binding site (site III) is used for recruitment of LIFR, OSMR or a second gp130 molecule (18,21,23,26,27,50). Research has shown that a conserved 'FXXK' motif at the core of site III is essential for all LIFR binding proteins for their interaction with LIFR (4,47,48). After recruiting the required receptors, these cytokines signal via activation of Jak/STAT (janus kinase/signal transducer and activator of transcription) and MAPK (mitogen activated protein kinase) pathways (52,313,318,319).

Among its family members, OSM resembles LIF most closely both in structure and function (320). The gene encoding for OSM, located on human chromosome 22q12, is only 20 kb away from LIF suggesting that these two genes evolved by gene duplication (320-323). In spite of the striking similarities, OSM differs from LIF in its receptor binding. While LIF first binds to leukemia inhibitory factor receptor (LIFR) and then recruits glycoprotein 130 (gp130) for its signal transduction (5,21,23,48), OSM first binds gp130 and then recruits LIFR (4,5,21,23,48,50,309,324). In addition, OSM can bind to gp130 and then recruit a unique receptor named Oncostatin M receptor (OSMR) forming a distinct signaling complex (23,50,309). Our aim was to identify the structural features on OSM that result in its unique ability to bind OSMR and the features that result in its higher affinity towards gp130 than towards LIFR or OSMR. Based on the structural alignments, we have identified a helical loop on OSM between its B and C helices that is unique to OSM and not found on LIF or any other IL-6 family cytokine (Figure 3.9). Using wild type and mutant OSM molecules that have shortened BC loops we show that the loop appears to present a steric hindrance for LIFR and OSMR, thus lowering the affinity for either receptor. Cytokines with deletions in the BC loop were able to activate LIFR:gp130 and OSMR:gp130 receptor complexes at 3 fold lower concentrations than the native OSM. Kinetic analysis of the ligand-receptor interactions show that improved activation is a consequence of increased affinity for the LIFR without altering the affinity for gp130. Together, these results suggest that the BC loop modulates OSM's affinity towards LIFR by presenting a steric hindrance for their interaction. Our

studies also indicate that the BC loop does not play a role in OSM's unique ability to bind OSMR.

3.2.2. Results

3.2.2.1. Structural analysis of hLIF and hOSM: Identification of the BC loop.

To determine the structural differences that might account for receptor specificity, we aligned the crystal structures of hOSM (PDB ID: 1EVS) onto hLIF (PDB ID: 1EMR) based on the trace of α-carbons using Delano Scientific's PyMol molecular viewer (http://pymol.org) (Figure 3.9). The alignment of the backbone structures fit well with a relatively low RMSD value of 4.342. The active sites II and III on both molecules exhibited good conservation in structural orientation. Previous reports showed that the FXXK motif is essential for OSM's interaction with both LIFR and OSMR (4,325). In spite of having a similar FXXK motif, other LIFR interacting cytokines LIF, CNTF, CT-1 and CLC however cannot activate OSMR (5). This suggested that the difference in receptor specificity between hOSM and other LIFR activating cytokines is the result of structural differences between these ligands in the vicinity of the core FXXK motif (4). One of the obvious structural differences in the alignments is the presence of an additional helical loop between its B and C helices in OSM that is not present in LIF (Figure 3.9). This BC loop is positioned in close proximity to the FXXK motif in active site III. Based on the crystal structures solved for LIF in complex with LIFR (PDB ID: 2Q7N) or gp130 (PDB ID: 1PVH), we have generated a model for the trimeric

complex of LIF:LIFR:gp130 using PyMol (Figure 3.9D). When OSM was superimposed over LIF in this trimeric model, the BC loop on OSM again stands out as a unique motif at the receptor binding interface of OSM. This suggested that the BC loop is possibly playing an essential role in recognizing OSMR.

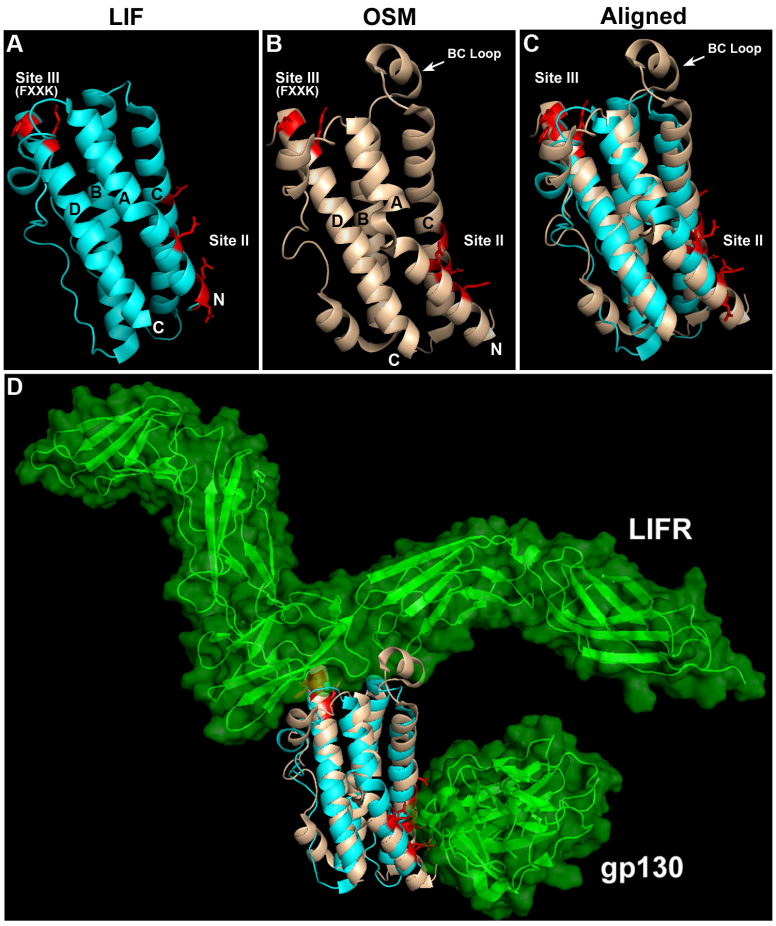


Figure 3.9 A, B) Crystal structures of LIF (PDB: 1EMR) and OSM (PDB: 1EVS) with their active sites and helices A, B, C and D identified.

Both structures have an “up-up-down-down” topology with the N-terminus and C-terminus indicated. Also identified is the helical loop on OSM between its B and C helices. C) Shown on right is the alignment of OSM structure onto LIF based on the α-carbon trace; RMSD = 4.342. While the overall structures and the active site orientation on LIF and OSM show remarkable conservation, the BC loop on OSM clearly projects out as a unique feature on OSM. This loop lies in close proximity to the active site III containing “FXXK” motif. D) Also shown on the bottom panel is the three dimensional model for LIF in complex with LIFR and gp130 in presence of OSM overlaid on LIF. Again, the BC loop on OSM clearly projects out into the space of LIFR suggesting a possible role for the loop in OSM’s unique ability to recognize OSMR.

To test this hypothesis, we generated substitution mutations in OSM that either remove or shorten the length of this BC loop. Wild type OSM contains 12 amino acids in the BC loop region. Using site directed mutagenesis, we have deleted or modified the amino acids in this region to generate OSM molecules that contained 7, 4 or 0 amino acids. Shown in figure 3.10 are the sequences of mutant OSM molecules with truncated BC loops (OSM-M1, OSM-M2 and OSM-M3) in comparison to the wild-type* OSM (OSM-WT*). Glycines (G) were incorporated into OSM-M1 and OSM-M2 to induce flexibility into the loop region thus minimizing the impact of this BC loop modification on the overall structure of OSM. In OSM-M1, the proline (P) was introduced to bend the loop back towards helix C and the alanine (A) served as a linker. OSM-WT*, OSM-M1 and OSM-M2 were expressed at high levels in bacteria but not OSM-M3 suggesting that complete removal of the BC loop from OSM leads to instability in the overall structure of the protein (Figure 3.10).

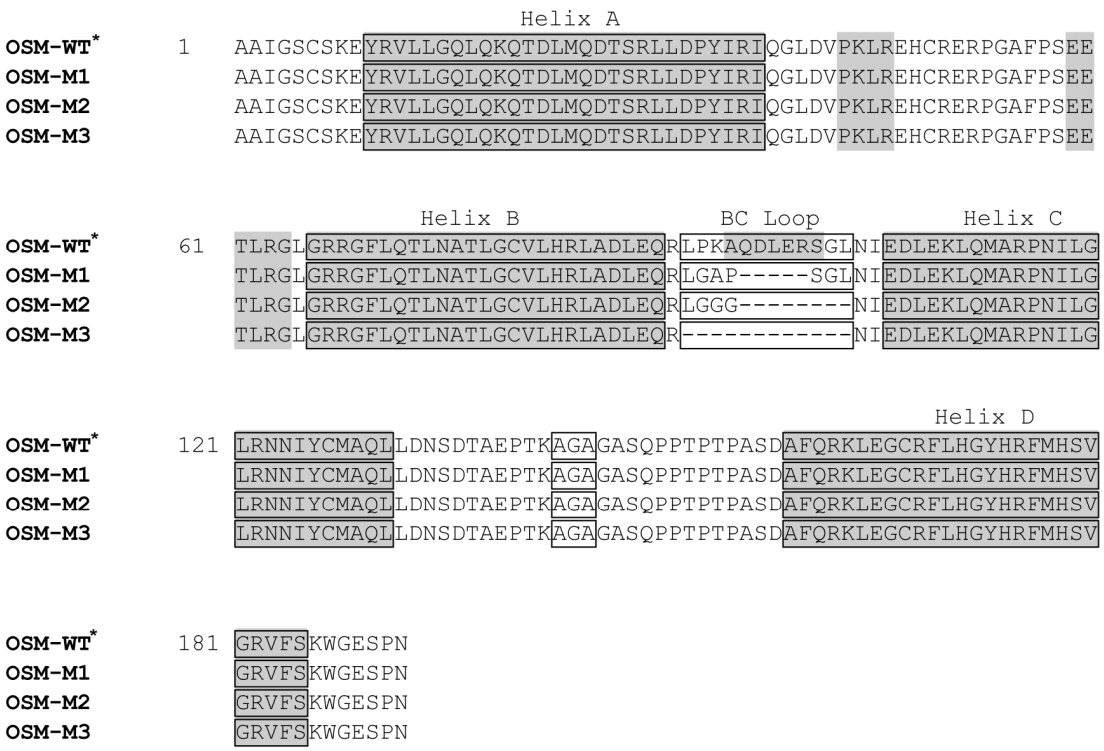


Figure 3.10 Amino acid sequences of wild type OSM and the mutant variants of OSM with truncated BC loops

Shown in gray are the α-helices present in the secondary structure of OSM as identified in the crystal structure (PDB: 1EVS). Each of the helices A, B, C and D are identified along with the BC loop region. Also highlighted in open box is the mutated thrombin cleavage site “AGA”.

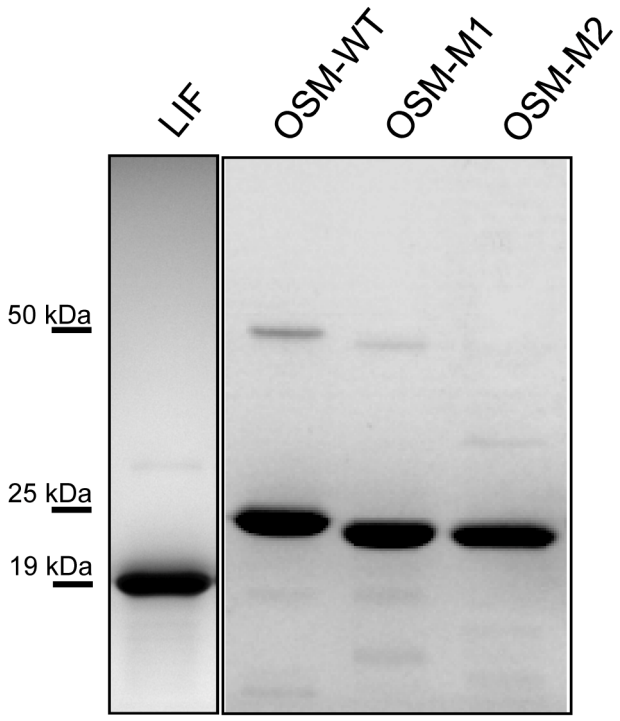


Figure 3.11 SDS-PAGE analysis of purified proteins

8 μg of purified protein is loaded into each lane.

3.2.2.2. Structural characterization of OSM-M1 and OSM-M2

Minor alterations in the size and composition of BC loop could potentially induce a global change in the overall structure of OSM. To determine whether the modified proteins (OSM-M1 and OSM-M2) still retained native alpha helical content we analyzed the recombinant proteins using circular dichroism (CD). Figure 3.12 shows the molar ellipticity [θ] plotted against the wavelength for LIF, OSM-WT*, OSM-M1 and OSM-M2. All molecules displayed similar absorption behavior. Analysis using the software programs SELCON3, CONTINLL and CDSSTR revealed that both LIF and OSM-WT* have approximately 60% alpha helical content with the remaining primarily being loop regions. This is in good agreement with the crystal structures available for LIF and OSM. Analysis also showed that both OSM-M1 and OSM-M2 have similar 60% alpha helical content with the remaining being loop regions. These results suggest that shortening the length of BC loop in OSM from 12 amino acids to 7 or 4 amino acids did not induce a significant global change in the overall secondary structure of OSM.

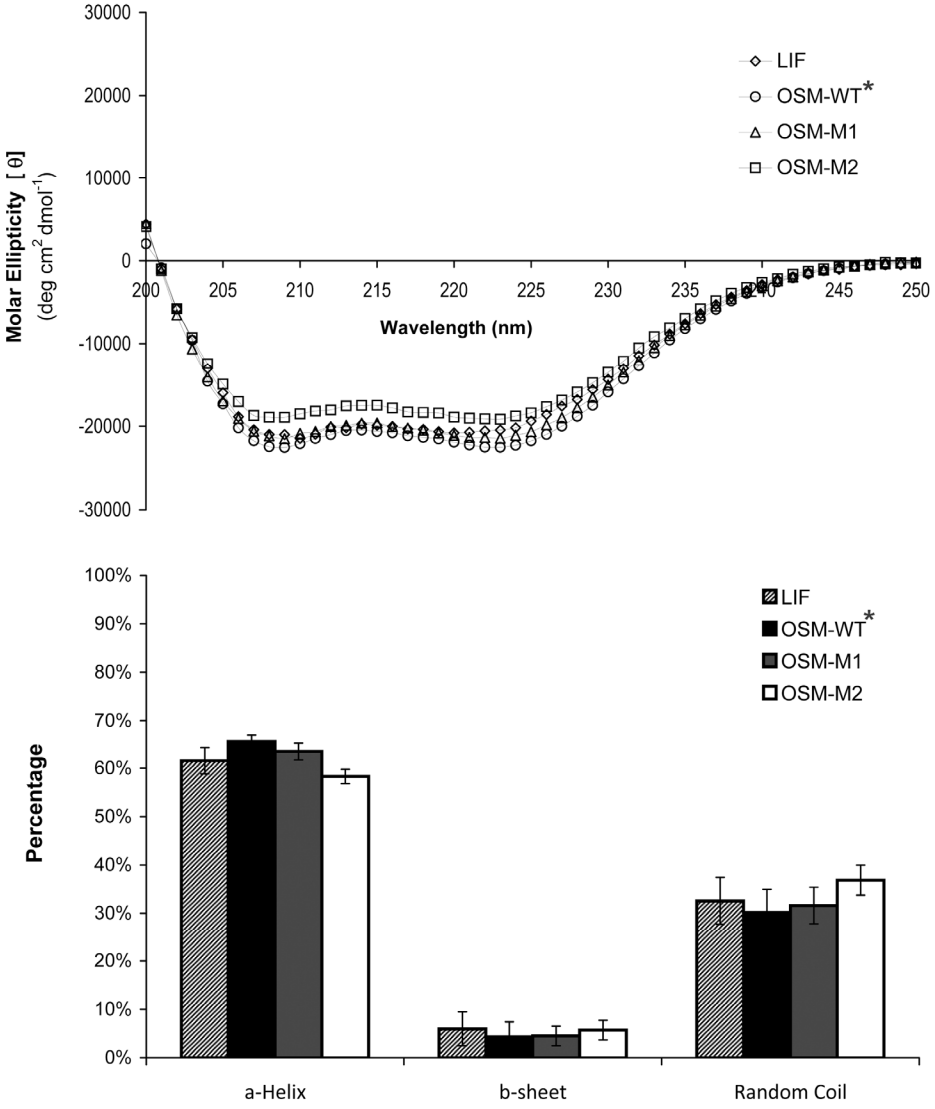


Figure 3.12 Modifications in the BC loop area of OSM did not induce a global change in the protein's structure.

A) Average of 3 CD spectra of the purified proteins plotted as molar ellipticity (θ) versus the wavelength. B) Theoretical estimation of the secondary structural content for each protein using SELCON3, CDSSTR and CONTINNL. Values are presented as mean of estimations given by the three programs ± SD.

3.2.2.3. Functional Evaluation of wild-type* and mutant OSMs in their activation of OSMR:gp130 complexes

To determine whether the BC loop on hOSM is required for OSMR binding, we stimulated A375 melanoma cells with the wild type and mutant forms of OSM. A375 melanoma cells express OSMR and gp130 on their cell surface but not LIFR (50). To confirm the absence of LIFR, A375 melanoma cells were treated with increasing doses of LIF and OSM-WT*. In agreement with previous observations, these cells did not respond to LIF but responded to OSM-WT* in a linear, dose dependent manner as demonstrated by activation of STAT3 (Figure 3.13A). In addition, pretreatment of A375 melanoma cells with LIFR specific antagonist, LIF05, showed no effect on hOSM-WT* activity while pretreatment with anti-gp130 antibody completely abolished hOSM-WT* activity (Figure 3.13B). These results again confirm that hOSM-WT* utilizes OSMR:gp130, but not LIFR:gp130 to activate STAT3 in A375 melanoma cells. When treated with OSM-M1 and OSM-M2 which have truncated BC loops, to our surprise, the A375 cells exhibited a 3 – 4 fold increase in their STAT3 activation relative to OSM-WT* (Figure 3.14). The mutant molecules however did not show any change in Erk 1/2 activation compared to OSM-WT*. Since OSM with truncated BC loops were able to activate OSMR:gp130 better than the wild-type* OSM (OSM-WT*), the BC loop is clearly not essential for OSM's unique ability to bind OSMR but is rather lowering the ability of OSM to form a stable complex with OSMR and gp130.

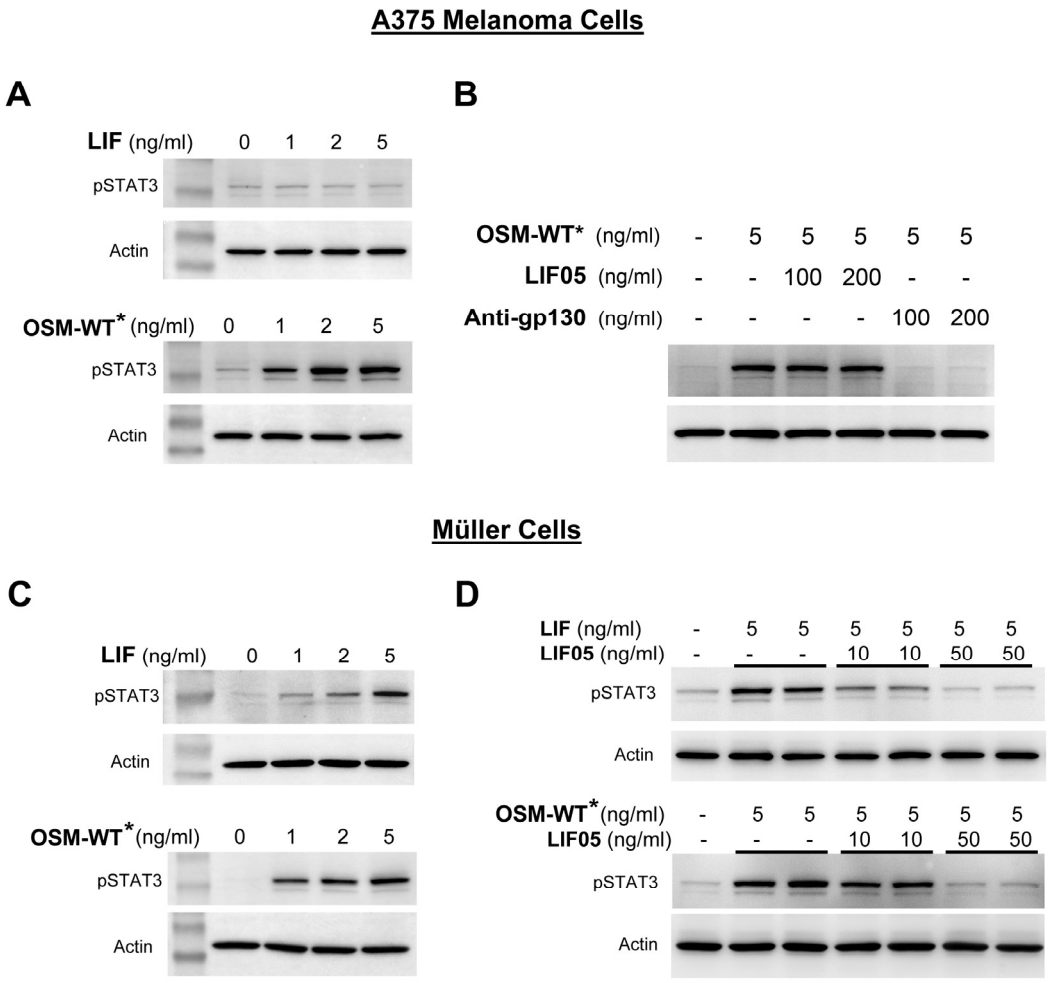


Figure 3.13 Human Müller cells express LIFR, gp130 while A375 melanoma cells express OSMR, gp130 on their cell surface.

A) Both LIF and OSM activate STAT3 in human retinal Müller cells in a dose dependent manner B) LIF05 (LIFR antagonist) is able to completely antagonize the STAT3 activation induced by both LIF and OSM suggesting that both LIF and OSM utilize LIFR:gp130 to activate STAT3 in Müller cells C) In A375 melanoma cells, only OSM is able to activate STAT3 in a dose dependent manner while LIF is not able to activate any STAT3 demonstrating that these cells express OSMR and gp130 on their surface but do not express LIFR.

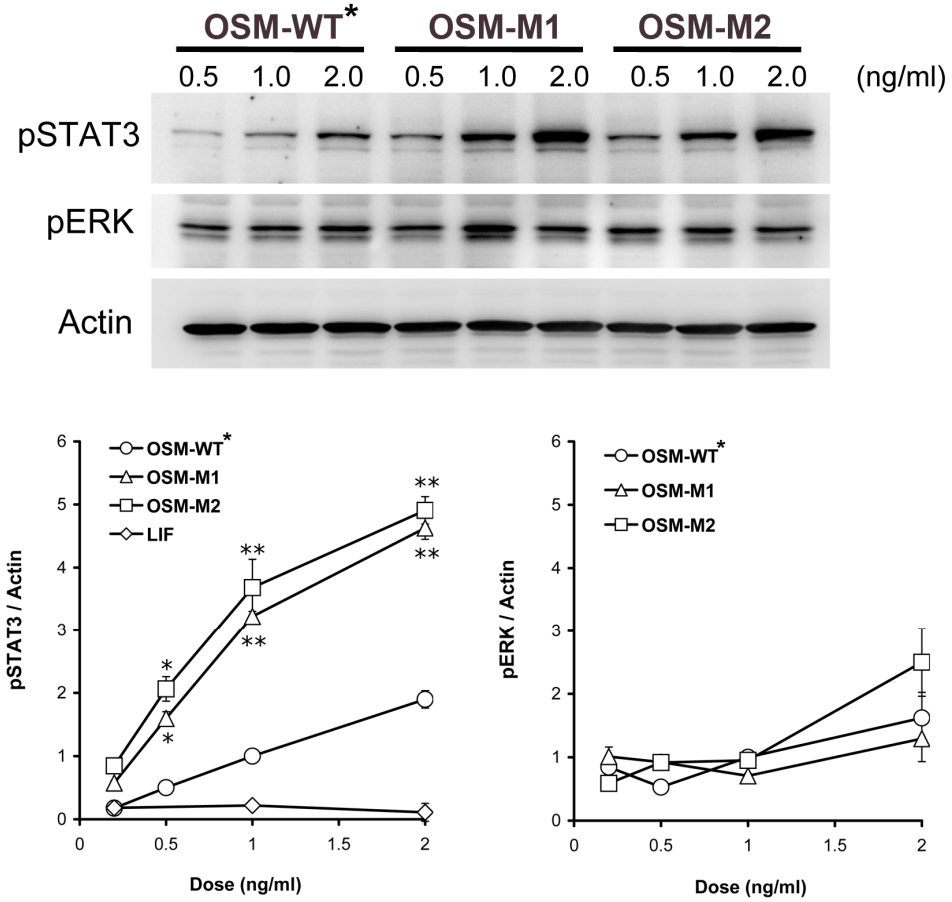


Figure 3.14 Activation of STAT3 and Erk 1/2 in A375 melanoma cells in response to different doses of wild type (OSM-WT) and the mutant forms of OSM (OSM-M1 and OSM-M2).

Values are presented as mean ± SE. n ≥ 4. (*p<0.01, **p<0.001, compared to OSM-WT treatment at same dose). Contrary to our expectation, mutant OSMs with truncated BC loops (OSM-M1 and OSM-M2) exhibited 3-4 fold higher potency in activating STAT3 downstream OSMR:gp130. STAT3 activation in induced by LIF estimated by the representative data shown in figure 3.13C is shown for comparison. However, compared to the wild type, OSM-M1 and OSM-M2 did not exhibit any difference in activating ERK1/2.

3.2.2.4. Functional Evaluation of wild-type and mutant OSMs in their activation of LIFR:gp130 complexes.

To determine whether shortening the BC loop in OSM affected the ability of OSM to activate LIFR:gp130 receptors we used the recombinant proteins to stimulate human retinal Müller cell line. Müller cells respond to both LIF and OSM-WT* stimulation in a dose dependent manner by activating STAT3 (Figure 3.13C). To determine the receptor expression, the cells were pre-treated with recombinant LIF05 (a mutant LIF molecule that specifically antagonizes the activation of LIFR but not OSMR or gp130 (48,294)), before stimulating with LIF or OSM-WT*. At doses of 50 ng/ml, LIF05 was able to completely antagonize the STAT3 activation induced both LIF and OSM-WT* demonstrating that the STAT3 activation in Müller cells is dependent upon utilization of LIFR:gp130 and not OSMR:gp130 (Figure 3.13D). Treatment of Müller cells with wild-type* and mutant OSM molecules again show that OSM-M1 and OSM-M2 induce a 2 to 3 fold greater activation of STAT3 compared to OSM-WT* at similar doses (Figure 3.15). Also, OSM-M1 and OSM-M2 exhibited a similar 2 – 3 fold higher activation of Erk1/2 compared to wild type* OSM. Clearly, these data demonstrate that reducing the size of BC loop significantly improves OSM's ability to bind and activate both LIFR:gp130 and OSMR:gp130 receptor complexes.

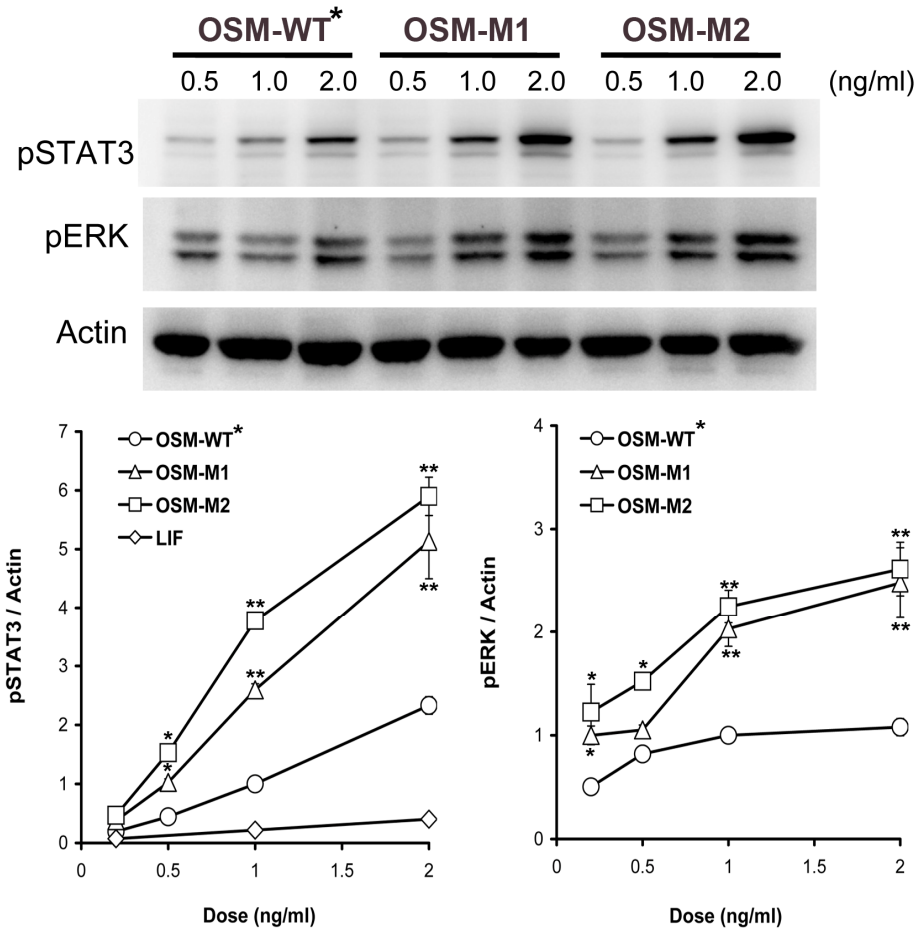


Figure 3.15 Activation of STAT3 and Erk 1/2 in human Müller cells in response to different doses of wild type (OSM-WT) and mutant forms of OSM (OSM-M1 and OSM-M2)

Values are presented as mean ± SE. n ≥ 4. (*p<0.05, **p<0.01, compared to OSM-WT treatment at same dose). As seen in A375 melanoma cells, mutant OSMs with truncated BC loops (OSM-M1 and OSM-M2) exhibited higher potency in activating STAT3 downstream OSMR:gp130. STAT3 activation induced by LIF estimated by the representative data shown in figure 3.13A is shown for comparison. Unlike in A375 melanoma cells, OSM-M1 and OSM-M2 exhibit 2-3 fold higher activation of ERK1/2 in Müller cells.

3.2.2.5. Removal of BC loop does not alter the requirement of core FXXK motif in active site III.

Given its proximity to the site III, it is possible that removal of the BC loop created an alternative site III that could facilitate a stronger binding to LIFR and OSMR. In order to determine whether the mutant OSMs, OSM-M1 and OSM-M2 still utilize the FXXK motif to interact with LIFR or OSMR, we mutated both F160 and K163 to alanines (A) and evaluated their activity on Müller cells and A375 cells. Müller cells were serum starved for 30 minutes before stimulation with 1 ng/ml concentration of either the wild type (FXXK) or the alanine mutant versions (AXXA) of OSM-WT*, OSM-M1 and OSM-M2 (Figure 3.16). As expected, mutating FXXK to AXXA in OSM-WT* completely abolishes its activity on both A375 melanoma and Müller cells. In a similar manner, both OSM-M1 and OSM-M2 showed complete loss of activity upon alanine substitution at the active site III. This suggests that the mutant OSMs with shorter BC loop still utilize the FXXK motif to interact with LIFR and OSMR.

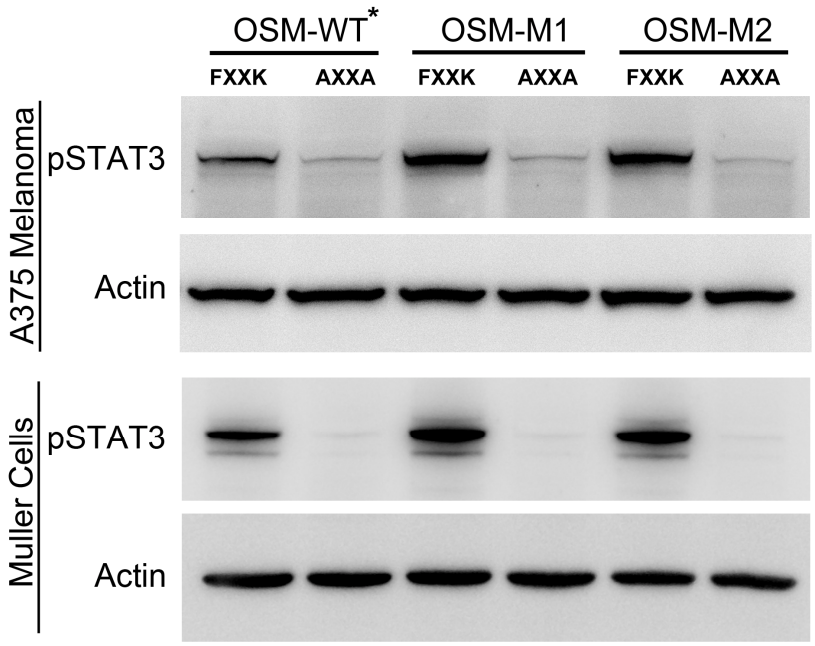


Figure 3.16 OSM with truncated BC loop still utilizes the FXXK motif to activate LIFR and OSMR.

A375 melanoma and Müller cells are stimulated with 1 ng/ml doses of various forms of OSM containing either the wild type (FXXK) or alanine substituted (AXXA) active site III. As expected, alanine substitution in wild-type OSM leads to complete abolition of its activity on both A375 melanoma and Müller cells. In a similar way, both OSM-M1 and OSM-M2 showed complete loss of activity upon alanine substitution at the active site III.

3.2.2.6. Reducing the size of BC loop improves OSM's affinity towards LIFR and OSMR

The ability of OSM-M1 and -M2 to activate receptor signaling at lower concentrations implied that these proteins have higher affinity towards LIFR and OSMR. To directly measure the binding kinetics of these ligand-receptor interactions, we used surface plasmon resonance (SPR). The cytokines (LIF, OSM-WT*, OSM-M1 and OSM-M2) were immobilized on the sensor chip surface while recombinant soluble receptors were used as the analytes (Figure 3.17). The analysis revealed that LIF had a 23 fold higher affinity towards LIFR (K_D = 3.10 nM) than gp130 (K_D = 72.38 nM) while OSM had a 2 fold higher affinity towards gp130 (K_D = 22.69 nM) than LIFR (K_D = 43.79 nM) (Table 3.2). This explains the sequential disparity between LIF and OSM in binding to LIFR and gp130 complexes. LIF, which exhibits a higher affinity towards LIFR would first bind LIFR and then bind to gp130 to form the stable trimeric complex. On the other hand, OSM which exhibits a higher affinity towards gp130, would first bind to it and then binds LIFR to form the trimeric complex. When the size of BC loop is reduced from 12 aa to 7 aa (OSM-M1) the affinity of OSM towards LIFR improved dramatically (K_D: 7.62 nM). When the size of BC loop is further reduced to 4 aa the affinity improved even more (K_D: 2.74 nM). However, changing the size of BC loop did not affect OSM's affinity towards gp130 significantly (K_D: OSM-WT* = 22.69 nM, OSM-M1 = 26.26 nM and OSM-M2 = 21.49 nM) (Table

3.2). OSM-M1 and -M2 proteins with shorter BC loops clearly display a higher affinity for LIFR still retaining their relatively high affinity towards gp130.

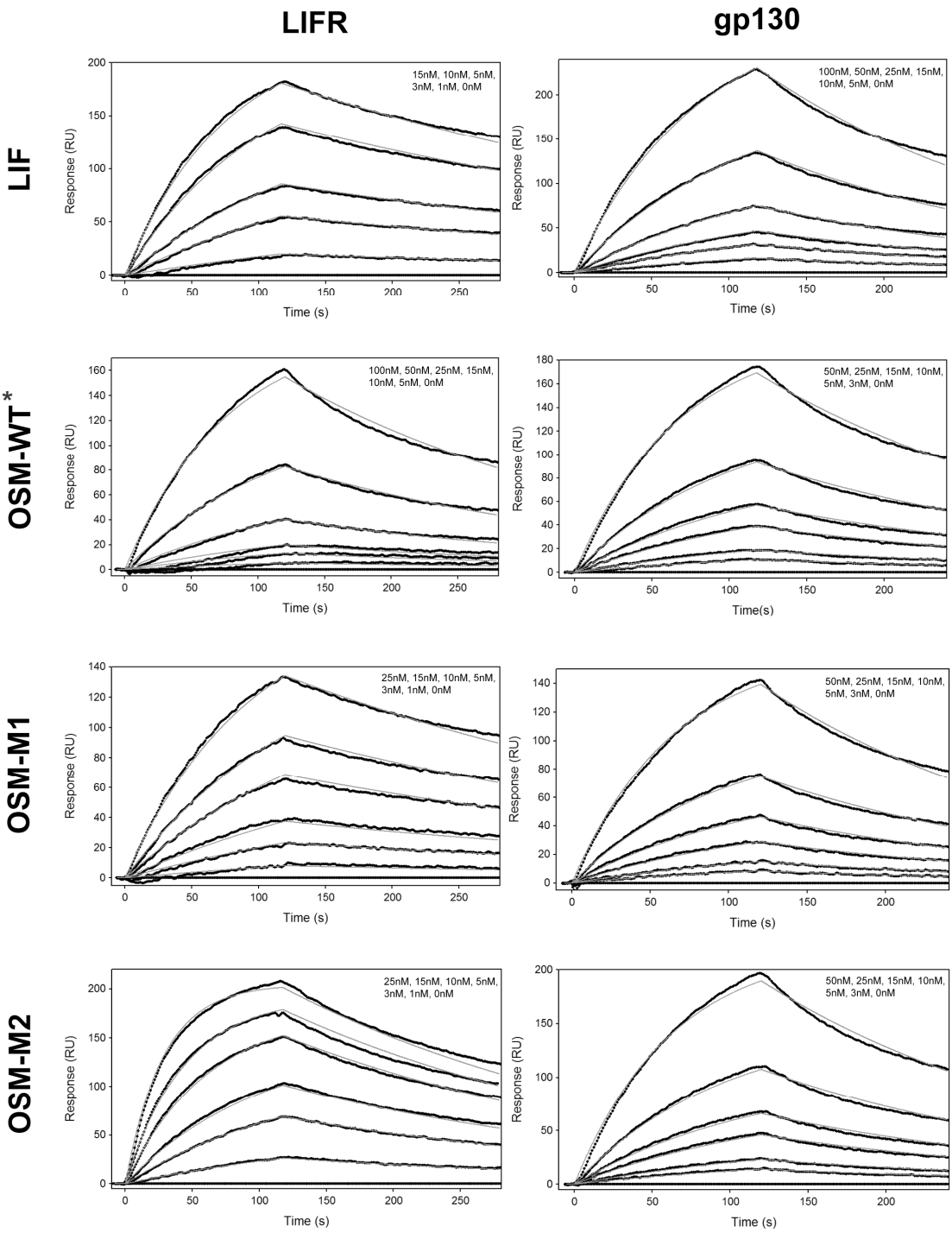


Figure 3.17 Kinetic analysis of LIFR and gp130 interaction towards LIF, OSM-WT, OSM-M1 or OSM-M2.

Soluble LIFR (left panel) or soluble gp130 (right panel) at various concentrations were injected over an SPR sensor chip with immobilized ligand (LIF, OSM-WT, OSM-M1 or OSM-M2) at flow rates of 25 μl/min. Responses obtained were corrected for background signal using a control flow cell. Association and dissociation rates are derived by global analysis of the response curves fit to a 1:1 kinetic model using QDat software (BioLogic Software, Ltd. Knoxville TN and Nomadics, Inc. Stillwater, OK) using 1:1 stoichiometry. Models are indicated in smooth gray line overlaid over response curve traces. *[Experiments were performed with assistance from ICX Technologies, Oklahoma City, OK]*

Table 3.2 Comparison of association (k_a), dissociation (k_d) and equilibrium dissociation (K_D) constants for LIFR and gp130 binding to LIF, OSM-WT, OSM-M1 and OSM-M2.

	LIFR			***gp130***		
	k_a (x 10^5 $M^{-1}s^{-1}$)	k_d (x 10^{-3} s^{-1})	K_D (nM)	k_a (x 10^5 $M^{-1}s^{-1}$)	k_d (x 10^{-3} s^{-1})	K_D (nM)
LIF	7.40	2.30	3.10	0.74	5.33	72.38
OSM-WT*	0.91	4.00	43.79	2.07	4.70	22.69
OSM-M1	3.31	2.52	7.62	2.03	5.34	26.26
OSM-M2	13.0	3.56	2.74	2.27	4.87	21.49

Together, these results suggest that the BC loop on OSM is presenting a steric hindrance for OSM's direct interaction with LIFR. Also, reducing its size not only enhances its affinity towards the receptor but also its ability to form a stable complex with cell surface receptors as demonstrated by the improved STAT3 activation.

Similar binding studies with OSMR showed that neither the wild-type* nor the mutant OSMs (OSM-M1 and OSM-M2) exhibit a direct interaction with OSMR (Figure 3.18). This is in agreement with previous results which reported a lack of direct interaction between OSM and OSMR in the absence of gp130 (4). In order to evaluate the binding kinetics of OSMR towards gp130 bound wild-type* or mutant OSMs, we have immobilized soluble gp130 on the sensor chip surface and treated with human OSM followed by OSMR. However, accurate association and dissociation constants could not be determined for these interactions since there was a progressive loss in the binding capacity of gp130 with each round of binding and regeneration. To overcome this issue, we used ELISA and performed similar binding assays where gp130 immobilized on the ELISA plate was sequentially treated with saturating amounts of wild-type* or mutant OSMs followed by increasing concentrations of soluble OSMR. Results show that after binding to gp130, both the wild type and the mutant OSMs start exhibiting a strong affinity towards OSMR (Figure 3.19B; Table 3.3). However, when tested for direct interaction, again, none of these cytokines displayed detectable affinities towards OSMR (Figure 3.19A; Table 3.3). This suggests that prior

bidning to gp130 is required for OSM to start displaying detectable affinities OSMR (Figure 3.19, Panel A vs. B). Again, as observed towards LIFR, there is a significant improvement in OSM's affinity towards OSMR when the BC loop is truncated ($K_{D,App}$: OSM-WT* – 10.86±1.7 nM; OSM-M1 – 3.71±0.67 nM; OSM-M2 – 2.19±0.28 nM). This represents a 3 – 4 fold increase in the affinity towards OSMR upon BC loop truncation on OSM. These results again confirm that the BC loop on OSM presents a steric hindrance for both LIFR and OSMR interaction towards OSM and its truncation results in significant improvement in both the affinity towards the receptors and also the biological activity.

The gp130 induced co-operativity for OSM binding towards OSMR prompted us to check if a similar co-operativity is induced towards LIFR binding. However, our results revealed that prior gp130 binding to OSM or LIF did not affect their affinities towards LIFR significantly (Figure 3.19, Table 3.3). This suggests that, unlike in the case of OSMR, LIFR and gp130 bind to the cytokines in a non-cooperative manner. Again, as observed in SPR, the mutant OSMs with truncated BC loop exhibited a stronger affinity towards LIFR compared to the wild-type* (Figure 3.19C and 3.19D, Table 3.3). However, to be noticed is the fact that the equilibrium dissociation constants obtained for LIFR binding using ELISA were significantly higher than the values obtained using SPR. This could be the result of structural distortions involved ELISA immobilization and also the indirect method of bidning analysis which involves series of washing and incubation steps that shifts the equilibrium.

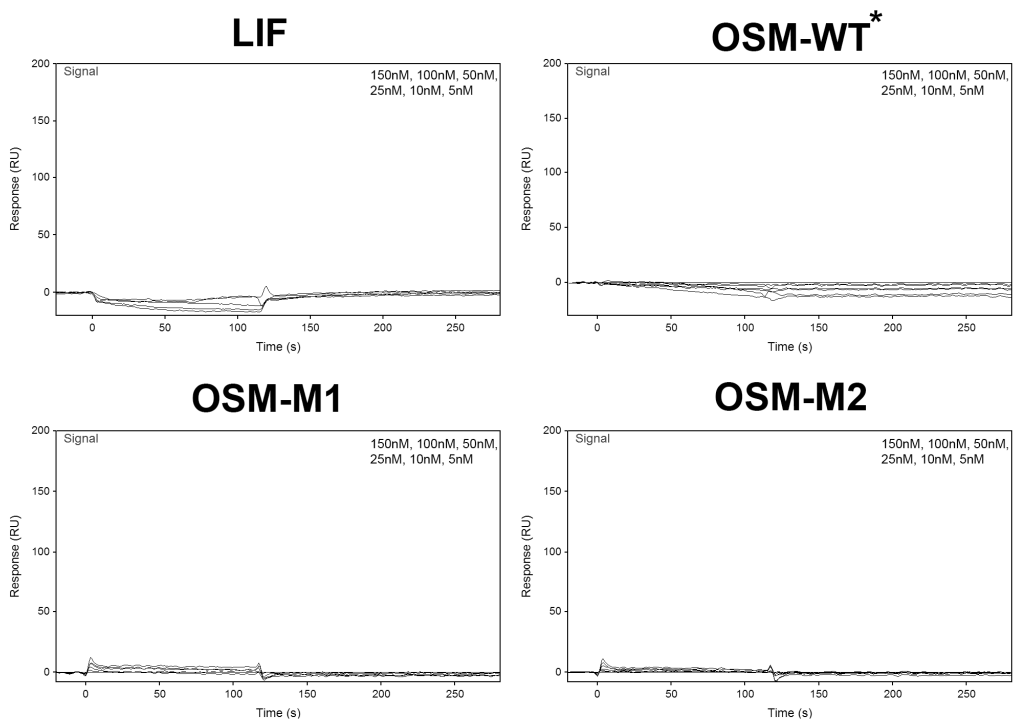


Figure 3.18 Neither wild type (OSM-WT) nor the mutant forms of OSM with truncated BC loop (OSM-M1 and OSM-M2) exhibit a direct affinity towards OSMR.

Soluble OSMR at various concentrations were injected over an SPR sensor chip with immobilized ligands (LIF, OSM-WT, OSM-M1 or OSM-M2) at flow rates of 25 μl/min. Responses obtained were corrected for background signal using a control flow cell. Association and dissociation rates are derived by global analysis of the response curves fit to a 1:1 kinetic model using QDat software (BioLogic Software, Ltd. Knoxville TN and Nomadics, Inc. Stillwater, OK) using 1:1 stoichiometry. Models are indicated by a smooth gray line overlaid over response curve traces.

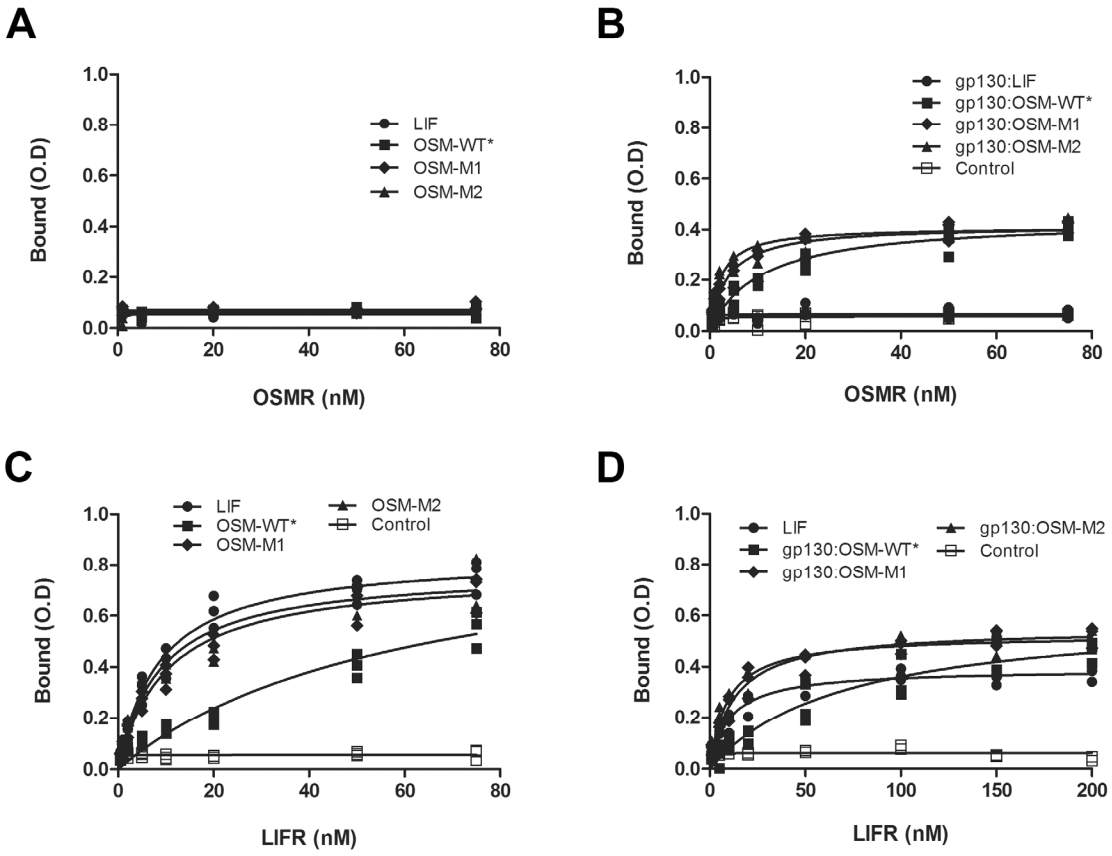


Figure 3.19 ELISA analysis of OSMR and LIFR binding towards LIF, OSM-WT*, OSM-M1 and OSM-M2 or gp130 bound LIF (gp130:LIF), OSM-WT* (gp130:OSM-WT*), OSM-M1 (gp130:OSM-M1) and OSM-M2 (gp130:OSM-M2). Cytokines (LIF, OSM-WT*, OSM-M1 or OSM-M2) immobilized on ELISA plate in the absence (A,C) or presence (B,D) of gp130 were treated with various concentrations of soluble OSMR (A,B) or soluble LIFR (C,D). Equilibrium K_D values were estimated using a non-linear curve fitting to the binding data using GraphPad Prism (Graph Pad Software. LaJolla, CA) (See Table 3.3)

Table 3.3 Comparison of apparent equilibrium dissociation constant ($K_{D,App}$) values (nM) for direct interaction of LIFR and OSMR with LIF, OSM-WT*, OSM-M1 and OSM-M2 or the interaction of LIFR and OSMR with gp130 bound LIF, OSM-WT*, OSM-M1 and OSM-M2)

	OSMR Binding		***LIFR Binding***	
	Direct	***With gp130***	***Direct***	***With gp130***
LIF	ND	ND	8.58 ± 0.99	10.33 ± 1.59
OSM-WT*	ND	10.86 ± 1.70	60.02 ± 17.54	70.29 ± 18.90
OSM-M1	ND	3.71 ± 0.67	10.06 ± 1.34	12.56 ± 1.73
OSM-M2	ND	2.19 ± 0.28	8.75 ± 1.34	9.13 ± 1.53

3.2.2.7. Inhibition of A375 melanoma cell proliferation

OSM was initially discovered by its ability to suppress proliferation of several melanoma cell lines including A375 melanoma cells (1). To test whether the improvement in OSM's affinity towards OSMR with truncation of BC loop has any functional consequence we monitored the growth of A375 melanoma cells in the presence or absence of wild-type* and mutant OSMs. As expected, treating A375 cells with wild-type* OSM inhibited their proliferation in a dose dependent manner (Figure 3.20). At concentrations of 20 ng/ml, OSM-WT* was able to suppress A375 melanoma cell proliferation by ~40% while a concentration of 50 ng/ml was able to suppress the proliferation by ~80%. In contrast, both OSM-M1 and OSM-M2 were both able to suppress the proliferation of A375 melanoma cells at significantly lower concentrations. While 10 ng/ml concentrations were enough for the mutant OSM molecules to inhibit the proliferation by ~60%, 20 ng/ml concentrations suppressed their proliferation by ~80%. These data clearly suggest that reducing the size of BC loop improves the ability of OSM to activate OSMR:gp130 and suppress the proliferation of A375 melanoma cells.

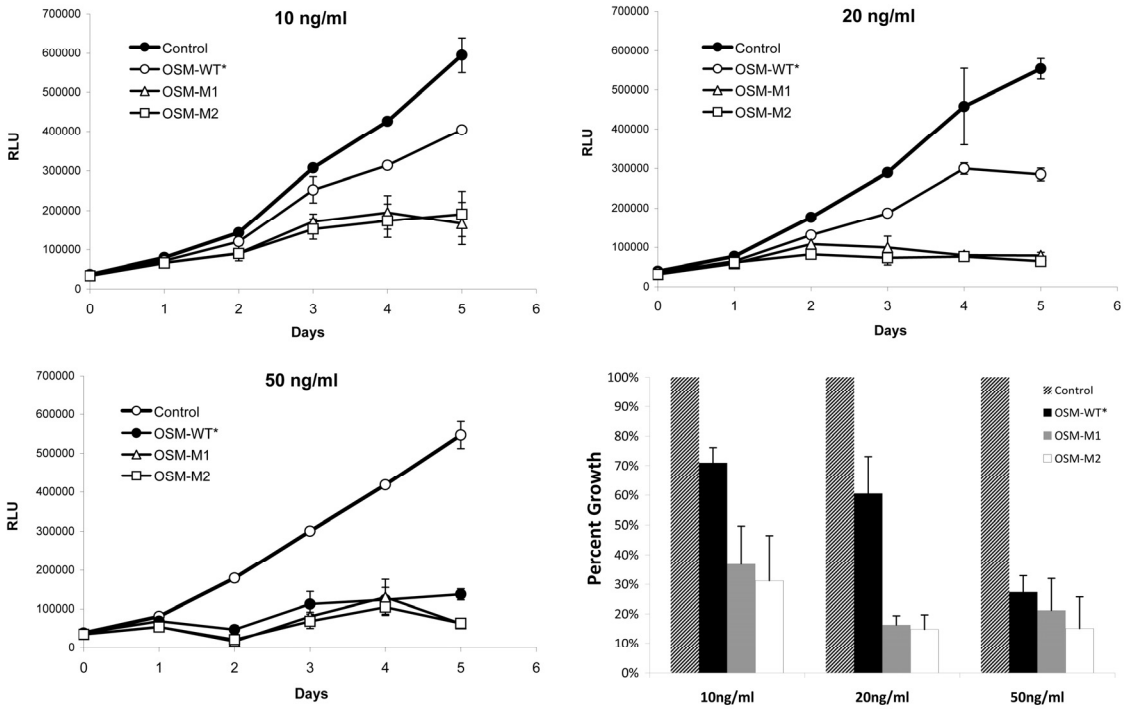


Figure 3.20 A375 melanoma cell proliferation in the presence or absence of OSM-WT, OSM-M1 and OSM-M2.

OSM inhibited the proliferation of A375 melanoma cells in a dose dependent manner with 50 ng/ml being able to exhibit a near complete suppression. However, at similar dosages, OSM-M1 and OSM-M2 were more potent in suppressing the proliferation of A375 melanoma cells. Average of cell numbers on 4^{th} and 5^{th} day of proliferation are normalized against the control cells and plotted for comparison. Values are presented as mean ± SD. n = 4.

3.2.2.8. Protection of retinal photoreceptors

As described in chapter 3.1, IL-6 family cytokines are strongly implicated in neuroprotection. Previous studies by LaVail et al., (146,301) and Ueki et al., (149) have shown that IL-6 family cytokines rescue photoreceptors from damaging effects of constant light and retinal degenrations induced by inherited genetic mutations. To test whether the mutant OSM's (OSM-M1 and OSM-M2) which display improved ability in binding and activating LIFR:gp130 and OSMR:gp130 complexes exhibit an enhanced ability in protecting the retinal photoreceptors compared to wild-type* OSM we injected 0.25 μg of OSM-WT*, OSM-M1 or OSM-M2 in a total volume of 1 μl in the left eye of Balb/cJ mice while the right eye, injected with PBS, served as control. 2 days following intravitreal injection, the mice were exposed to damaging light (4000 lux) for 4 hours. Following a 4 day recovery period after the light damage, eyes were enucleated and processed for histological analysis. Photoreceptor cell death in each group was assessed my morphometric analysis. Representative sections for each treatment is shown in figure 3.21A while quantitative analysis of the number of photoreceptors in each group are shown in figure 3.21B. Exposure to 4000 lux for 4 hours caused significant damage to retinal photoreceptors injected with PBS. Compared to normal eyes, which

contain ~12 rows of photoreceptor nuclei in their outer nuclear layer (ONL), PBS injected eyes retained only 3-4 nuclei layers in the ONL. While OSM-WT* did not show significant protection of photoreceptors, OSM-M1 and OSM-M2 were clearly more potent and lead to retainment of 6-7 photoreceptor nuclei layers after the light damage. Again, this clearly suggests that the improved affinity of OSM towards OSMR and LIFR by truncating the BC loop has a functional consequence.

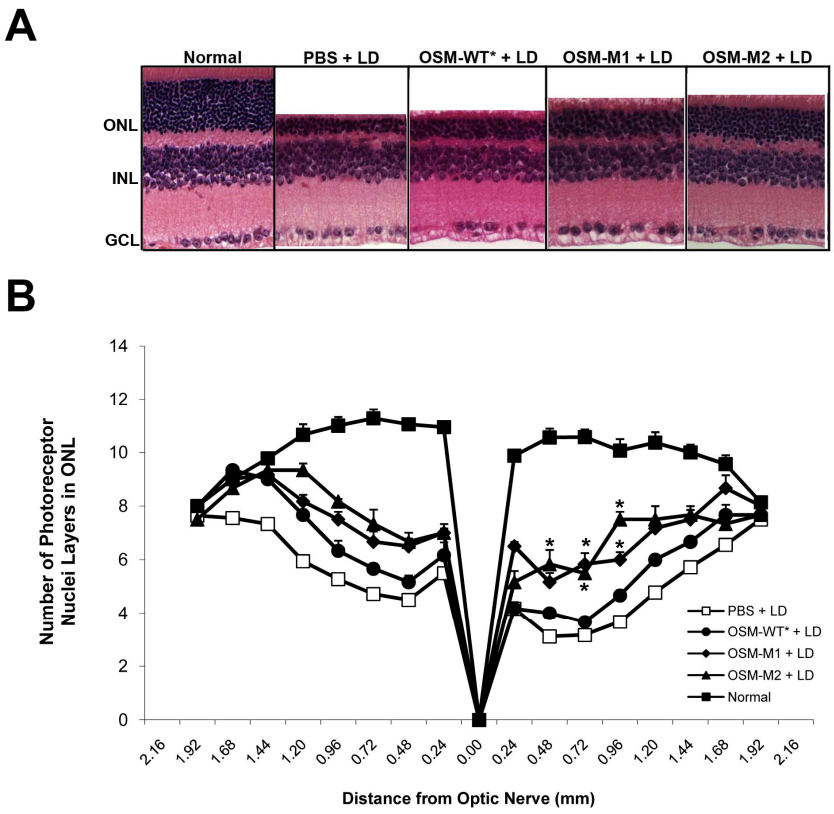


Figure 3.21 Mutant OSM's with truncated BC loop (OSM-M1 and OSM-M2) are more potent than the wild-type* OSM (OSM-WT) in protecting the photoreceptor cells from light damage (LD).

A) Representative sections and B) quantification of number of rows of photoreceptor nuclei in the outer nuclear layer (ONL) along the vertical meridian of the retinas treated with PBS (□), OSM-WT* (●), OSM-M1 (♦) or OSM-M2 (▲) and subjected to light damage (4000 lux for 4 hours). Quantification of photoreceptor nuclei layers from a normal retina (■) is shown for comparison. n = 3; value = mean SD (*$p<0.05$, vs. LD eyes, paired t-test). ONL – outer nuclear layer; INL – Inner nuclear layer; GCL – ganglion cell layer).

Discussion

IL-6 family cytokines are pleitropic cytokines that elicit a wide variety of responses *in vivo* mediated by the activation of signal transducing receptors gp130, LIFR and OSMR. Among these cytokines, OSM is unique in terms of its ability to signal through two different receptor complexes, LIFR:gp130 (type I) and OSMR:gp130 (type II). Also, OSM is unique in the order in which it binds to its receptors i.e. gp130 followed by LIFR or OSMR (5,21,25,324). Based on the crystal structures and mutational analysis conducted, it has been proposed that the ability of OSM to interact with OSMR must result from the involvement of additional residues in the vicinity of its "FXXK" motif which is required for OSM's binding to LIFR and OSMR (4). In comparison to other IL-6 family cytokines, we have identified that OSM has a unique α-helical loop between its B and C helices. This BC loop lies in close proximity to site III which contains the core "FXXK" motif. The size and location of this loop suggested that it is possibly playing an essential role in OSM's unique ability to bind OSMR. However, contrary to our expectation, shortening this loop resulted in proteins that display higher affinity towards OSMR as indicated by improved activation of signal transduction and inhibition of A375 melanoma cell proliferation. Additional studies using Müller cells showed that the truncation of BC loop on OSM improves its ability to activate LIFR:gp130 complexes also. These observations suggest that while the alpha helix in BC loop of OSM is not responsible for binding to OSMR, its primary role seems to be to modulate the function of OSM.

It has been reported that LIF has a strong preference for binding LIFR prior to binding gp130 while OSM has a preference for binding gp130 prior to binding LIFR (21,23,48). Affinity measurements by SPR suggest that the mechanism behind the unique ability of OSM to first bind gp130 can be explained by its relative affinity to each receptor subunit. OSM has a two fold higher affinity for gp130 than for LIFR. LIF, which lacks the BC loop, has a 23 fold higher affinity for LIFR than for gp130. When the BC loop on OSM is truncated, OSM starts displaying a higher affinity towards LIFR than towards gp130. Clearly, the reduced affinity of OSM towards LIFR is caused by the BC loop and is likely playing a role in the difference in sequential binding between LIF and OSM.

The inability of OSM to bind soluble OSMR directly is consistent with previous observations (4). Like IL-6 and CNTF which require binding to their alpha receptor before they can bind to their signal transducing receptors, these results suggest that OSM requires binding to gp130 before it can bind OSMR. To test this, we conducted OSMR binding analysis for these cytokines in the presence of gp130. Results showed that gp130 binding induces remarkable co-operativity towards OSMR binding in both the wild type and mutant OSMs (OSM-WT*, OSM-M1 and OSM-M2) i.e. the cytokines by themselves do not exhibit any direct interaction with OSMR, but upon prior binding to gp130 they start exhibiting a strong affinity towards OSMR. While the data clearly showed that OSM utilizes the ‘FXXK’ motif for OSMR binding, binding to gp130 might expose otherwise

hidden residues on OSM required for OSMR binding or alter the OSM structure to move hindering residues away from the binding interface leading to the strong binding. Solving the structure of OSM in complex with gp130 would prove valuable in identifying these changes.

Finally, a number of studies conducted over the last decade have revealed the diverse biological roles of OSM. One among them is the growth modulation of cells which include tumor cells, epithelial cells, fibroblasts and plasmacytoma cells (1,170,171,174,326,327). In agreement with earlier studies, our results show that OSM inhibits the growth of A375 melanoma cells in a dose dependent manner (Figure 3.15). Mutant OSM proteins with a shorter BC loop exhibit increased potency in suppressing their proliferation (Figure 3.15). This improvement in OSM's function could prove valuable in treating diseases associated with melanoma. Previous research in our lab has shown that STAT3 activation induced by IL-6 family cytokines is neuroprotective and prevents photoreceptor cell death under oxidative stress (149,328). Our experiments show that the mutant OSM molecules, OSM-M1 and OSM-M2 are more potent than the native cytokine (OSM-WT*) in protecting the photoreceptor cells from oxidative damage. These molecules could thus serve as potent therapeutic agents in preventing photoreceptor degeneration induced by inherited genetic mutations such as retinitis pigmentosa. Also, OSM plays a key role in the inflammatory response to injury and infection. OSM secreted from activated T cells and monocytes stimulates expression of 1) acute phase proteins (APPs) in

the liver (87) 2) P-selectin and E-selectin on endothelial cells and (97,98) 3) TIMP-1 in fibroblasts (105,329) all of which promote wound repair. The mutant OSM proteins could thus potentially find therapeutic application in promoting wound healing also.

3.3. Sustained Delivery of human Oncostatin M (hOSM) to Retina using poly(ethylene glycol) (PEG) based hydrogels

3.3.1. Introduction

Diseases of the posterior eye segment pose a major challenge in ophthalmology. Several of these diseases, such as age related macular degeneration (AMD), retinitis pigmentosa (RP), glaucoma and diabetic retinopathy, necessitate long-term treatment with appropriate drugs. However, delivering drugs to the posterior eye has been a problem for decades because of various physiological and anatomical barriers. As summarized by Geroski and Edelhauser (330), there are four major routes for delivering drugs to the posterior segment: systemic, topical, intravitreal and transscleral. The systemic route has the obvious advantage of easy administration, but is largely ineffective because of the relatively small volume of vasculature present in the eye and also the resistance imposed by blood-retinal barriers (331). Topical delivery is very effective for delivering drugs to anterior segment. However losses to the tear film, convection of the drug by circulating aqueous humor (which flows posterior-to-anterior, away from target area) and the long distance to the retina combine to reduce the efficiency of topical delivery to a level only slightly above that of systemic delivery (332). Intravitreal injection of drugs has proven very effective and has been the method of choice for a long time since it offers the advantage of delivering the drug near target tissue and eliminates the necessity to cross retinal barriers. This mode of

delivery has gained popularity since the advent of new antibody based treatments for age-related macular degeneration (AMD) (eg. Avastin®, Lucentis®). However, many drugs that are used to treat vitreoretinal diseases have a narrow concentration range within which they are effective (333). Higher concentrations can be toxic, and lower concentrations can be insufficient to treat the disease. Hence, it is critical to maintain desired concentrations of drug inside the eye and this mandates frequent injection of drugs. Unfortunately, this increases the risk of infection and also poses the threat of serious side effects like vitreous hemorrhage and retinal detachment (334). Therefore other less invasive and long acting treatment modes are needed. Recent studies have shown that transscleral delivery of drugs can provide the localization of drugs similar to intravitreal injection and also offer safety levels comparable to topical administration if a constant release vehicle is employed (272,335-339). The sclera has a large surface area and is highly diffusible to drugs below molecular weight of 70kDa, making it an appealing route for delivery of small drugs to the posterior eye (335,340-342). Figure 3.22 shows a simplified anatomy of the barriers involved in transscleral drug delivery.

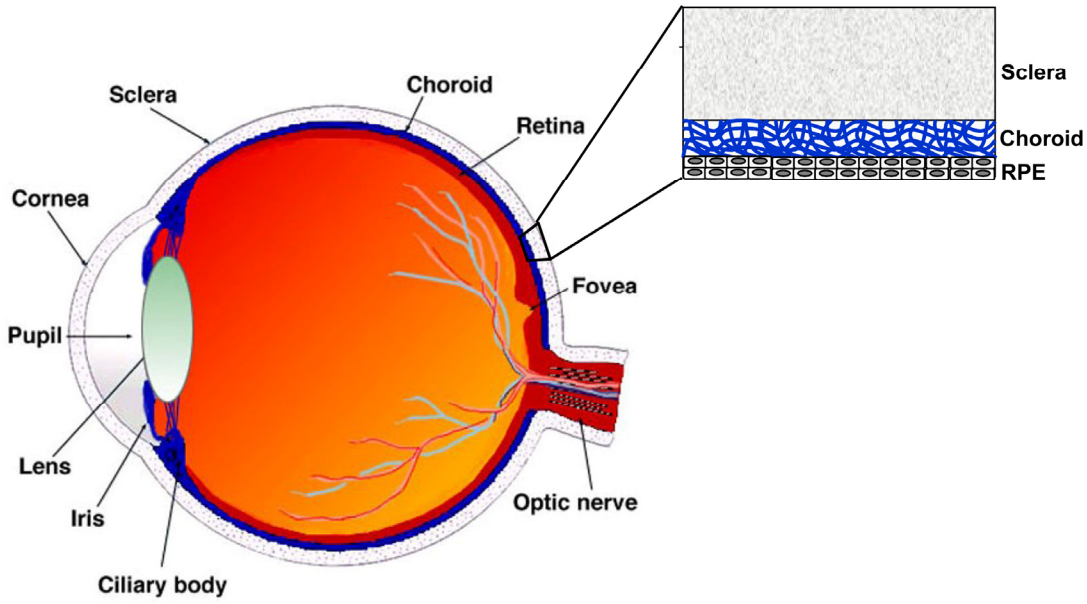


Figure 3.22 Schematic representation of the eye.

Shown in the inset is the representation of various barriers along the route for transscleral drug delivery.

[Modified and used with permission from http://webvision.med.utah.edu/sretina .html]

Since the pioneering work of Wichterle in the 1960s (215-217) hydrogels have generated great interest among scientists as potential vehicles that can deliver drugs in a controlled, pre-dictated manner. Hydrogels offer a number of advantages over traditional methods; they trigger minimal immune response when implanted, can hold large amounts of drug, prevent their rapid clearance and release drugs in a sustained manner over long periods of time (343). A number of polymers have been studied for creating transscleral drug delivery implants. Examples include polyvinyl alcohol (PVA), ethylene vinyl acetate (EVA), poly(ethylene glycol) (PEG), poly(lactic acid) (PLA), poly(glycolic acid) (PGA), their co-polymer, poly(lactic-co-glycolic acid) (PLGA) (272,291,335,336,338,339,344-347).

Previous work and our results have shown that STAT3 activation induced by IL-6 family cytokines protect the photoreceptor cells in the retina from oxidative stress induced by bright light and inherited genetic mutations (149,150,328). However, we have also shown that when delivered in large doses, these cytokines can induce photostasis leading to transient loss of visual function (149). Thus, a judicious release of these drugs in a controlled manner is essential for these molecules to be used in therapy for treatments. Since these molecules are small (M.W ~20kDa), controlled delivery via the transscleral route using hydrogel implants proves to be an effective way to get these drugs to the photoreceptors. We have used functionalized PEG monomers to create hydrogel matrices encapsulated with human oncostatin M (hOSM) and release studies *in vitro* have

shown that the macromer concentration can be varied effectively to tailor the release rates of the drug from these matrices. When implanted sub-conjunctivally in a mouse eye, the PEG hydrogel released hOSM in a controlled manner leading to sustained activation of STAT3 as predicted by *in vitro* and mathematical model studies.

3.3.2. Results

3.3.2.1. Estimation of volumetric swelling ratio (Q), mesh size (ξ) and diffusivity of the drugs in hydrogel (Dg)

Hydrogels with varying amounts of PEG 5000 macromer (10%, 20%, 30% 40% and 50% by weight) were made for this analysis. Immediately after photo-polymerization, the hydrogels were each weighed and placed in a reservoir of continuously agitated PBS solution. At regular time intervals, the hydrogels were taken out of the swelling medium and weighed. This process was continued until the gel stopped swelling as indicated by a constant final weight. The weight of gel at this equilibrium swelling point was noted as (M_{eq}). Results indicated that by 2 hours of incubation, gels of all compositions reached a steady-state equilibrium swelling. The gels were then dried under vacuum for 2 days to obtain the dry weight of the hydrogels (M_d). Equilibrium mass swelling ratio of the hydrogels was obtained by dividing the weight of hydrogel at equilibrium swelling point (M_{eq}) with dry weight of the hydrogel (M_d).

$$\text{Mass Swelling Ratio } (Q_m) = \frac{M_{eq}}{M_d}$$

Results show that the mass swelling ratio of the PEG hydrogels showed an inversely proportionate correlation with the weight percent of the macromer in the hydrogel. While 10% hydrogel has an equilibrium mass swelling ratio (Q_m) of 11.9 ± 0.15, 20%, 30%, 40% and 50% hydrogels displayed an equilibrium mass swelling ratio (Q_m) of 7.1 ± 0.09, 5.3 ± 0.02, 3.9 ± 0.04 and 2.5 ± 0.12 respectively (Figure 3.23A).

These values of mass swelling ratios are then used to determine the volumetric swelling ratio (Q) and the polymer mesh size (ξ), using the scaling laws developed by Peppas and co-workers (250,348).

$$Q = \frac{(Q_m - 1)\upsilon_1 + \upsilon_2}{\upsilon_2}$$

Where, υ_1 is the specific volume of PBS and υ_2 is the specific volume of PEG. Using the volumetric swelling ratio, one can estimate the mesh size of the hydrogel network using the equation:

$$\xi = Q^{1/3}\, rms_o$$

Where, rms_o is the root mean squared end-to-end distance of the PEG macromer. This can be estimated using the equation:

$$rms_o = l_{avg} (C_n)^{1/2} (n)^{1/2}$$

Where, l_{avg} is the average bond length of the PEG macromer, C_n is the characteristic ratio of the macromer and n is the total number of bonds present in each macromer.

Estimation of volumetric swelling ratios revealed a similar inverse correlation with weight percentage of the macromer in the hydrogel. Volumetric swelling ratio (Q) of 10%, 20%, 30%, 40% and 50% gels were 13.0 ± 0.16, 7.7 ± 0.10, 5.7 ± 0.03, 4.2 ± 0.04 and 2.7 ± 0.14 respectively (Figure 3.23B). In agreement with the above two values, estimation of mesh size of the hydrogel revealed that as the amount of macromer content in the hydrogel increased, there is a corresponding decrease in mesh size of the hydrogel network. Mesh sizes (ξ) of 10%, 20%, 30%, 40% and 50% gels were 12.9 ± 0.05 x 10^{-7} cm, 10.8 ± 0.05 x 10^{-7} cm, 9.8 ± 0.01 x 10^{-7} cm, 8.9 ± 0.03 x 10^{-7} cm and 7.9 ± 0.13 x 10^{-7} cm respectively (Figure 3.23B). These results clearly suggest that the macromer content inside a hydrogel can be varied to effectively tailor the physical properties of the hydrogel.

For a given drug molecule, one can easily estimate its diffusion coefficient inside the hydrogel (D_g) using equation developed by Anseth et al., (244).

$$D_g = D_o \left(1 - \frac{r_s}{\xi}\right)$$

Where, D_o is the diffusion coefficient of a drug molecule in aqueous solution, r_s is hydrodynamic radius of the drug molecule. D_o can be readily estimated using the 'Stokes-Einstein equation' given below:

$$D_o = \frac{k_B T}{6 \pi \mu r_s}$$

Where, k_B - Boltzmann's constant (= 1.38 x 10^{-16} cm^2g/s^2K), T – temperature in Kelvin, μ - viscosity of PBS and, the hydrodynamic radius of the drug molecule (r_s) can be estimated using the equation:

$$r_s = \left(\frac{3\,MW}{4\,\pi\,\rho\,N_A} \right)^{1/3}$$

Where, MW – molecular weight of the drug molecule, ρ - density of PBS, N_A – Avogadro's number (= 6.023 x 10^{23}).

However, it must be understood that these predictions for D_g, D_o and r_s assume that the drug molecule is spherical, while in reality the proteins exist in a wide range of shapes often deviating from the spherical shape. The molecule employed for our studies here, hOSM, exists in a conformation more closer to the cylindrical shape. Thus, empirical observations for the drug release rates could show significant deviation from the theoretical predictions particularly, when the theoretically predicted mesh sizes are closer to drug radius.

As expected, theoretical predictions revealed that as the macromer content inside the hydrogel increased, the diffusivity of hOSM decreased in a proportionate manner (Figure 3.24). This is expected since increasing the macromer content decreases the mesh size of the hydrogel leading to a corresponding decrease in diffusivity of the drug molecule in the hydrogel.

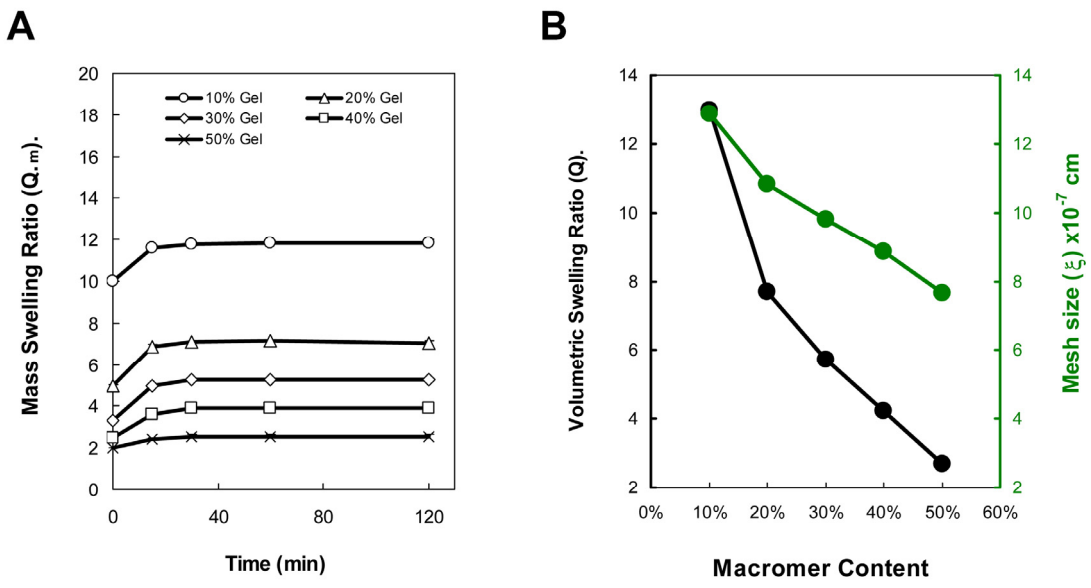


Figure 3.23 Changes in mass swelling ratio, volumetric swelling ratio and mesh size of PEG hydrogels as a function of macromer content

A) Changes in mass swelling ratio (Q_m) of PEG hydrogels with various amounts of macromer (10%, 205, 30%, 40% and 50% by weight) as a function of time. All hydrogels reached an equilibrium within first 40 mins and remained stable later. B) Changes in volumetric swelling ratio (Q) and mesh size (ξ) as a function of macromer content in the hydrogel. As expected, both the swelling ratio and mesh size decrease with increase in macromer content.

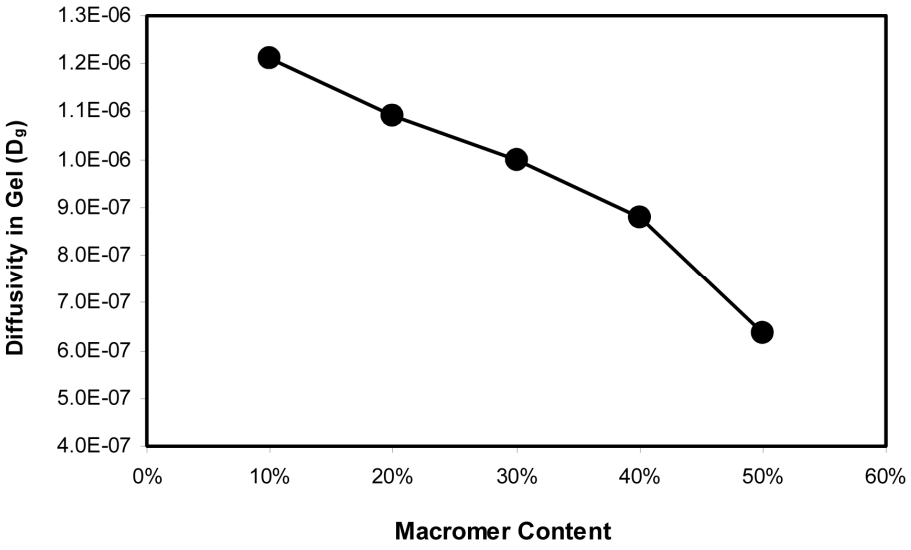


Figure 3.24 Changes in diffusivity (D_g) of hOSM through PEG 5000 DA hydrogels as a function of macromer content in the hydrogel.

3.3.2.2. Theoretical Estimation of Drug Diffusion from Hydrogels

As described in the materials and methods section, the rate of drug diffusion from the polymeric hydrogels can be estimated by solving the Fick's law of diffusion equation. Since we are synthesizing hydrogels of high aspect ratio, a valid assumption of unsteady-state 'one-dimensional' diffusion from either face of the gel can be made.

3.3.2.2.1 Concentration profile in drug loaded hydrogel

Fick's Law:

$$\frac{\partial C}{\partial t} = D_g \frac{\partial^2 C}{\partial x^2} \qquad \text{Eqn 1}$$

Where, C is the concentration of drug inside the gel at time t and position x, and D_g is the diffusion coefficient of the drug inside swollen hydrogel. The hydrogel is non-degradable and thus the structural properties of the hydrogel and thus diffusion coefficient of the drug will stay constant throughout the release process.

Boundary Conditions:

BC 1 $\quad C(\pm L, t) = 0$

BC2 $\quad C(x,0) = C_o \qquad\qquad -L < x < +L$

BC3 $\quad \left.\frac{\partial C}{\partial x}\right|_{x=0} = 0$

Using the boundary conditions listed above, Crank (349) has derived the equation for estimating concentration profile with respect to time and position (See Appendix A1 for details of derivation).

$$C_{(x,t)} = \frac{4C_o}{\pi} \sum_{n=0}^{\infty} \frac{(-1)^n}{(2n+1)} \exp\left[\frac{-D_g (2n+1)^2 \pi^2 t}{4L^2} \right] Cos \frac{(2n+1)}{L} \frac{\pi}{2} x$$

Based on the diffusivity (D_g) values obtained earlier (figure 3.24), we have solved for changes in the concentration profile of hOSM in 10% and 50% PEG 5000 diacrylate hydrogels. Shown in figure 3.25 is the comparison of changes in concentration profiles with respect to time and position in a 10% and 50% PEG hydrogel. As expected, the concentration of hOSM in both hydrogels decreases with time and this decrease is symmetric with the central plane of the hydrogel.

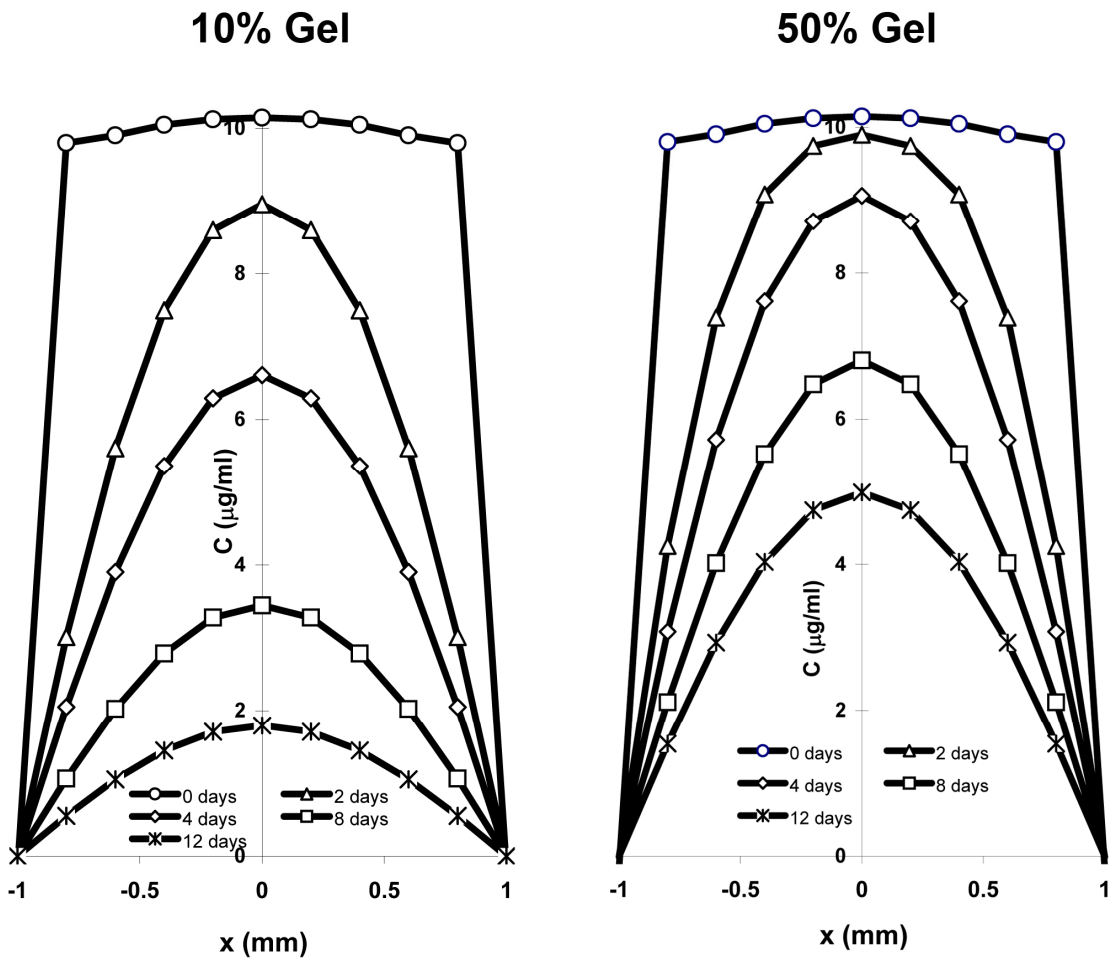


Figure 3.25 Theoretical predictions for changes in the concentration profile of hOSM through a hydrogel slab as a function of time.

An initial loading of hOSM at a concentration of 10μg/ml is assumed. Diffusion is one-dimensional and symmetrical about the central plane as described in the materials and methods section.

3.3.2.2.2 Fractional Release of the Drug

Release of the drug from a hydrogel is normally represented in terms of fractional release with respect to time. To obtain this, one can integrate the concentration '$C_{(x,t)}$' with respect to 'x' and obtain the mass of the drug inside the hydrogel and thus the mass of drug released from the hydrogel as function of time.

Mass retained in the one-dimensional plane at time (t) = 0 is $C_o \cdot 2L$

Mass retained at time (t) = t is $\int_{-L}^{L} C_{(x,t)} dx$

Mass retained at time (t) = ∞ is 0

Thus, mass of the drug (M_t) released in time, t is $M_{(\text{in pellet at } t = 0)} - M_{(\text{in pellet at } t = t)}$

$$= 2C_o l - \int_{-L}^{L} C_{(x,t)} dx$$

Total mass of the drug that can be released (M_∞) is $M_{(\text{in pellet at } t = 0)}$

$$= 2C_o L$$

We can obtain for the fractional release by solving the equation;

$$\frac{\mathrm{M_t}}{\mathrm{M_\infty}} = \frac{2C_o L - \int_{-L}^{L} C_{(x,t)} dx}{2C_o L}$$

Solving for the integral on the numerator, we can get (See Appendix A2 for details of the derivation);

$$\frac{M_t}{M_\infty} = 1 - 8\sum_{n=0}^{\infty} \frac{1}{(2n+1)^2 \pi^2} \exp\left[\frac{-D_g (2n+1)^2 \pi^2 t}{4L^2}\right]$$

Using this equation, we have solved for the fractional release of hOSM from 10% and 50% PEG 5000 hydrogels.

Shown in figure 3.26A is a comparison of the release profiles from these two hydrogels. Again, as expected, the release of hOSM from 10% hydrogel was significantly faster than that from 50% gel at earlier time points (Figure 3.26B). These results predict that for 10% gel, ~50% of the drug comes out within the first 2 days. While the next 45% of the drug takes about 10 days to come out of the hydrogel. Clearly, as the concentration gradient between the hydrogel and outside sink decreases with time, the release rate of the drug decreases and takes a longer duration to come out. In comparison, about 40% of the drug comes out of the 50% PEG 5000 hydrogel in the first 2 days. And, in the next 10 days, another 50% of the drug comes out. When the release rates are compared, a similar trend of lowering release rate with time is observed for both gels (Figure 3.26B). However, in the 50% gel, the decrease in release rates is not as rapid as in the 10% gel (Figure 3.26B). This can be attributed to the slow decrease in concentration gradient in 50% gel compared to 10% gel. Thus, at 12 days, the average release rate in a 50% gel is higher than that in 10% gel.

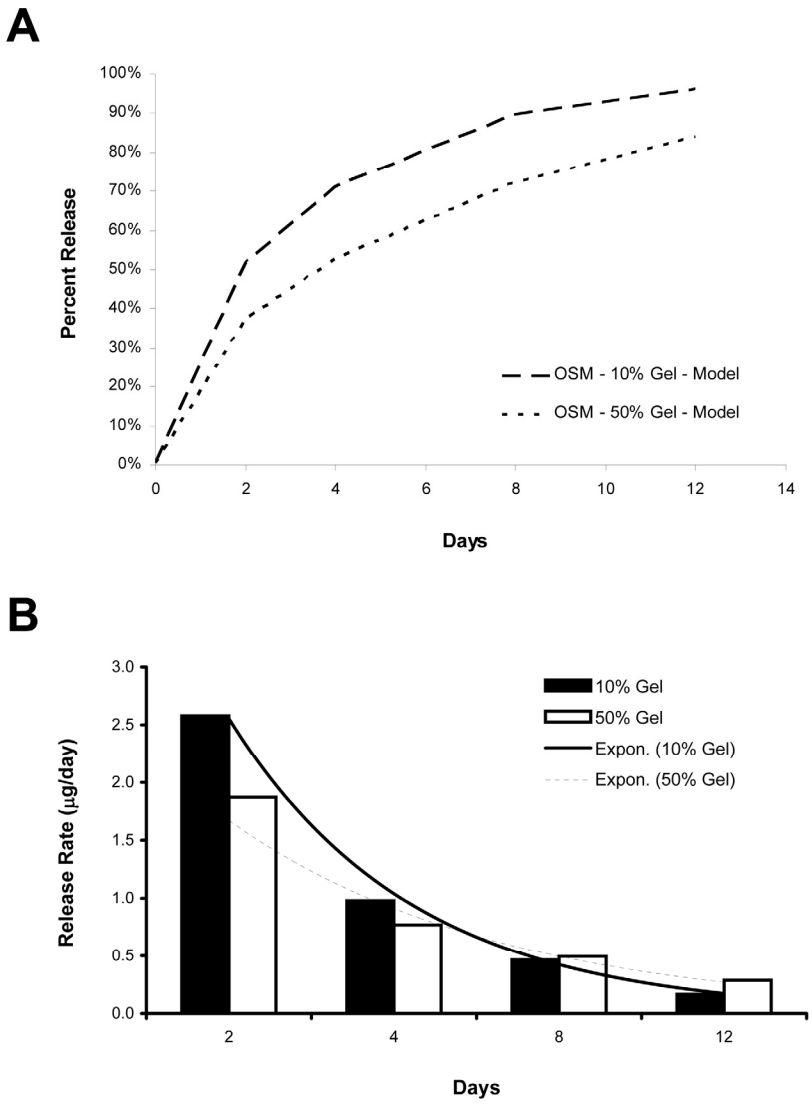


Figure 3.26 Theoretical predictions for fractional release (A) and average release rate (B) of hOSM through 10 wt% and 50 wt% PEG hydrogels.

hOSM is relased out of both hydrogels in a time dependent manner, and as would be predicted, the drug comes out of 10% hydrogel at a faster rate than through the 50% hydrogel. The release rates of hOSM from both hydrogels decreases with time. However, the rate of decrease in the release rate is slower in the 50% hydrogel compared to 10% hydrogel (thin dotted line vs. thick solid line).

3.3.2.3. Drug Release Studies – *In Vitro*

For empirical estimation of drug release from the PEG 5000 hydrogels, 100 μg of hOSM (MW: 23kDa, r_s: 2.09x10^{-7} cm) encapsulated in 10 wt% and 50 wt% PEG hydrogels were synthesized as described in materials and methods. Immediately after polymerization, the hydrogels were weighed and placed in a 0.5 ml reservoir of PBS and maintained under continuous agitation. Agitation was carried out in a humidified environment to prevent evaporation of the aqueous solution. After 2 days, 4 days, 8 days and 12 days of agitation, 10 μl samples were taken out of the reservoir solution and replaced with an equal amount of PBS to maintain the same volume. Samples taken out at different time points were subjected to BCA assay for determination of protein concentration. Percent release of OSM from the hydrogel was estimated using these values. As expected, results revealed that OSM diffused out of both the 10% and 50% hydrogels in a time dependent manner (Figure 3.27). In agreement with previous observations, hydrogel with higher macromer content (50% gel) showed a slow release of the drug in comparison to the hydrogel with a low macromer content (10% gel). In 10% gel, ~95% of the drug diffused out by 12 days while in 50% gel, only 75% of the drug diffused out (Figure 3.27). When the drug encapsulated inside the hydrogel is changed to bovine serum albumin (BSA) which has a higher molecular weight and is bigger in size (MW: 69kDa, r_s: 3.02x10^{-7} cm), the release rates were clearly slower than those for hOSM. While ~95% of hOSM diffused out of the 10% gel by 12 days, only ~82% of BSA diffused out of a similar 10% PEG

hydrogel by the end of 12 days (compare figure 3.27 with 3.28). Again, while about 75% of hOSM diffused out of a 50% hydrogel by 12 days, only ~60% of BSA diffused out of a similar 50% hydrogel by the end of 12 days. Thus, both macromer composition and the size of the drug affect the release rates of a drug from hydrogel.

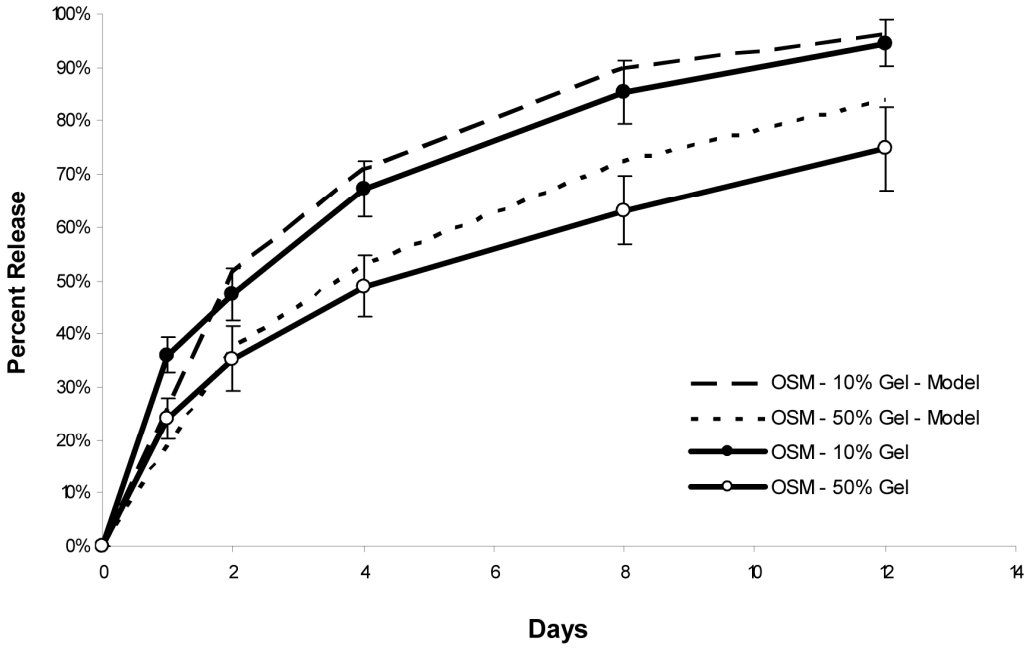


Figure 3.27 Percent release of hOSM from a 10% and 50% PEG hydrogel as a function of time.

In good agreement with the model, hOSM is released out of the PEG hydrogels in a time dependent manner. And, the release rate from 10% hydrogel is faster than the release rate from 50% hydrogel.

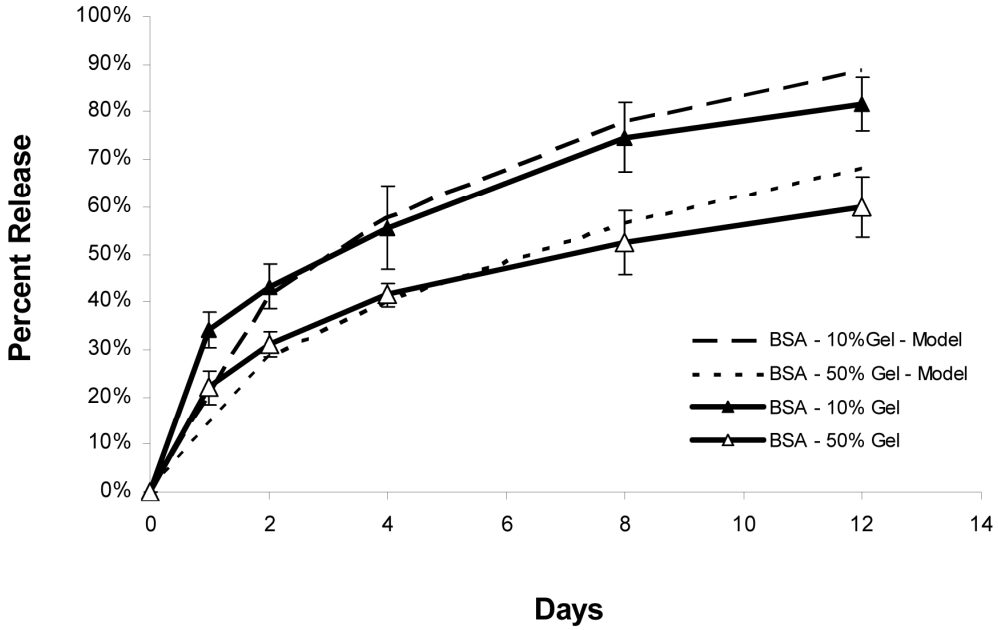


Figure 3.28 Percent release of BSA from a 10% and 50% PEG hydrogel as a function of time.

Again, in good agreement with the model, hOSM is released out of the PEG hydrogels in a time dependent manner. However, compared to the release of hOSM from similar hydrogels, release of BSA is significantly slower.

These empirical values for drug release from the hydrogel were in reasonably good agreement with the theoretically predicted values (Figures 3.27 and 3.28). However, there were two major deviations from the predictions. First, the empirically observed release rate was significantly higher during the first day in comparison to the model prediction. This could be because of sudden swelling of the hydrogel when placed in the reservoir, thus leading to a burst release of the drug. However, as shown earlier, the hydrogel stops swelling after the first two hours (Figure 3.23), thus preventing any further accelerated release thereafter. Second, in 50% gels, the final release of the drug by the end of 12 days found in these experiments was significantly lower than that predicted by the theoretical models. There are two factors that might potentially be playing a role here a) geometry of the protein and b) cross-reaction between the macromers and the proteins. Theoretical predictions for the release rates are based on the assumption that the drug molecules are spherical in shape (OSM radius: ~2.09 $x10^{-7}$ cm; BSA radius ~3.02 $x10^{-7}$ cm). However, unlike BSA, which is closer to a spherical geometry, hOSM assumes a cylindrical geometry with a height of ~5.0 $x10^{-7}$ cm and a radius of ~1.0 $x10^{-7}$ cm. In 10% gels, where the mesh size is ~12.1 $x10^{-7}$ cm, the drug sizes are relatively smaller and the shape does not affect the release rates significantly. However, in 50% gels where the mesh size is ~7.9 $x10^{-7}$ cm, the shape of the drugs would play a significant role and lead to deviations from theoretical predictions. Secondly, the highly reactive free radicals generated by the acrylate groups during photopolymerization can cross-react with the free amines present in proteins, thus leading to their permanent

immobilization in the hydrogels. Again, this effect is more pronounced in the 50% gels because of the high abundance of macromers and the reactive acrylate groups.

3.3.2.4. Drug Release Studies – *In Vivo*

PEG hydrogels (10% and 50%) loaded with 10μg of hOSM were implanted sub-conjunctivally at the posterior segment in Balb/cj mouse. The left eye was implanted with a blank gel to serve as a control. The mice were then placed back into their cages and maintained under normal cage room conditions. At desired time points, the mice were euthanized and the eyes were enucleated for Western blot analysis. In agreement with *in vitro* studies and release rate predictions (Figures 3.27 and 3.26B), Western blots show that there is a peak activation of STAT3 two days after the implantation followed by a decline in subsequent days (Figure 3.29). STAT3 activation sustained until 8 days post implantation and returned to basal levels by 12 days. The comparison between theoretical predictions and *in vivo* STAT3 activation pattern (Figure 3.30) also suggests that a release rate of at least 0.45 – 0.5 μg/day from the hydrogel is required to allow hOSM to overcome the clearance at choroid and RPE layers and induce STAT3 activation inside the retina. A 50% gel made with the PEG 5000 did not show a significant difference in terms of STAT3 activation profile. Theoretical estimation of release rates from the hydrogel explains the reason for this observation. In spite of a slower release from the 50% gel, the release rates were still well below

the 0.45 – 0.5 μg/day release rate at the 12th day. Clearance at the choroid layer renders this release rate insufficient for hOSM to reach the retina and induce detectable levels of STAT3 activation.

In agreement with the predictions, there is peak activation of STAT3 in the retina 2 days after implantation followed by a steady decrease. The model suggests that a release rate of at least 0.5 μg/day is required for OSM to pass through the choroid and RPE barriers to induce STAT3 activation in retina.

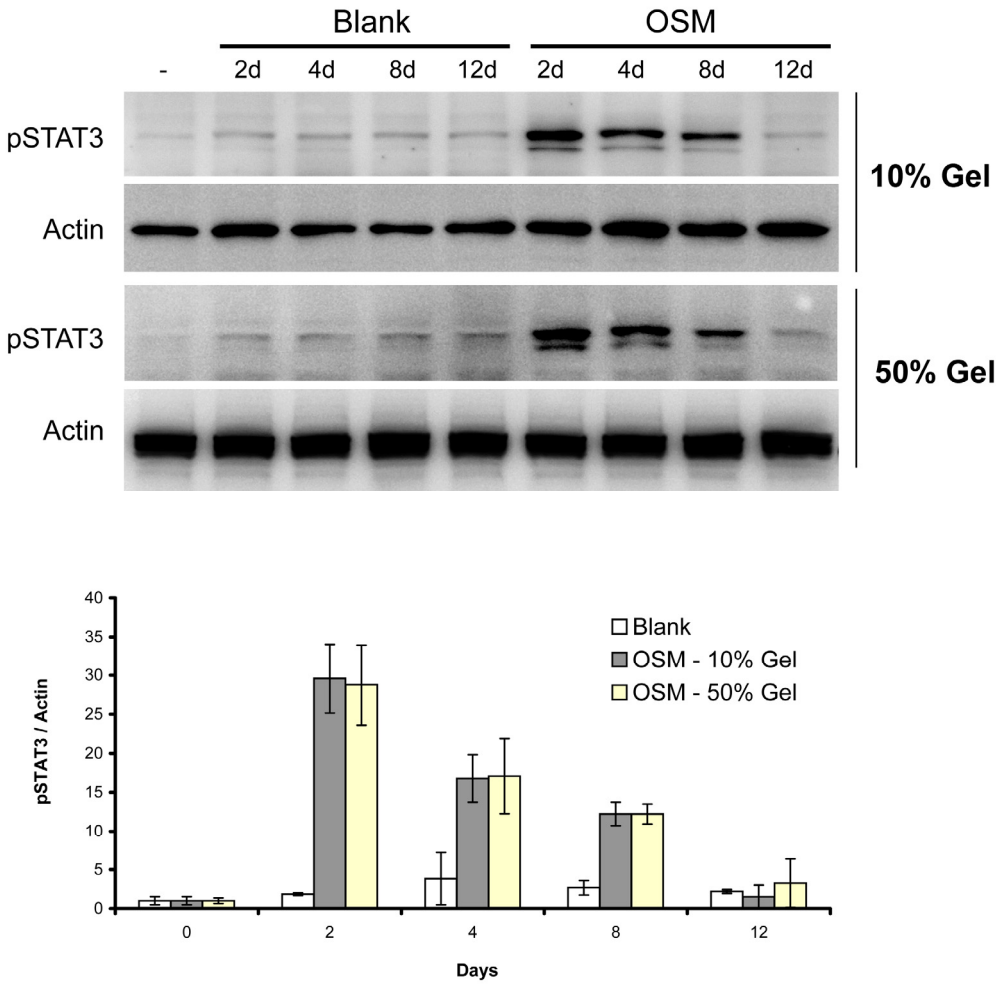


Figure 3.29 STAT3 activation profile in mouse retina after sub-conjunctival implantation with PEG hydrogels releasing hOSM.

In agreement with *in vitro* studies and theoretical predictions, STAT3 showed peak activation 2 days after implantation followed by a steady decline until it reached basal levels by the end of 12 days. While mathematical equations predicted a slightly slower and longer release from 50% gel, *in vivo* STAT3 activation showed a similar profile for both 10% and 50% gels.

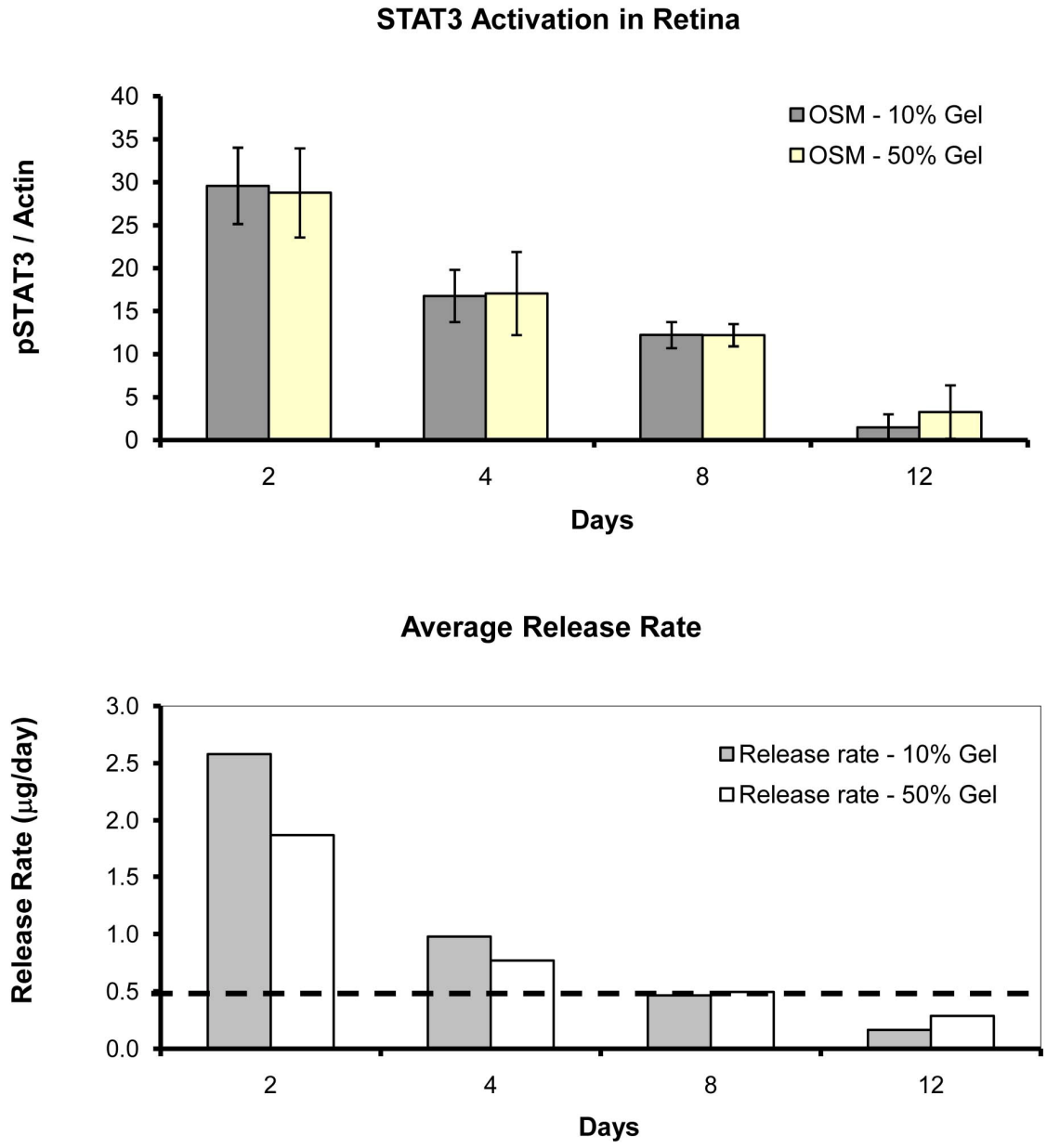


Figure 3.30 Comparison of STAT3 activation in the retina with theoretical predictions for release rate from the hydrogel (Figure 3.30 with Figure 3.27B).

3.3.3. Discussion

Most diseases in the posterior eye segment require treatment over long durations of time eg. AMD, retinitis pigmentosa, diabetic retinopahy. Owing to difficulties in delivery, intravitreal injection has been the method of choice for targeted delivery of therapeutic drugs to the posterior segment of the eye. However, repeated intravitreal injections often lead to serious complications such as vitreous hemorrhage, endophthalmitis and retinal detachment. On the other hand, one time delivery of large doses of drug can also lead to serious undesired side effects. Recently, transscleral drug delivery has been hypothesized to be an effective means for achieving therapeutic concentrations of drugs in the posterior part of the eye (330,335-337,339). It has been reported that scleral permeability is comparable to that of the corneal stroma (340,341). Similar to the corneal stroma route, the primary route for solute transport through sclera is by passive diffusion through an aqueous pathway.

Results in chapter 3.1 have shown that STAT3 activation induced by IL-6 family cytokines protect the retina from oxidative injury induced by bright light. Sustained delivery of these molecules to retina would thus prove valuable in treating a number of blinding diseases like retinitis pigmentosa, which lead to photoreceptor cell death mediated by oxidative stress. To aid this attempt, we have designed PEG based hydrogels to release hOSM in a sustained, time-dependent manner. Results have shown that the macromer content in hydrogels can be manipulated effectively to tailor the physical properties of the hydrogel.

Higher macromer content in a hydrogel leads to the fabrication of a more compact hydrogel network with smaller mesh sizes leading to low diffusivity of the drug molecule encapsulate inside the hydrogel. It takes about 12 days for 95% of hOSM to come out of a 10 wt% PEG 5000 hydrogel, while a 50 wt% PEG 5000 hydrogel allows only 75% of hOSM to diffuse out by the end of 12 days. When compared to theoretical model predictions, the empirical results showed good agreement in terms of drug release pattern from the PEG based hydrogels. However, empirical results showed the presence of a burst release of the drug initially. This can be attributed to the sudden swelling of the hydrogel when placed in PBS reservoir. Also, in gels made with 50% macromer, the release of the drug was significantly slower than that predicted by the models by the end of 12 days. This is probably an effect of the cross-reaction between highly reactive acrylate groups with the free amines on hOSM and also its non-spherical geometry.

When placed *in vivo*, hOSM released from the hydrogels induced STAT3 activation in the retina in a time-dependent manner as predicted by the model. Results suggest that a release rate of at least 0.45 – 0.5 μg/day is required for the hOSM to cross the choroids, RPE barriers and reach the retina to induce STAT3 activation. Together these results suggest that the physical properties of PEG hydrogels can be effectively manipulated to obtain desired drug release rates and when implanted in the eye, these hydrogels successfully release

hOSM in a sustained time-dependent manner leading to STAT3 activation in the retina.

4. CONCLUSIONS AND RECOMMENDATIONS

The current research has characterized the neuroprotective roles of IL-6 family cytokines in the context of retina followed by structural analysis of OSM and identifying its features that are responsible for its unique ability to display higher affinity towards gp130 rather than towards LIFR. As a result of this study, we have generated two mutant molecules of OSM that display higher potency in terms of activating the cell surface receptors and thereby executing the functions. In order to extend the therapeutic application of these molecules, we have characterized the utilization of PEG based hydrogels for controlled drug delivery.

Previous work has shown that preconditioning with moderate oxidative stress (e.g. light-induced stress, mechanical stress or hypoxic stress) can protect retinal photoreceptor cells from a subsequent lethal dose of oxidative stress (151-155,301,306). However, the mechanism for this inducible protection remained poorly understood. Based on previous studies (151,152), we have developed a preconditioning model by cyclically exposing the mice to stress inducing moderate bright light (600 lux) for 6 days (See figure 2.4 for model). Functional and morphological studies have revealed that this preconditioning shows remarkable protection of retinal photoreceptor cells from subsequent lethal dose of light stress (4000 lux for 4hrs). Real time RT-PCR analyses have shown that the neuroprotective cytokines belonging to IL-6 family are strongly up regulated in response to moderate oxidative stress. To check whether these cytokines are

playing a functional role in this preconditioning induced protection, we have exposed the retinal cells to LIFR inhibitor, LIF05, during preconditioning. Functional and morphological analyses following this inhibition showed a clear attenuation in the preconditioning-induced protection of the retinal photoreceptors. However, injection of LIF05 alone without preconditioning did not induce any photoreceptor cell death. This suggests that the activation of LIFR-gp130 pathway mediated by IL-6 family cytokines plays an essential role in bright cyclic light preconditioning induced protection of retinal photoreceptor cells. In addition, the results also suggested that LIFR activation is not required for the normal function and survival of photoreceptors at physiological conditions. In agreement with the studies by Joly et al., (150) our results demonstrate that IL-6 family cytokines endogenously upregulated in response to stress inside the retina are playing an essential role in protecting the photoreceptors from succumbing to oxidative stress.

While the Müller glial cells are widely hypothesized to be the source of these cytokines (150) it is not yet clear how the stress signals sensed by the photoreceptors are transmitted to the Müller cells and induce them to express IL-6 family cytokines. Joly et al., (150) and Rattner et al., (133) hypothesized that endothelin 2 (Edn2) secreted from photoreceptor cells in response to light stress stimulate Müller cells and induce them to express IL-6 family cytokines. However, it was again not clear whether the IL-6 family cytokines secreted from Müller cells directly act upon photoreceptor cells or induce an indirect signaling pathway via

activation of other cells in the retina that ultimately lead to protection of photoreceptor cells. Previous studies in our lab by Ueki et al., (149) have shown that IL-6 family cytokines can directly activate STAT3 in the photoreceptor cells (149). And, current studies in our lab show that the STAT3 activation, specifically in photoreceptor cells, is essential for the preconditioning induced protection. This suggests that, under stressed conditions, the IL-6 family cytokines secreted by Müller glial cells directly act upon the photoreceptor cells to trigger the activation of protective pathways which help the photoreceptors tolerate lethal stress and promote their survival (Figure 4.1). Future definitive studies on 1) identifying the molecules involved in transmitting the stress signals from photoreceptor cells to Müller glial cells and 2) identifying the molecular mechanism by which activated gp130 and STAT3 in photoreceptor cells leads to their survival would be very beneficial to the field. Studies identifying the target genes that are regulated by the activated transcription factor STAT3 in response to stress will provide clues for identifying the molecular mechanism involved in this induced protection. In addition, these results also suggest that designing potent agonists that can promote the actions of gp130 would prove very valuable in treating a number of blinding diseases like retinitis pigmentosa and age-related macular degeneration.

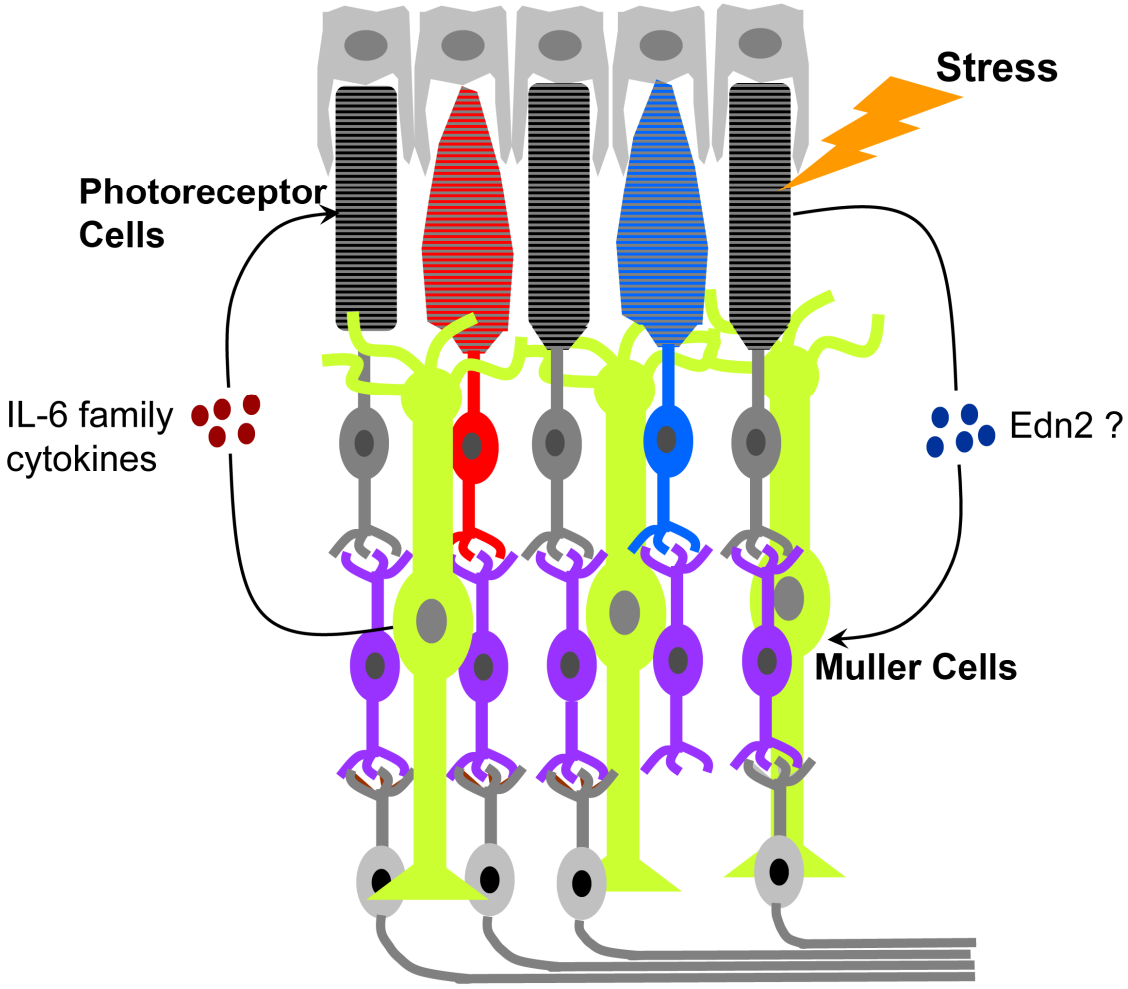


Figure 4.1 Schematic representation of hypothesized model for stress induced protection of photoreceptor cells.

Photoreceptor cells exposed to stress are hypothesized to release endothelin-2 (Edn2) which acts upon Müller cells to induce expression of IL-6 family cytokines. These IL-6 family cytokines directly activate LIFR:gp130 on the surface of photoreceptor cells triggering activation of signaling pathways that lead to photoreceptor survival.

In an attempt to design agonists for IL-6 family cytokines, we have closely studied the crystal structures of various IL-6 family cytokines. During this study we have identified a unique loop structure between the B and C helices of OSM which was not present on any other IL-6 family cytokine, including LIF which is closely related to OSM both in structure and function. Among IL-6 family cytokines, there has been an as yet unanswered question on how OSM, unlike other IL-6 family cytokines, can bind to a unique receptor called OSMR. Mutational analyses have revealed that OSM utilizes the same 'FXXK' motif, which is responsible for LIFR binding, to bind OSMR too (4). This has lead to a hypothesis that the difference in receptor specificity between hOSM and other LIFR activating cytokines is the result of structural differences between these ligands in the vicinity of the core 'FXXK' motif (4). Structural proximity to the 'FXXK' motif and the orientation of the unique BC loop we have identified on OSM has lead us to hypothesize that the BC loop might be playing an important role in OSM's unique ability to recognize OSMR. To test this, we have created mutant OSM proteins (OSM-M1 and OSM-M2) that have truncated BC loops. Surprisingly, OSMs with truncated BC loops (OSM-M1 and OSM-M2) displayed a

dramatic increase in potency in terms of activating the cell surface receptors OSMR: gp130. When tested for function on Müller cells that express LIFR and gp130, we found a similar behavior i.e. the mutant OSM molecules with truncated BC loops were more potent than the native cytokine. Re-analysis of OSM structure in comparison to LIF's structure in complex with its receptors LIFR and gp130 suggested that the BC loop on OSM might be presenting a steric hindrance for LIFR's interaction with OSM. In addition to the unique ability of OSM to bind OSMR, there is another abnormal behavior displayed by OSM i.e. unlike its other family members, OSM displays a high affinity towards gp130 than towards LIFR (21,23). Based on structural observations and the results we obtained, we hypothesized that the unique BC loop present on OSM is responsible for OSM's lowered affinity towards LIFR. Kinetic and equilibrium binding studies using SPR and ELISA have revealed that OSM with truncated BC loops display dramatic increase in their affinity towards both LIFR and OSMR compared to native OSM. This suggests that the BC loop on OSM presents a steric hindrance for OSM's interaction with LIFR. This is the first demonstration showing that a structural motif on OSM modulates its affinity towards LIFR by presenting a steric hindrance. The functional relevance of this lowered affinity towards LIFR is not known yet. However, during pregnancy there is a robust increase in the concentrations of soluble LIFR (sLIFR) in circulation (350) and this sLIFR negatively influences LIF levels by competitively binding the free LIF thus preventing it from activating membrane bound LIFR on cells. However, like LIF, if OSM were to exhibit a strong affinity towards LIFR it would also be

scavenged out of circulation severely compromising its ability to promote wound healing during period of pregnancy. *In vivo* studies investigating the role of BC loop in this context would be beneficial in assigning a functional role for the BC loop on OSM.

While conducting the binding experiments, we were however not able to detect any direct affinity for either OSM or its mutants towards OSMR. Similar observation has been reported for OSM earlier (4). However, in the presence of gp130, these molecules showed a strong affinity towards OSMR. This suggests that binding to gp130 might expose otherwise hidden residues on OSM required for OSMR binding or alter the OSM structure to move hindering residues away from the binding interface. Structural studies of OSM in complex with gp130 would be useful in characterizing the structural changes induced in OSM by gp130 binding. Similar affinity conversion was not observed towards LIFR. This suggests that unlike OSMR, LIFR and gp130 participate in a non-coopertaive binding to form the signaling complex with the cytokines.

Also, during this study we have demonstrated that the increase in potency of OSM by truncating its BC loop is functional; compared to the native OSM, both OSM-M1 and OSM-M2 display significantly higher ability in suppressing the proliferation of A375 melanoma cells. This increased potency in suppressing the melanoma cells would prove very valuable in treating cancer patients. However,

in vivo studies optimizing the dose ranges are needed to demonstrate the applicability of these mutant molecules for therapy.

Finally, for therapy, a proper drug delivery mode is needed to deliver these molecules, since high doses of these cytokines in circulation can be toxic and lead to serious side effects. For example, Ueki et al., (149) have shown that LIF protects the photoreceptors from oxidative stress induced by light damage. However, when delivered in large doses, it causes the unwanted side effect of lowering retinal function. Thus, for treatment of diseases like retinitis pigmentosa, a drug delivery mode which can deliver appropriate doses of IL-6 family cytokines in a sustained manner over long durations is highly desired. PEG hydrogels have been widely investigated for use in delivering a number of therapeutics *in vivo*. These hydrogels proved very biocompatible triggering minimal immune response. We have conducted studies and shown that the hydrogel properties can be effectively manipulated by varying the concentrations of macromer content. PEG hydrogels with 5000Da macromer size were found to be effective for delivering the cytokines over a period of 8 days *in vivo*. However, for treating the retinal degenerations, release rates over the order of months and years would be highly desirable. Manipulating the PEG macromer size might prove effective in attaining such release rates. Results also revealed that a release rate of at least 0.45 – 0.50 μg/day is required for hOSM to cross the choroid and RPE barriers to reach and induce STAT3 activation in retina. Thus,, further work in altering the molecular properties of hydrogels to obtain a steady

release rate of at least 0.5 μg/day OSM would prove very helpful in treating retinal degenerations.

BIBLIOGRAPHY

1. Zarling, J. M., Shoyab, M., Marquardt, H., Hanson, M. B., Lioubin, M. N., and Todaro, G. J. (1986) *Proc. Natl. Acad. Sci. U. S. A* **83,** 9739-9743

2. Malik, N., Kallestad, J. C., Gunderson, N. L., Austin, S. D., Neubauer, M. G., Ochs, V., Marquardt, H., Zarling, J. M., Shoyab, M., Wei, C. M., and . (1989) *Mol. Cell Biol.* **9,** 2847-2853

3. Linsley, P. S., Kallestad, J., Ochs, V., and Neubauer, M. (1990) *Mol. Cell Biol.* **10,** 1882-1890

4. Deller, M. C., Hudson, K. R., Ikemizu, S., Bravo, J., Jones, E. Y., and Heath, J. K. (2000) *Structure.* **8,** 863-874

5. Tanaka, M. and Miyajima, A. (2003) *Rev. Physiol Biochem. Pharmacol.* **149,** 39-52

6. Gomez-Lechon, M. J. (1999) *Life Sci.* **65,** 2019-2030

7. Bazan, J. F. (1990) *Immunol. Today* **11,** 350-354

8. Bazan, J. F. (1990) *Proc. Natl. Acad. Sci. U. S. A* **87,** 6934-6938

9. Bazan, J. F. (1993) *Curr. Biol.* **3,** 603-606

10. Nicola, N. A. and Hilton, D. J. (1998) *Adv. Protein Chem.* **52,** 1-65

11. Davies, D. R. and Wlodawer, A. (1995) *FASEB J.* **9,** 50-56

12. Boulay, J. L. and Paul, W. E. (1993) *Curr. Biol.* **3,** 573-581

13. Heinrich, P. C., Behrmann, I., Muller-Newen, G., Schaper, F., and Graeve, L. (1998) *Biochem. J.* **334 (Pt 2),** 297-314

14. Heinrich, P. C., Behrmann, I., Haan, S., Hermanns, H. M., Muller-Newen, G., and Schaper, F. (2003) *Biochem. J.* **374,** 1-20

15. Boulanger, M. J. and Garcia, K. C. (2004) *Adv. Protein Chem.* **68,** 107-146

16. Cosman, D. (1993) *Cytokine* **5,** 95-106

17. Boulton, T. G., Stahl, N., and Yancopoulos, G. D. (1994) *J. Biol. Chem.* **269,** 11648-11655

18. Davis, S., Aldrich, T. H., Stahl, N., Pan, L., Taga, T., Kishimoto, T., Ip, N. Y., and Yancopoulos, G. D. (1993) *Science* **260,** 1805-1808

19. Davis, S., Aldrich, T. H., Valenzuela, D. M., Wong, V. V., Furth, M. E., Squinto, S. P., and Yancopoulos, G. D. (1991) *Science* **253,** 59-63

20. Sleeman, M. W., Anderson, K. D., Lambert, P. D., Yancopoulos, G. D., and Wiegand, S. J. (2000) *Pharm. Acta Helv.* **74,** 265-272

21. Gearing, D. P., Comeau, M. R., Friend, D. J., Gimpel, S. D., Thut, C. J., McGourty, J., Brasher, K. K., King, J. A., Gillis, S., Mosley, B., and . (1992) *Science* **255,** 1434-1437

22. Gearing, D. P., Thut, C. J., VandeBos, T., Gimpel, S. D., Delaney, P. B., King, J., Price, V., Cosman, D., and Beckmann, M. P. (1991) *EMBO J.* **10,** 2839-2848

23. Mosley, B., De, I. C., Friend, D., Boiani, N., Thoma, B., Park, L. S., and Cosman, D. (1996) *J. Biol. Chem.* **271,** 32635-32643

24. Kishimoto, T., Hibi, M., Murakami, M., Narazaki, M., Saito, M., and Taga, T. (1992) *Ciba Found. Symp.* **167,** 5-16

25. Liu, J., Modrell, B., Aruffo, A., Marken, J. S., Taga, T., Yasukawa, K., Murakami, M., Kishimoto, T., and Shoyab, M. (1992) *J. Biol. Chem.* **267,** 16763-16766

26. Murakami, M., Hibi, M., Nakagawa, N., Nakagawa, T., Yasukawa, K., Yamanishi, K., Taga, T., and Kishimoto, T. (1993) *Science* **260,** 1808-1810

27. Taga, T., Hibi, M., Murakami, M., Saito, M., Yawata, H., Narazaki, M., Hirata, Y., Sugita, T., Yasukawa, K., Hirano, T., and . (1992) *Chem. Immunol.* **51,** 181-204

28. Hilton, D. J., Hilton, A. A., Raicevic, A., Rakar, S., Harrison-Smith, M., Gough, N. M., Begley, C. G., Metcalf, D., Nicola, N. A., and Willson, T. A. (1994) *EMBO J.* **13,** 4765-4775

29. Yamasaki, K., Taga, T., Hirata, Y., Yawata, H., Kawanishi, Y., Seed, B., Taniguchi, T., Hirano, T., and Kishimoto, T. (1988) *Science* **241,** 825-828

30. Robledo, O., Fourcin, M., Chevalier, S., Guillet, C., Auguste, P., Pouplard-Barthelaix, A., Pennica, D., and Gascan, H. (1997) *J. Biol. Chem.* **272,** 4855-4863

31. Jones, S. A., Richards, P. J., Scheller, J., and Rose-John, S. (2005) *J. Interferon Cytokine Res.* **25,** 241-253

32. Marz, P., Otten, U., and Rose-John, S. (1999) *Eur. J. Neurosci.* **11,** 2995-3004

33. Marz, P., Herget, T., Lang, E., Otten, U., and Rose-John, S. (1997) *Eur. J. Neurosci.* **9,** 2765-2773

34. Thier, M., Marz, P., Otten, U., Weis, J., and Rose-John, S. (1999) *J. Neurosci. Res.* **55,** 411-422

35. Klouche, M., Bhakdi, S., Hemmes, M., and Rose-John, S. (1999) *J. Immunol.* **163,** 4583-4589

36. Romano, M., Sironi, M., Toniatti, C., Polentarutti, N., Fruscella, P., Ghezzi, P., Faggioni, R., Luini, W., van, H., V, Sozzani, S., Bussolino, F., Poli, V., Ciliberto, G., and Mantovani, A. (1997) *Immunity.* **6,** 315-325

37. Mackiewicz, A., Wiznerowicz, M., Roeb, E., Nowak, J., Pawlowski, T., Baumann, H., Heinrich, P. C., and Rose-John, S. (1995) *Ann. N. Y. Acad. Sci.* **762,** 361-373

38. Bazan, J. F. (1990) *Cell* **61,** 753-754

39. de Vos, A. M., Ultsch, M., and Kossiakoff, A. A. (1992) *Science* **255,** 306-312

40. Yawata, H., Yasukawa, K., Natsuka, S., Murakami, M., Yamasaki, K., Hibi, M., Taga, T., and Kishimoto, T. (1993) *EMBO J.* **12,** 1705-1712

41. Boulanger, M. J., Bankovich, A. J., Kortemme, T., Baker, D., and Garcia, K. C. (2003) *Mol. Cell* **12,** 577-589

42. Livnah, O., Stura, E. A., Johnson, D. L., Middleton, S. A., Mulcahy, L. S., Wrighton, N. C., Dower, W. J., Jolliffe, L. K., and Wilson, I. A. (1996) *Science* **273,** 464-471

43. Boulanger, M. J., Chow, D. C., Brevnova, E. E., and Garcia, K. C. (2003) *Science* **300,** 2101-2104

44. Cunningham, B. C., Ultsch, M., de Vos, A. M., Mulkerrin, M. G., Clauser, K. R., and Wells, J. A. (1991) *Science* **254,** 821-825

45. Inoue, M., Nakayama, C., Kikuchi, K., Kimura, T., Ishige, Y., Ito, A., Kanaoka, M., and Noguchi, H. (1995) *Proc. Natl. Acad. Sci. U. S. A* **92,** 8579-8583

46. Paonessa, G., Graziani, R., De, S. A., Savino, R., Ciapponi, L., Lahm, A., Salvati, A. L., Toniatti, C., and Ciliberto, G. (1995) *EMBO J.* **14,** 1942-1951

47. Di, M. A., Gloaguen, I., Graziani, R., Paonessa, G., Saggio, I., Hudson, K. R., and Laufer, R. (1996) *Proc. Natl. Acad. Sci. U. S. A* **93,** 9247-9252

48. Hudson, K. R., Vernallis, A. B., and Heath, J. K. (1996) *J. Biol. Chem.* **271,** 11971-11978

49. Heinrich, P. C., Graeve, L., Rose-John, S., Schneider-Mergener, J., Dittrich, E., Erren, A., Gerhartz, C., Hemann, U., Lutticken, C., Wegenka, U., and . (1995) *Ann. N. Y. Acad. Sci.* **762,** 222-236

50. Auguste, P., Guillet, C., Fourcin, M., Olivier, C., Veziers, J., Pouplard-Barthelaix, A., and Gascan, H. (1997) *J. Biol. Chem.* **272,** 15760-15764

51. Murray, P. J. (2007) *J. Immunol.* **178,** 2623-2629

52. Darnell, J. E., Jr., Kerr, I. M., and Stark, G. R. (1994) *Science* **264,** 1415-1421

53. Schindler, C., Levy, D. E., and Decker, T. (2007) *J. Biol. Chem.* **282,** 20059-20063

54. Ihle, J. N. (2001) *Curr. Opin. Cell Biol.* **13,** 211-217

55. Leonard, W. J. and O'Shea, J. J. (1998) *Annu. Rev. Immunol.* **16,** 293-322

56. Dong, C., Davis, R. J., and Flavell, R. A. (2002) *Annu. Rev. Immunol.* **20,** 55-72

57. Cantley, L. C. (2002) *Science* **296,** 1655-1657

58. Kelly-Welch, A., Hanson, E. M., and Keegan, A. D. (2005) *Sci. STKE.* **2005,** cm9

59. Bravo, J., Staunton, D., Heath, J. K., and Jones, E. Y. (1998) *EMBO J.* **17,** 1665-1674

60. Horsten, U., Muller-Newen, G., Gerhartz, C., Wollmer, A., Wijdenes, J., Heinrich, P. C., and Grotzinger, J. (1997) *J. Biol. Chem.* **272,** 23748-23757

61. Skiniotis, G., Lupardus, P. J., Martick, M., Walz, T., and Garcia, K. C. (2008) *Mol. Cell* **31,** 737-748

62. Somers, W., Stahl, M., and Seehra, J. S. (1997) *EMBO J.* **16,** 989-997

63. Tacken, I., Dahmen, H., Boisteau, O., Minvielle, S., Jacques, Y., Grotzinger, J., Kuster, A., Horsten, U., Blanc, C., Montero-Julian, F. A.,

Heinrich, P. C., and Muller-Newen, G. (1999) *Eur. J. Biochem.* **265,** 645-655

64. Huyton, T., Zhang, J. G., Luo, C. S., Lou, M. Z., Hilton, D. J., Nicola, N. A., and Garrett, T. P. (2007) *Proc. Natl. Acad. Sci. U. S. A* **104,** 12737-12742

65. Barton, V. A., Hudson, K. R., and Heath, J. K. (1999) *J. Biol. Chem.* **274,** 5755-5761

66. Ehlers, M., Grotzinger, J., deHon, F. D., Mullberg, J., Brakenhoff, J. P., Liu, J., Wollmer, A., and Rose-John, S. (1994) *J. Immunol.* **153,** 1744-1753

67. Czupryn, M., Bennett, F., Dube, J., Grant, K., Scoble, H., Sookdeo, H., and McCoy, J. M. (1995) *Ann. N. Y. Acad. Sci.* **762,** 152-164

68. Kruttgen, A., Grotzinger, J., Kurapkat, G., Weis, J., Simon, R., Thier, M., Schroder, M., Heinrich, P., Wollmer, A., Comeau, M., and . (1995) *Biochem. J.* **309 (Pt 1),** 215-220

69. Thier, M., Simon, R., Kruttgen, A., Rose-John, S., Heinrich, P. C., Schroder, J. M., and Weis, J. (1995) *J. Neurosci. Res.* **40,** 826-835

70. Plun-Favreau, H., Elson, G., Chabbert, M., Froger, J., deLapeyriere, O., Lelievre, E., Guillet, C., Hermann, J., Gauchat, J. F., Gascan, H., and Chevalier, S. (2001) *EMBO J.* **20,** 1692-1703

71. Skiniotis, G., Boulanger, M. J., Garcia, K. C., and Walz, T. (2005) *Nat. Struct. Mol. Biol.* **12,** 545-551

72. Chen, R. W. and Postlethwait, R. W. (1964) *Monogr Surg. Sci.* **16,** 215-276

73. Teller, P. and White, T. K. (2009) *Surg. Clin. North Am.* **89,** 599-610

74. Korpos, E., Wu, C., Song, J., Hallmann, R., and Sorokin, L. (2009) *Cell Tissue Res.*

75. Korpos, E., Wu, C., and Sorokin, L. (2009) *Curr. Pharm. Des* **15,** 1349-1357

76. Saharinen, P., Eklund, L., Miettinen, J., Wirkkala, R., Anisimov, A., Winderlich, M., Nottebaum, A., Vestweber, D., Deutsch, U., Koh, G. Y., Olsen, B. R., and Alitalo, K. (2008) *Nat. Cell Biol.* **10,** 527-537

77. Vestweber, D., Winderlich, M., Cagna, G., and Nottebaum, A. F. (2009) *Trends Cell Biol.* **19,** 8-15

78. Garrido-Urbani, S., Bradfield, P. F., Lee, B. P., and Imhof, B. A. (2008) *Biochem. Soc. Trans.* **36,** 203-211

79. Adamson, R. (2009) *J. Wound. Care* **18,** 349-351

80. Glaros, T., Larsen, M., and Li, L. (2009) *Front Biosci.* **14,** 3988-3993

81. Hoenig, M. R., Bianchi, C., and Sellke, F. W. (2008) *Curr. Drug Targets.* **9,** 422-435

82. Ochoa, O., Torres, F. M., and Shireman, P. K. (2007) *Vascular.* **15,** 350-355

83. Yager, D. R., Kulina, R. A., and Gilman, L. A. (2007) *Int. J. Low Extrem. Wounds.* **6,** 262-272

84. Grenier, A., Dehoux, M., Boutten, A., rce-Vicioso, M., Durand, G., Gougerot-Pocidalo, M. A., and Chollet-Martin, S. (1999) *Blood* **93,** 1413-1421

85. Boniface, K., Diveu, C., Morel, F., Pedretti, N., Froger, J., Ravon, E., Garcia, M., Venereau, E., Preisser, L., Guignouard, E., Guillet, G., Dagregorio, G., Pene, J., Moles, J. P., Yssel, H., Chevalier, S., Bernard, F. X., Gascan, H., and Lecron, J. C. (2007) *J. Immunol.* **178,** 4615-4622

86. Brown, T. J., Rowe, J. M., Liu, J. W., and Shoyab, M. (1991) *J. Immunol.* **147,** 2175-2180

87. Richards, C. D., Brown, T. J., Shoyab, M., Baumann, H., and Gauldie, J. (1992) *J. Immunol.* **148,** 1731-1736

88. Koj, A., Rokita, H., Pierzchalski, P., Kordula, T., Guzdek, A., and Bereta, J. (1992) *Folia Histochem. Cytobiol.* **30,** 143-145

89. Koj, A., Rokita, H., Kordula, T., Kurdowska, A., and Travis, J. (1991) *Biomed. Biochim. Acta* **50,** 421-425

90. Kordula, T., Rokita, H., Koj, A., Fiers, W., Gauldie, J., and Baumann, H. (1991) *Lymphokine Cytokine Res.* **10,** 23-26

91. Rokita, H., Falus, A., Biro, J., Smolen, J., Kordula, T., and Stalinska, K. (1992) *Scand. J. Immunol.* **35,** 681-685

92. Nesbitt, J. E., Fuentes, N. L., and Fuller, G. M. (1993) *Biochem. Biophys. Res. Commun.* **190,** 544-550

93. Schooltink, H., Stoyan, T., Lenz, D., Schmitz, H., Hirano, T., Kishimoto, T., Heinrich, P. C., and Rose-John, S. (1991) *Biochem. J.* **277 (Pt 3),** 659-664

94. Barton, B. E. (1997) *Clin. Immunol. Immunopathol.* **85,** 16-20

95. Kaibara, A., Espat, N. J., Auffenberg, T., Abouhamze, A. S., Martin, D., Kalra, S., and Moldawer, L. L. (1998) *Cytokine* **10,** 452-456

96. Gabay, C., Singwe, M., Genin, B., Meyer, O., Mentha, G., LeCoultre, C., Vischer, T., and Guerne, P. A. (1996) *Clin. Exp. Immunol.* **105,** 260-265

97. Modur, V., Feldhaus, M. J., Weyrich, A. S., Jicha, D. L., Prescott, S. M., Zimmerman, G. A., and McIntyre, T. M. (1997) *J. Clin. Invest* **100,** 158-168

98. Yao, L., Pan, J., Setiadi, H., Patel, K. D., and McEver, R. P. (1996) *J. Exp. Med.* **184,** 81-92

99. Woessner, J. F., Jr. (1991) *FASEB J.* **5,** 2145-2154

100. Cawston, T., Plumpton, T., Curry, V., Ellis, A., and Powell, L. (1994) *Ann. N. Y. Acad. Sci.* **732,** 75-83

101. Cawston, T., Billington, C., Cleaver, C., Elliott, S., Hui, W., Koshy, P., Shingleton, B., and Rowan, A. (1999) *Ann. N. Y. Acad. Sci.* **878,** 120-129

102. Cawston, T. E. and Billington, C. (1996) *J. Pathol.* **180,** 115-117

103. Clark, I. M., Powell, L. K., and Cawston, T. E. (1994) *Biochem. Biophys. Res. Commun.* **203,** 874-880

104. Ellis, A. J., Curry, V. A., Powell, E. K., and Cawston, T. E. (1994) *Biochem. Biophys. Res. Commun.* **201,** 94-101

105. Richards, C. D., Shoyab, M., Brown, T. J., and Gauldie, J. (1993) *J. Immunol.* **150,** 5596-5603

106. Korzus, E., Nagase, H., Rydell, R., and Travis, J. (1997) *J. Biol. Chem.* **272,** 1188-1196

107. Carroll, G., Bell, M., Wang, H., Chapman, H., and Mills, J. (1998) *Inflamm. Res.* **47,** 1-7

108. Houssiau, F. A., Devogelaer, J. P., Van, D. J., de Deuxchaisnes, C. N., and Van, S. J. (1988) *Arthritis Rheum.* **31,** 784-788

109. De, B. F., Robbioni, P., Massa, M., Viola, S., Albani, S., and Martini, A. (1992) *Clin. Exp. Rheumatol.* **10,** 493-498

110. De, B. F., Massa, M., Robbioni, P., Ravelli, A., Burgio, G. R., and Martini, A. (1991) *Arthritis Rheum.* **34,** 1158-1163

111. De, B. F., Massa, M., Pignatti, P., Albani, S., Novick, D., and Martini, A. (1994) *J. Clin. Invest* **93,** 2114-2119

112. Guerne, P. A., Zuraw, B. L., Vaughan, J. H., Carson, D. A., and Lotz, M. (1989) *J. Clin. Invest* **83,** 585-592

113. Kotake, S., Sato, K., Kim, K. J., Takahashi, N., Udagawa, N., Nakamura, I., Yamaguchi, A., Kishimoto, T., Suda, T., and Kashiwazaki, S. (1996) *J. Bone Miner. Res.* **11,** 88-95

114. Robak, T., Gladalska, A., Stepien, H., and Robak, E. (1998) *Mediators. Inflamm.* **7,** 347-353

115. Lotz, M., Moats, T., and Villiger, P. M. (1992) *J. Clin. Invest* **90,** 888-896

116. Okamoto, H., Yamamura, M., Morita, Y., Harada, S., Makino, H., and Ota, Z. (1997) *Arthritis Rheum.* **40,** 1096-1105

117. Waring, P. M., Carroll, G. J., Kandiah, D. A., Buirski, G., and Metcalf, D. (1993) *Arthritis Rheum.* **36,** 911-915

118. Hui, W., Bell, M., and Carroll, G. (1997) *Ann. Rheum. Dis.* **56,** 184-187

119. Cornish, J., Callon, K., King, A., Edgar, S., and Reid, I. R. (1993) *Endocrinology* **132,** 1359-1366

120. Lowe, C., Cornish, J., Martin, T. J., and Reid, I. R. (1991) *Calcif. Tissue Int.* **49,** 394-397

121. Reid, L. R., Lowe, C., Cornish, J., Skinner, S. J., Hilton, D. J., Willson, T. A., Gearing, D. P., and Martin, T. J. (1990) *Endocrinology* **126,** 1416-1420

122. Hamilton, J. A., Waring, P. M., and Filonzi, E. L. (1993) *J. Immunol.* **150,** 1496-1502

123. Bell, M. C., Carroll, G. J., Chapman, H. M., Mills, J. N., and Hui, W. (1999) *Arthritis Rheum.* **42,** 2543-2551

124. Carroll, G. J., Bell, M. C., Chapman, H. M., Mills, J. N., and Robinson, W. F. (1995) *J. Interferon Cytokine Res.* **15,** 567-573

125. Cornish, J., Callon, K. E., Edgar, S. G., and Reid, I. R. (1997) *Bone* **21,** 243-247

126. Lowe, C., Cornish, J., Callon, K., Martin, T. J., and Reid, I. R. (1991) *J. Bone Miner. Res.* **6,** 1277-1283

127. Takagi, N., Mihara, M., Moriya, Y., Nishimoto, N., Yoshizaki, K., Kishimoto, T., Takeda, Y., and Ohsugi, Y. (1998) *Arthritis Rheum.* **41,** 2117-2121

128. DeChiara, T. M., Vejsada, R., Poueymirou, W. T., Acheson, A., Suri, C., Conover, J. C., Friedman, B., McClain, J., Pan, L., Stahl, N., Ip, N. Y., and Yancopoulos, G. D. (1995) *Cell* **83,** 313-322

129. Stewart, C. L., Kaspar, P., Brunet, L. J., Bhatt, H., Gadi, I., Kontgen, F., and Abbondanzo, S. J. (1992) *Nature* **359,** 76-79

130. Ware, C. B., Horowitz, M. C., Renshaw, B. R., Hunt, J. S., Liggitt, D., Koblar, S. A., Gliniak, B. C., McKenna, H. J., Papayannopoulou, T., Thoma, B., and . (1995) *Development* **121,** 1283-1299

131. Li, M., Sendtner, M., and Smith, A. (1995) *Nature* **378,** 724-727

132. Chen, S. H., Gillespie, G. Y., and Benveniste, E. N. (2006) *Glia* **53,** 191-200

133. Rattner, A. and Nathans, J. (2005) *J. Neurosci.* **25,** 4540-4549

134. Rattner, A., Toulabi, L., Williams, J., Yu, H., and Nathans, J. (2008) *J. Neurosci.* **28,** 9880-9889

135. Choi, J. S., Kim, S. Y., Cha, J. H., Choi, Y. S., Sung, K. W., Oh, S. T., Kim, O. N., Chung, J. W., Chun, M. H., Lee, S. B., and Lee, M. Y. (2003) *Glia* **41,** 237-246

136. Weiss, T. W., Samson, A. L., Niego, B., Daniel, P. B., and Medcalf, R. L. (2006) *FASEB J.* **20,** 2369-2371

137. Linker, R. A., Maurer, M., Gaupp, S., Martini, R., Holtmann, B., Giess, R., Rieckmann, P., Lassmann, H., Toyka, K. V., Sendtner, M., and Gold, R. (2002) *Nat. Med.* **8,** 620-624

138. Anderson, K. D., Panayotatos, N., Corcoran, T. L., Lindsay, R. M., and Wiegand, S. J. (1996) *Proc. Natl. Acad. Sci. U. S. A* **93,** 7346-7351

139. Emerich, D. F., Winn, S. R., Hantraye, P. M., Peschanski, M., Chen, E. Y., Chu, Y., McDermott, P., Baetge, E. E., and Kordower, J. H. (1997) *Nature* **386,** 395-399

140. Sendtner, M., Schmalbruch, H., Stockli, K. A., Carroll, P., Kreutzberg, G. W., and Thoenen, H. (1992) *Nature* **358,** 502-504

141. Sendtner, M., Arakawa, Y., Stockli, K. A., Kreutzberg, G. W., and Thoenen, H. (1991) *J. Cell Sci. Suppl* **15,** 103-109

142. Sendtner, M., Kreutzberg, G. W., and Thoenen, H. (1990) *Nature* **345,** 440-441

143. Murphy, M., Reid, K., Ford, M., Furness, J. B., and Bartlett, P. F. (1994) *Development* **120,** 3519-3528

144. Murphy, M., Reid, K., Hilton, D. J., and Bartlett, P. F. (1991) *Proc. Natl. Acad. Sci. U. S. A* **88,** 3498-3501

145. Adler, R. (1993) *Curr. Opin. Neurobiol.* **3,** 785-789

146. LaVail, M. M., Unoki, K., Yasumura, D., Matthes, M. T., Yancopoulos, G. D., and Steinberg, R. H. (1992) *Proc. Natl. Acad. Sci. U. S. A* **89,** 11249-11253

147. LaVail, M. M., Yasumura, D., Matthes, M. T., Lau-Villacorta, C., Unoki, K., Sung, C. H., and Steinberg, R. H. (1998) *Invest Ophthalmol. Vis. Sci.* **39,** 592-602

148. LaVail, M. M., Faktorovich, E. G., Hepler, J. M., Pearson, K. L., Yasumura, D., Matthes, M. T., and Steinberg, R. H. (1991) *Ann. N. Y. Acad. Sci.* **638,** 341-347

149. Ueki, Y., Wang, J., Chollangi, S., and Ash, J. D. (2008) *J. Neurochem.* **105,** 784-796

150. Joly, S., Lange, C., Thiersch, M., Samardzija, M., and Grimm, C. (2008) *J. Neurosci.* **28,** 13765-13774

151. Li, F., Cao, W., and Anderson, R. E. (2003) *Invest Ophthalmol. Vis. Sci.* **44,** 4968-4975

152. Li, F., Cao, W., and Anderson, R. E. (2001) *Exp. Eye Res.* **73,** 569-577

153. Liu, C., Peng, M., Laties, A. M., and Wen, R. (1998) *J. Neurosci.* **18,** 1337-1344

154. Grimm, C., Wenzel, A., Groszer, M., Mayser, H., Seeliger, M., Samardzija, M., Bauer, C., Gassmann, M., and Reme, C. E. (2002) *Nat. Med.* **8,** 718-724

155. Grimm, C., Hermann, D. M., Bogdanova, A., Hotop, S., Kilic, U., Wenzel, A., Kilic, E., and Gassmann, M. (2005) *Semin. Cell Dev. Biol.* **16,** 531-538

156. Muckenthaler, M. U., Galy, B., and Hentze, M. W. (2008) *Annu. Rev. Nutr.* **28,** 197-213

157. Yoshimura, A., Ichihara, M., Kinjyo, I., Moriyama, M., Copeland, N. G., Gilbert, D. J., Jenkins, N. A., Hara, T., and Miyajima, A. (1996) *EMBO J.* **15,** 1055-1063

158. Ikebuchi, K., Wong, G. G., Clark, S. C., Ihle, J. N., Hirai, Y., and Ogawa, M. (1987) *Proc. Natl. Acad. Sci. U. S. A* **84,** 9035-9039

159. Leary, A. G., Ikebuchi, K., Hirai, Y., Wong, G. G., Yang, Y. C., Clark, S. C., and Ogawa, M. (1988) *Blood* **71,** 1759-1763

160. Wong, G. G., Witek-Giannotti, J. S., Temple, P. A., Kriz, R., Ferenz, C., Hewick, R. M., Clark, S. C., Ikebuchi, K., and Ogawa, M. (1988) *J. Immunol.* **140,** 3040-3044

161. Ishibashi, T., Kimura, H., Shikama, Y., Uchida, T., Kariyone, S., Hirano, T., Kishimoto, T., Takatsuki, F., and Akiyama, Y. (1989) *Blood* **74,** 1241-1244

162. Asano, S., Okano, A., Ozawa, K., Nakahata, T., Ishibashi, T., Koike, K., Kimura, H., Tanioka, Y., Shibuya, A., Hirano, T., and . (1990) *Blood* **75,** 1602-1605

163. Suzuki, H., Ikebuchi, K., Wada, Y., Okano, A., Nakamiya, T., Akiyama, Y., Sawada, T., Asano, S., and Nakahata, T. (1997) *Transplantation* **64,** 1468-1473

164. Suzuki, H., Okano, A., Ejima, C., Konishi, A., Akiyama, Y., Ozawa, K., and Asano, S. (1996) *Jpn. J. Cancer Res.* **87,** 938-944

165. Metcalf, D., Nicola, N. A., and Gearing, D. P. (1990) *Blood* **76,** 50-56

166. Mayer, P., Geissler, K., Ward, M., and Metcalf, D. (1993) *Blood* **81,** 3226-3233

167. Shabo, Y., Lotem, J., Rubinstein, M., Revel, M., Clark, S. C., Wolf, S. F., Kamen, R., and Sachs, L. (1988) *Blood* **72,** 2070-2073

168. Oritani, K., Kaisho, T., Nakajima, K., and Hirano, T. (1992) *Blood* **80,** 2298-2305

169. Revel, M. (1992) *Res. Immunol.* **143,** 769-773

170. Horn, D., Fitzpatrick, W. C., Gompper, P. T., Ochs, V., Bolton-Hansen, M., Zarling, J., Malik, N., Todaro, G. J., and Linsley, P. S. (1990) *Growth Factors* **2,** 157-165

171. Liu, J., Spence, M. J., Wallace, P. M., Forcier, K., Hellstrom, I., and Vestal, R. E. (1997) *Cell Growth Differ.* **8,** 667-676

172. Halfter, H., Lotfi, R., Westermann, R., Young, P., Ringelstein, E. B., and Stogbauer, F. T. (1998) *Growth Factors* **15,** 135-147

173. Lacreusette, A., Nguyen, J. M., Pandolfino, M. C., Khammari, A., Dreno, B., Jacques, Y., Godard, A., and Blanchard, F. (2007) *Oncogene* **26,** 881-892

174. Liu, J., Hadjokas, N., Mosley, B., Estrov, Z., Spence, M. J., and Vestal, R. E. (1998) *Cytokine* **10,** 295-302

175. Miles, S. A., Martinez-Maza, O., Rezai, A., Magpantay, L., Kishimoto, T., Nakamura, S., Radka, S. F., and Linsley, P. S. (1992) *Science* **255,** 1432-1434

176. Nair, B. C., DeVico, A. L., Nakamura, S., Copeland, T. D., Chen, Y., Patel, A., O'Neil, T., Oroszlan, S., Gallo, R. C., and Sarngadharan, M. G. (1992) *Science* **255,** 1430-1432

177. Murakami-Mori, K., Taga, T., Kishimoto, T., and Nakamura, S. (1995) *J. Clin. Invest* **96,** 1319-1327

178. Ihn, H. and Tamaki, K. (2000) *J. Immunol.* **165,** 2149-2155

179. Grundy, S. M. (1998) *Circulation* **97,** 1436-1439

180. Ansell, B. J., Watson, K. E., Fogelman, A. M., Navab, M., and Fonarow, G. C. (2005) *J. Am. Coll. Cardiol.* **46,** 1792-1798

181. Ansell, B. J., Watson, K. E., and Fogelman, A. M. (1999) *JAMA* **282,** 2051-2057

182. Watson, K. E., Ansell, B. J., Watson, A. D., and Fonarow, G. C. (2007) *Rev. Cardiovasc. Med.* **8,** 1-8

183. Goldstein, J. L. and Brown, M. S. (1986) *Trans. Assoc. Am. Physicians* **99,** ccxxxi-ccxlvii

184. Goldstein, J. L. and Brown, M. S. (1990) *Nature* **343,** 425-430

185. Brown, M. S. and Goldstein, J. L. (1986) *Science* **232,** 34-47

186. Klotz, U. (2003) *Arzneimittelforschung.* **53,** 605-611

187. Parini, P., Angelin, B., Lobie, P. E., Norstedt, G., and Rudling, M. (1995) *Endocrinology* **136,** 3767-3773

188. Rudling, M., Norstedt, G., Olivecrona, H., Reihner, E., Gustafsson, J. A., and Angelin, B. (1992) *Proc. Natl. Acad. Sci. U. S. A* **89,** 6983-6987

189. Ostlund, R. E., Jr., Yang, J. W., Heath-Monnig, E., and Semenkovich, C. F. (1994) *Mol. Endocrinol.* **8,** 904-909

190. Semenkovich, C. F. and Ostlund, R. E., Jr. (1987) *Biochemistry* **26,** 4987-4992

191. Streicher, R., Kotzka, J., Muller-Wieland, D., and Krone, W. (1998) *Z. Ernahrungswiss.* **37 Suppl 1,** 85-87

192. Streicher, R., Kotzka, J., Muller-Wieland, D., Siemeister, G., Munck, M., Avci, H., and Krone, W. (1996) *J. Biol. Chem.* **271,** 7128-7133

193. Parini, P., Angelin, B., and Rudling, M. (1997) *Arterioscler. Thromb. Vasc. Biol.* **17,** 1800-1805

194. Pak, Y. K., Kanuck, M. P., Berrios, D., Briggs, M. R., Cooper, A. D., and Ellsworth, J. L. (1996) *J. Lipid Res.* **37,** 985-998

195. Stopeck, A. T., Nicholson, A. C., Mancini, F. P., and Hajjar, D. P. (1993) *J. Biol. Chem.* **268,** 17489-17494

196. Gierens, H., Nauck, M., Roth, M., Schinker, R., Schurmann, C., Scharnagl, H., Neuhaus, G., Wieland, H., and Marz, W. (2000) *Arterioscler. Thromb. Vasc. Biol.* **20,** 1777-1783

197. Scharnagl, H., Schinker, R., Gierens, H., Nauck, M., Wieland, H., and Marz, W. (2001) *Biochem. Pharmacol.* **62,** 1545-1555

198. Grove, R. I., Mazzucco, C., Allegretto, N., Kiener, P. A., Spitalny, G., Radka, S. F., Shoyab, M., Antonaccio, M., and Warr, G. A. (1991) *J. Lipid Res.* **32,** 1889-1897

199. Liu, J., Grove, R. I., and Vestal, R. E. (1994) *Cell Growth Differ.* **5,** 1333-1338

200. Liu, J., Shoyab, M., and Grove, R. I. (1993) *Cell Growth Differ.* **4,** 611-616

201. Liu, J., Streiff, R., Zhang, Y. L., Vestal, R. E., Spence, M. J., and Briggs, M. R. (1997) *J. Lipid Res.* **38,** 2035-2048

202. Li, C., Kraemer, F. B., Ahlborn, T. E., and Liu, J. (1999) *J. Biol. Chem.* **274,** 6747-6753

203. Kong, W., Abidi, P., Kraemer, F. B., Jiang, J. D., and Liu, J. (2005) *J. Lipid Res.* **46,** 1163-1171

204. Liu, J., Zhang, F., Li, C., Lin, M., and Briggs, M. R. (2003) *Arterioscler. Thromb. Vasc. Biol.* **23,** 90-96

205. Zhang, F., Lin, M., Abidi, P., Thiel, G., and Liu, J. (2003) *J. Biol. Chem.* **278,** 44246-44254

206. Johns, M. W. (1975) *Drugs* **9,** 448-478

207. Jefferson, J. W. (1975) *Psychosom. Med.* **37,** 160-179

208. Becker, C. E. (1979) *Adv. Intern. Med.* **24,** 183-202

209. Benowitz, N. L., Rosenberg, J., and Becker, C. E. (1979) *Med. Clin. North Am.* **63,** 267-296

210. Zaffaroni, A. (1991) *Ann. N. Y. Acad. Sci.* **618,** 405-421

211. Garcia, C. R., Siqueiros, A., and Benet, L. Z. (1978) *Pharm. Acta Helv.* **53,** 99-109

212. Shaw, J. E. and Chandrasekaran, S. K. (1978) *Drug Metab Rev.* **8,** 223-233

213. Heller, J. (1980) *Biomaterials* **1,** 51-57

214. Mikos, A. G. and Peppas, N. A. (1988) *Biomaterials* **9,** 419-423

215. Wichterle, O., LIM, D., and DREIFUS, M. (1961) *Cesk. Oftalmol.* **17,** 70-75

216. DREIFUS, M. and Wichterle, O. (1964) *Cesk. Oftalmol.* **20,** 393-399

217. Wichterle, O. and Lim, D. (1960) Hydrophilic gels in biologic use.

218. Murphy, G. F., Orgill, D. P., and Yannas, I. V. (1990) *Lab Invest* **62,** 305-313

219. Yannas, I. V., Lee, E., Orgill, D. P., Skrabut, E. M., and Murphy, G. F. (1989) *Proc. Natl. Acad. Sci. U. S. A* **86,** 933-937

220. Brown, L. R., Wei, C. L., and Langer, R. (1983) *J. Pharm. Sci.* **72,** 1181-1185

221. Langer, R. (1983) *Pharmacol. Ther.* **21,** 35-51

222. Rosen, H. B., Chang, J., Wnek, G. E., Linhardt, R. J., and Langer, R. (1983) *Biomaterials* **4,** 131-133

223. Hsu, F. Y., Tsai, S. W., Lan, C. W., and Wang, Y. J. (2005) *J. Mater. Sci. Mater. Med.* **16,** 341-345

224. Tsai, S. W., Chen, C. C., Liou, H. M., and Hsu, F. Y. (2009) *J. Biomed. Mater. Res. A*

225. Tsai, S. W., Chen, C. C., Chen, P. L., and Hsu, F. Y. (2008) *J. Biomed. Mater. Res. A*

226. Tsai, S. W., Hsu, F. Y., and Chen, P. L. (2008) *Acta Biomater.* **4,** 1332-1341

227. Tsai, S. W., Liu, R. L., Hsu, F. Y., and Chen, C. C. (2006) *Biopolymers* **83,** 381-388

228. Matthew, H. W., Basu, S., Peterson, W. D., Salley, S. O., and Klein, M. D. (1993) *J. Pediatr. Surg.* **28,** 1423-1427

229. Matthew, H. W., Salley, S. O., Peterson, W. D., and Klein, M. D. (1993) *Biotechnol. Prog.* **9,** 510-519

230. Matthew, H. W., Salley, S. O., Peterson, W. D., Jr., Deshmukh, D. R., Mukhopadhyay, A., and Klein, M. D. (1991) *ASAIO Trans.* **37,** M328-M330

231. Duconseille, E., Woerly, S., Kelche, C., Will, B., and Cassel, J. C. (1998) *Restor. Neurol. Neurosci.* **13,** 193-203

232. Lesny, P., De, C. J., Pradny, M., Vacik, J., Michalek, J., Woerly, S., and Sykova, E. (2002) *J. Chem. Neuroanat.* **23,** 243-247

233. Marchand, R., Woerly, S., Bertrand, L., and Valdes, N. (1993) *Brain Res. Bull.* **30,** 415-422

234. Plant, G. W., Woerly, S., and Harvey, A. R. (1997) *Exp. Neurol.* **143,** 287-299

235. Woerly, S., Doan, V. D., Sosa, N., de, V. J., and Espinosa-Jeffrey, A. (2004) *J. Neurosci. Res.* **75,** 262-272

236. Woerly, S., Doan, V. D., Evans-Martin, F., Paramore, C. G., and Peduzzi, J. D. (2001) *J. Neurosci. Res.* **66,** 1187-1197

237. Woerly, S., Pinet, E., de, R. L., Van, D. D., and Bousmina, M. (2001) *Biomaterials* **22,** 1095-1111

238. Woerly, S., Doan, V. D., Sosa, N., de, V. J., and Espinosa, A. (2001) *Int. J. Dev. Neurosci.* **19,** 63-83

239. Woerly, S., Petrov, P., Sykova, E., Roitbak, T., Simonova, Z., and Harvey, A. R. (1999) *Tissue Eng* **5,** 467-488

240. Woerly, S., Plant, G. W., and Harvey, A. R. (1996) *Biomaterials* **17,** 301-310

241. Woerly, S. (1993) *Biomaterials* **14,** 1056-1058

242. Campoccia, D., Doherty, P., Radice, M., Brun, P., Abatangelo, G., and Williams, D. F. (1998) *Biomaterials* **19,** 2101-2127

243. Prestwich, G. D., Marecak, D. M., Marecek, J. F., Vercruysse, K. P., and Ziebell, M. R. (1998) *J. Control Release* **53,** 93-103

244. Anseth, K. S., Metters, A. T., Bryant, S. J., Martens, P. J., Elisseeff, J. H., and Bowman, C. N. (2002) *J. Control Release* **78,** 199-209

245. Metters, A. T., Anseth, K. S., and Bowman, C. N. (1999) *Biomed. Sci. Instrum.* **35,** 33-38

246. van de, W. P., Metters, A. T., Schoenmakers, R. G., and Hubbell, J. A. (2005) *J. Control Release* **102,** 619-627

247. Lu, S. and Anseth, K. S. (1999) *J. Control Release* **57,** 291-300

248. Rhine, W. D., Hsieh, D. S., and Langer, R. (1980) *J. Pharm. Sci.* **69,** 265-270

249. Tamada, J. A. and Langer, R. (1993) *Proc. Natl. Acad. Sci. U. S. A* **90,** 552-556

250. Canal, T. and Peppas, N. A. (1989) *J. Biomed. Mater. Res.* **23,** 1183-1193

251. Lin, C. C. and Metters, A. T. (2006) *Adv. Drug Deliv. Rev.* **58,** 1379-1408

252. Drury, J. L. and Mooney, D. J. (2003) *Biomaterials* **24,** 4337-4351

253. Gander, B., Gurny, R., Doelker, E., and Peppas, N. A. (1989) *Pharm. Res.* **6,** 578-584

254. Zhong, Y., Zhang, L., Ding, A. G., Shenderova, A., Zhu, G., Pei, P., Chen, R. R., Mallery, S. R., Mooney, D. J., and Schwendeman, S. P. (2007) *J. Control Release* **122,** 331-337

255. Zhu, G., Mallery, S. R., and Schwendeman, S. P. (2000) *Nat. Biotechnol.* **18,** 52-57

256. Khoo, X., Hamilton, P., O'Toole, G. A., Snyder, B. D., Kenan, D. J., and Grinstaff, M. W. (2009) *J. Am. Chem. Soc.* **131,** 10992-10997

257. Delgado, C., Francis, G. E., and Fisher, D. (1992) *Crit Rev. Ther. Drug Carrier Syst.* **9,** 249-304

258. Delgado, C., Patel, J. N., Francis, G. E., and Fisher, D. (1990) *Biotechnol. Appl. Biochem.* **12,** 119-128

259. Francis, G. E., Fisher, D., Delgado, C., Malik, F., Gardiner, A., and Neale, D. (1998) *Int. J. Hematol.* **68,** 1-18

260. Francis, G. E., Delgado, C., Fisher, D., Malik, F., and Agrawal, A. K. (1996) *J. Drug Target* **3,** 321-340

261. Malik, F., Delgado, C., Knusli, C., Irvine, A. E., Fisher, D., and Francis, G. E. (1992) *Exp. Hematol.* **20,** 1028-1035

262. Veronese, F. M. (2001) *Biomaterials* **22,** 405-417

263. Veronese, F. M., Sacca, B., Polverino de, L. P., Sergi, M., Caliceti, P., Schiavon, O., and Orsolini, P. (2001) *Bioconjug. Chem.* **12,** 62-70

264. Veronese, F. M. and Harris, J. M. (2002) *Adv. Drug Deliv. Rev.* **54,** 453-456

265. Duncan, R. and Spreafico, F. (1994) *Clin. Pharmacokinet.* **27,** 290-306

266. Apicella, A., Cappello, B., Del Nobile, M. A., La Rotonda, M. I., Mensitieri, G., and Nicolais, L. (1993) *Biomaterials* **14,** 83-90

267. Middleton, J. C. and Tipton, A. J. (2000) *Biomaterials* **21,** 2335-2346

268. Gunatillake, P., Mayadunne, R., and Adhikari, R. (2006) *Biotechnol. Annu. Rev.* **12,** 301-347

269. Gunatillake, P. A. and Adhikari, R. (2003) *Eur. Cell Mater.* **5,** 1-16

270. Frazer, R. Q., Byron, R. T., Osborne, P. B., and West, K. P. (2005) *J. Long. Term. Eff. Med. Implants.* **15,** 629-639

271. Wang, J., Fonn, D., and Simpson, T. L. (2003) *Invest Ophthalmol. Vis. Sci.* **44,** 1070-1074

272. Okabe, K., Kimura, H., Okabe, J., Kato, A., Kunou, N., and Ogura, Y. (2003) *Invest Ophthalmol. Vis. Sci.* **44,** 2702-2707

273. Kato, A., Kimura, H., Okabe, K., Okabe, J., Kunou, N., and Ogura, Y. (2004) *Invest Ophthalmol. Vis. Sci.* **45,** 238-244

274. Bourges, J. L., Bloquel, C., Thomas, A., Froussart, F., Bochot, A., Azan, F., Gurny, R., BenEzra, D., and Behar-Cohen, F. (2006) *Adv. Drug Deliv. Rev.* **58,** 1182-1202

275. Chen, G. and Hoffman, A. S. (1995) *Nature* **373,** 49-52

276. Inoue, T., Chen, G., Nakamae, K., and Hoffman, A. S. (1998) *J. Control Release* **51,** 221-229

277. Kyriakides, T. R., Cheung, C. Y., Murthy, N., Bornstein, P., Stayton, P. S., and Hoffman, A. S. (2002) *J. Control Release* **78,** 295-303

278. Lackey, C. A., Press, O. W., Hoffman, A. S., and Stayton, P. S. (2002) *Bioconjug. Chem.* **13,** 996-1001

279. Chen, G. and Hoffman, A. S. (1994) *J. Biomater. Sci. Polym. Ed* **5,** 371-382

280. Chen, G. and Hoffman, A. S. (1993) *Bioconjug. Chem.* **4,** 509-514

281. Ding, Z., Chen, G., and Hoffman, A. S. (1998) *J. Biomed. Mater. Res.* **39,** 498-505

282. Ding, Z., Chen, G., and Hoffman, A. S. (1996) *Bioconjug. Chem.* **7,** 121-126

283. Kost, J., Horbett, T. A., Ratner, B. D., and Singh, M. (1985) *J. Biomed. Mater. Res.* **19,** 1117-1133

284. Langer, R. (1990) *Science* **249,** 1527-1533

285. Drobnik, J., Spacek, P., and Wichterle, O. (1974) *J. Biomed. Mater. Res.* **8,** 45-51

286. Creque, H. M., Langer, R., and Folkman, J. (1980) *Diabetes* **29,** 37-40

287. Verma, R. K., Mishra, B., and Garg, S. (2000) *Drug Dev. Ind. Pharm.* **26,** 695-708

288. Albisser, A. M., Jackman, W. S., Ferguson, R., Bahoric, A., and Goriya, Y. (1978) *Med. Prog. Technol.* **5,** 187-193

289. Chien, Y. W. (1985) *Methods Enzymol.* **112,** 461-470

290. Newhouse, M. T. and Dolovich, M. (1986) *Clin. Pharm.* **5,** 198-199

291. Yasukawa, T., Kimura, H., Tabata, Y., and Ogura, Y. (2001) *Adv. Drug Deliv. Rev.* **52,** 25-36

292. Katzhendler, I., Hoffman, A., Goldberger, A., and Friedman, M. (1997) *J. Pharm. Sci.* **86,** 110-115

293. Akbari, H., D'Emanuele, A., and Attwood, D. (1998) *Pharm. Dev. Technol.* **3,** 251-259

294. Vernallis, A. B., Hudson, K. R., and Heath, J. K. (1997) *J. Biol. Chem.* **272,** 26947-26952

295. Bird, A. C. (1995) *Am. J. Ophthalmol.* **119,** 543-562

296. Faktorovich, E. G., Steinberg, R. H., Yasumura, D., Matthes, M. T., and LaVail, M. M. (1992) *J. Neurosci.* **12,** 3554-3567

297. LaVail, M. M., Matthes, M. T., Yasumura, D., and Steinberg, R. H. (1997) *Exp. Eye Res.* **65,** 45-50

298. Penn, J. S., Naash, M. I., and Anderson, R. E. (1987) *Exp. Eye Res.* **44,** 779-788

299. Noell, W. K., Walker, V. S., Kang, B. S., and Berman, S. (1966) *Invest Ophthalmol.* **5,** 450-473

300. Chaum, E. (2003) *J. Cell Biochem.* **88,** 57-75

301. Cao, W., Wen, R., Li, F., LaVail, M. M., and Steinberg, R. H. (1997) *Exp. Eye Res.* **65,** 241-248

302. Wen, R., Cheng, T., Song, Y., Matthes, M. T., Yasumura, D., LaVail, M. M., and Steinberg, R. H. (1998) *Curr. Eye Res.* **17,** 494-500

303. Wen, R., Song, Y., Cheng, T., Matthes, M. T., Yasumura, D., LaVail, M. M., and Steinberg, R. H. (1995) *J. Neurosci.* **15,** 7377-7385

304. Samardzija, M., Wenzel, A., Aufenberg, S., Thiersch, M., Reme, C., and Grimm, C. (2006) *FASEB J.* **20,** 2411-2413

305. Sherry, D. M., Mitchell, R., Li, H., Graham, D. R., and Ash, J. D. (2005) *J. Neurosci. Res.* **82,** 316-332

306. Cao, W., Li, F., Steinberg, R. H., and LaVail, M. M. (2001) *Exp. Eye Res.* **72,** 591-604

307. Cao, W., Wen, R., Li, F., Cheng, T., and Steinberg, R. H. (1997) *Invest Ophthalmol. Vis. Sci.* **38,** 1358-1366

308. Pennica, D., King, K. L., Shaw, K. J., Luis, E., Rullamas, J., Luoh, S. M., Darbonne, W. C., Knutzon, D. S., Yen, R., Chien, K. R., and . (1995) *Proc. Natl. Acad. Sci. U. S. A* **92,** 1142-1146

309. Ichihara, M., Hara, T., Kim, H., Murate, T., and Miyajima, A. (1997) *Blood* **90,** 165-173

310. Glass, D. J., Nye, S. H., Hantzopoulos, P., Macchi, M. J., Squinto, S. P., Goldfarb, M., and Yancopoulos, G. D. (1991) *Cell* **66,** 405-413

311. Plun-Favreau, H., Perret, D., Diveu, C., Froger, J., Chevalier, S., Lelievre, E., Gascan, H., and Chabbert, M. (2003) *J. Biol. Chem.* **278,** 27169-27179

312. Robinson, R. C., Grey, L. M., Staunton, D., Vankelecom, H., Vernallis, A. B., Moreau, J. F., Stuart, D. I., Heath, J. K., and Jones, E. Y. (1994) *Cell* **77,** 1101-1116

313. Stahl, N., Boulton, T. G., Farruggella, T., Ip, N. Y., Davis, S., Witthuhn, B. A., Quelle, F. W., Silvennoinen, O., Barbieri, G., Pellegrini, S., and . (1994) *Science* **263,** 92-95

314. Taniguchi, T. (1995) *Science* **268,** 251-255

315. Amaravadi, R. and Thompson, C. B. (2005) *J. Clin. Invest* **115,** 2618-2624

316. Bravo, J. and Heath, J. K. (2000) *EMBO J.* **19,** 2399-2411

317. Simpson, R. J., Hammacher, A., Smith, D. K., Matthews, J. M., and Ward, L. D. (1997) *Protein Sci.* **6,** 929-955

318. Lutticken, C., Wegenka, U. M., Yuan, J., Buschmann, J., Schindler, C., Ziemiecki, A., Harpur, A. G., Wilks, A. F., Yasukawa, K., Taga, T., and . (1994) *Science* **263,** 89-92

319. Stahl, N., Farruggella, T. J., Boulton, T. G., Zhong, Z., Darnell, J. E., Jr., and Yancopoulos, G. D. (1995) *Science* **267,** 1349-1353

320. Rose, T. M., Lagrou, M. J., Fransson, I., Werelius, B., Delattre, O., Thomas, G., de Jong, P. J., Todaro, G. J., and Dumanski, J. P. (1993) *Genomics* **17,** 136-140

321. Jeffery, E., Price, V., and Gearing, D. P. (1993) *Cytokine* **5,** 107-111

322. Giovannini, M., Selleri, L., Hermanson, G. G., and Evans, G. A. (1993) *Cytogenet. Cell Genet.* **62,** 32-34

323. Giovannini, M., Djabali, M., McElligott, D., Selleri, L., and Evans, G. A. (1993) *Cytogenet. Cell Genet.* **64,** 240-244

324. Sporeno, E., Paonessa, G., Salvati, A. L., Graziani, R., Delmastro, P., Ciliberto, G., and Toniatti, C. (1994) *J. Biol. Chem.* **269,** 10991-10995

325. Liu, H., Fenollar-Ferrer, C., Cao, A., Anselmi, C., Carloni, P., and Liu, J. (2009) *Int. J. Mol. Med.* **23,** 161-172

326. Grant, S. L., Douglas, A. M., Goss, G. A., and Begley, C. G. (2001) *Growth Factors* **19,** 153-162

327. Nishimoto, N., Ogata, A., Shima, Y., Tani, Y., Ogawa, H., Nakagawa, M., Sugiyama, H., Yoshizaki, K., and Kishimoto, T. (1994) *J. Exp. Med.* **179,** 1343-1347

328. Chollangi, S., Wang, J., Martin, A., Quinn, J., and Ash, J. D. (2009) *Neurobiol. Dis.* **34,** 535-544

329. Richards, C. D., Kerr, C., Tanaka, M., Hara, T., Miyajima, A., Pennica, D., Botelho, F., and Langdon, C. M. (1997) *J. Immunol.* **159,** 2431-2437

330. Geroski, D. H. and Edelhauser, H. F. (2000) *Invest Ophthalmol. Vis. Sci.* **41,** 961-964

331. Hosoya, K. and Tomi, M. (2005) *Biol. Pharm. Bull.* **28,** 1-8

332. Maurice, D. M. (2002) *Surv. Ophthalmol.* **47 Suppl 1,** S41-S52

333. Pflugfelder, S. C., Hernandez, E., Fliesler, S. J., Alvarez, J., Pflugfelder, M. E., and Forster, R. K. (1987) *Arch. Ophthalmol.* **105,** 831-837

334. Maurice, D. (2001) *J. Ocul. Pharmacol. Ther.* **17,** 393-401

335. Ambati, J., Canakis, C. S., Miller, J. W., Gragoudas, E. S., Edwards, A., Weissgold, D. J., Kim, I., Delori, F. C., and Adamis, A. P. (2000) *Invest Ophthalmol. Vis. Sci.* **41,** 1181-1185

336. Ambati, J., Gragoudas, E. S., Miller, J. W., You, T. T., Miyamoto, K., Delori, F. C., and Adamis, A. P. (2000) *Invest Ophthalmol. Vis. Sci.* **41,** 1186-1191

337. Geroski, D. H. and Edelhauser, H. F. (2001) *Adv. Drug Deliv. Rev.* **52,** 37-48

338. Okabe, K., Kimura, H., Okabe, J., and Ogura, Y. (2007) *Retina* **27,** 770-777

339. Okabe, K., Kimura, H., Okabe, J., Kato, A., Shimizu, H., Ueda, T., Shimada, S., and Ogura, Y. (2005) *Invest Ophthalmol. Vis. Sci.* **46,** 703-708

340. Olsen, T. W., Aaberg, S. Y., Geroski, D. H., and Edelhauser, H. F. (1998) *Am. J. Ophthalmol.* **125,** 237-241

341. Olsen, T. W., Edelhauser, H. F., Lim, J. I., and Geroski, D. H. (1995) *Invest Ophthalmol. Vis. Sci.* **36,** 1893-1903

342. Marmor, M. F., Negi, A., and Maurice, D. M. (1985) *Exp. Eye Res.* **40,** 687-696

343. Hoffman, A. S. (2002) *Adv. Drug Deliv. Rev.* **54,** 3-12

344. Okabe, J., Kimura, H., Kunou, N., Okabe, K., Kato, A., and Ogura, Y. (2003) *Invest Ophthalmol. Vis. Sci.* **44,** 740-744

345. Yasukawa, T., Ogura, Y., Kimura, H., Sakurai, E., and Tabata, Y. (2006) *Expert. Opin. Drug Deliv.* **3,** 261-273

346. Yasukawa, T., Ogura, Y., Sakurai, E., Tabata, Y., and Kimura, H. (2005) *Adv. Drug Deliv. Rev.* **57,** 2033-2046

347. Yasukawa, T., Ogura, Y., Tabata, Y., Kimura, H., Wiedemann, P., and Honda, Y. (2004) *Prog. Retin. Eye Res.* **23,** 253-281

348. Harland, R. S. and Peppas, N. A. (1989) *J. Pharm. Sci.* **78,** 146-148

349. Crank, J. (1980) The Mathematics of Diffusion. Oxford University Press, Great Britain

350. Pitard, V., Lorgeot, V., Taupin, J. L., Aubard, Y., Praloran, V., and Moreau, J. F. (1998) *Eur. Cytokine Netw.* **9,** 599-605

APPENDIX

A1. Concentration profile as a function of position (x) and time (t):

Fick's Law:

$$\frac{\partial C}{\partial t} = D_g \frac{\partial^2 C}{\partial x^2} \qquad \text{---------- Eqn 1}$$

Where, C is the concentration of drug inside the gel at time t and position x, and D_g is the diffusion coefficient of the drug inside swollen hydrogel. The hydrogel is non-degradable and thus the structural properties of the hydrogel and thus diffusion coefficient of the drug will stay constant throughout the release process.

Boundary Conditions:

BC 1 $\quad C(\pm L, t) = 0$

BC2 $\quad C(x,0) = C_o \qquad\qquad -L < x < +L$

BC3 $\quad \left.\frac{\partial C}{\partial x}\right|_{x=0} = 0$

Since, concentration (C) is a function of position (x) and time (t), assuming the variables are separable, C can be defined as;

$$C = F(x)\,G(t) \qquad \text{---------- Eqn 2}$$

Thus, equation 1 can be rewritten as,

$$\frac{1}{G}\frac{\partial G}{\partial t} = \frac{D_g}{F}\frac{\partial^2 F}{\partial x^2} \qquad \text{---------- Eqn 3}$$

On the left hand side, we have an expression dependent on 't' while on the right hand side, we have an expression dependent on 'x'. For them to be equal, both sides must be equal to a constant. For computational ease, let this constant be $-\lambda^2 D_g$.

Thus,

$$\frac{1}{G}\frac{\partial G}{\partial t} = -\lambda^2 D_g \qquad \text{---------- Eqn 4}$$

$$\frac{1}{F}\frac{\partial^2 F}{\partial x^2} = -\lambda^2 \qquad \text{---------- Eqn 5}$$

Solving equations 4 and 5 give,

$$G = e^{-\lambda^2 D_g t} \qquad \text{---------- Eqn 6}$$

$$F = A\,Sin\lambda x + B\,Cos\lambda x \qquad \text{---------- Eqn 7}$$

Thus, concentration (C) can be redefined as;

$$C = \left(A\,Sin\lambda x + B\,Cos\lambda x\right)e^{-\lambda^2 D_g t} \qquad \text{---------- Eqn 8}$$

Since equation 1 is a linear equation, the most general solution is obtained by summing up all solutions of the type eqn 8. Thus, we have;

$$C = \sum_{n=0}^{\infty}\left(A_n\,Sin\lambda_n x + B_n\,Cos\lambda_n x\right)e^{-\lambda_n^2 D_g t} \qquad \text{---------- Eqn 9}$$

Using Boundary Condition 3 in equation 9;

$$\left.\frac{\partial C}{\partial x}\right|_{x=0} = 0 = \sum_{n=0}^{\infty}\left(\frac{A_n\,Cos\lambda_n x}{\lambda_n} - \frac{B_n\,Sin\lambda_n x}{\lambda_n}\right)e^{-\lambda_n^2 D_g t}\Bigg|_{x=0}$$

$$\Rightarrow \quad A_n Cos\lambda_n x\big|_{x=0} = B_n Sin\lambda_n x\big|_{x=0}$$

$$\Rightarrow \quad A_n\,(1) = 0$$

$$\Rightarrow \qquad A_n = 0$$

Using boundary condition 1 in equation 9;

$$0 = \sum_{n=0}^{\infty} B_n \, Cos\lambda_n x \, . \, e^{-\lambda_n^{\,2} D_g t}\Big|_{x=\pm L}$$

Since, $e^{-\lambda_n^{\,2} D_g t} \neq 0$ at $t = 0$

$$Cos\lambda_n x\big|_{x=\pm L} = 0$$

$$\Rightarrow \qquad \lambda_n L = \frac{(2n+1)\pi}{2}$$

$$\Rightarrow \qquad \lambda_n = \frac{(2n+1)}{L}\frac{\pi}{2}$$

Using boundary condition 2 in equation 9,

$$C_o = \sum_{n=0}^{\infty} B_n Cos\frac{(2n+1)}{2L}\pi x \qquad (-L < x < +L) \qquad \text{---------- Eqn 10}$$

Multiplying both sides of the equation 10 with $\left[Cos\frac{(2p+1)}{2L}\pi x \right]$

$$\sum_{p=0}^{\infty} C_o . Cos\frac{(2p+1)}{2L}\pi x = \sum_{n=0}^{\infty}\sum_{p=0}^{\infty} B_n Cos\frac{(2n+1)}{2L}\pi x . Cos\frac{(2p+1)}{2L}\pi x$$

Integrating with respect to 'x';

$$\sum_{p=0}^{\infty} C_o \cdot \int_{-L}^{L} Cos\frac{(2p+1)}{2L}\pi x dx = \sum_{n=0}^{\infty}\sum_{p=0}^{\infty} B_n \int_{-L}^{L} Cos\frac{(2n+1)}{2L}\pi x \cdot Cos\frac{(2p+1)}{2L}\pi x dx \quad \text{-- Eqn 11}$$

Consider $\int_{-L}^{L} Cos\frac{(2n+1)}{2L}\pi x \cdot Cos\frac{(2p+1)}{2L}\pi x dx$

$$= \frac{1}{2}\int_{-L}^{L}\left(Cos\left[\frac{(2n+1)+(2p+1)}{2L}\right]\pi x + Cos\left[\frac{(2n+1)-(2p+1)}{2L}\right]\pi x\right)dx$$

$$= \frac{1}{2}\int_{-L}^{L}\left(Cos\frac{(n+p+1)}{L}\pi x + Cos\frac{(n-p)}{L}\pi x\right)dx$$

Consider, n = p

$$= \frac{1}{2}\int_{-L}^{L}\left(Cos\frac{(2n+1)}{L}\pi x + 1\right)dx$$

$$= \frac{1}{2}\left[\frac{Sin\frac{(2n+1)}{L}\pi x}{\frac{(2n+1)\pi}{L}} + x\right]_{-L}^{L}$$

$$= \frac{1}{2}\left[\frac{2LSin(2n+1)\pi}{(2n+1)\pi} + 2L\right]$$

$= L$ Since, $Sin(2n+1)\pi = 0$

Consider $n \neq p$;

$$= \frac{1}{2}\left[\frac{Sin\left(\frac{n+p+1}{L}\right)\pi x}{\left(\frac{n+p+1}{L}\right)\pi} + \frac{Sin\left(\frac{n-p}{L}\right)\pi x}{\left(\frac{n-p}{L}\right)\pi}\right]_{-L}^{L}$$

$$= \frac{L}{2\pi}\left[\frac{Sin\left(\frac{n+p+1}{L}\right)\pi x}{(n+p+1)} + \frac{Sin\left(\frac{n-p}{L}\right)\pi x}{(n-p)}\right]_{-L}^{L}$$

$$= \frac{L}{\pi}\left[\frac{Sin(n+p+1)\pi}{(n+p+1)} + \frac{Sin(n-p)\pi}{(n-p)}\right]$$

For any value of n and p, both terms are equal to zero.

Thus;

$$\int_{-L}^{L} Cos\frac{(2n+1)}{2L}\pi x \cdot Cos\frac{(2p+1)}{2L}\pi x dx \qquad = 0 \; for \; n \neq p$$

$$= L \; for \; n = p$$

Taking n = p, equation 11 can be rewritten as,

$$\sum_{n=0}^{\infty} C_o \int_{-L}^{L} Cos\frac{(2n+1)}{2L}\pi x \, dx = \sum_{n=0}^{\infty} B_n L$$

$$\Rightarrow \qquad \sum_{n=0}^{\infty} C_o \left[\frac{Sin\left(\frac{2n+1}{2L}\right)\pi x}{\left(\frac{2n+1}{2L}\right)\pi}\right]_{-L}^{L} = \sum_{n=0}^{\infty} B_n L$$

$$\Rightarrow \qquad \sum_{n=0}^{\infty} C_o \cdot \left(\frac{2L}{2n+1}\right)\frac{1}{\pi} \cdot 2Sin\left(\frac{2n+1}{2}\right)\pi = \sum_{n=0}^{\infty} B_n L$$

$$\Rightarrow \qquad \sum_{n=0}^{\infty} \frac{4C_o L}{(2n+1)\pi} \cdot Sin(2n+1)\frac{\pi}{2} = \sum_{n=0}^{\infty} B_n L$$

Thus,

$$\sum_{n=0}^{\infty} \frac{4C_o L}{(2n+1)\pi} \cdot (-1)^n = \sum_{n=0}^{\infty} B_n L$$

$$B_n = (-1)^n \frac{4C_o}{(2n+1)\pi}$$

Substituting,

$$A_n = 0$$

$$\lambda_n = \frac{(2n+1)}{L}\frac{\pi}{2}$$

$$B_n = (-1)^n \frac{4C_o}{(2n+1)\pi}$$

in equation 9, we finally get

$$\boxed{C_{(x,t)} = \frac{4C_o}{\pi}\sum_{n=0}^{\infty}\frac{(-1)^n}{(2n+1)}\exp\left[\frac{-D_g(2n+1)^2\pi^2 t}{4L^2}\right]Cos\frac{(2n+1)}{L}\frac{\pi}{2}x}$$

A2. Fractional Release of Drug as a function of time (t)

Mass retained in the one-dimensional plane at time (t) = 0 is $C_o \cdot 2L$

Mass retained at time (t) = t is $\int_{-L}^{L} C_{(x,t)} dx$

Mass retained at time (t) = ∞ is 0

Thus, mass of the drug (M_t) released in time, t is $M_{(\text{in pellet at } t = 0)} - M_{(\text{in pellet at } t = t)}$

$$= 2C_o L - \int_{-L}^{L} C_{(x,t)} dx$$

Total mass of the drug that can be released (M_∞) is $M_{(\text{in pellet at } t = 0)}$

$$= 2C_o L$$

Thus,

$$\frac{M_t}{M_\infty} = \frac{2C_o L - \int_{-L}^{L} C_{(x,t)} dx}{2C_o L} \qquad \text{---------- Eqn 12}$$

Consider $\int_{-L}^{L} C_{(x,t)} dx$

$$= \int_{-L}^{L} \frac{4C_o}{\pi} \sum_{n=0}^{\infty} \frac{(-1)^n}{(2n+1)} \exp\left[\frac{-D_g (2n+1)^2 \pi^2 t}{4L^2}\right] \; Cos \frac{(2n+1)}{L} \frac{\pi}{2} x dx$$

$$= \frac{4C_o}{\pi}\sum_{n=0}^{\infty}\frac{(-1)^n}{(2n+1)}\exp\left[\frac{-D_g(2n+1)^2\pi^2 t}{4L^2}\right]\int_{-L}^{L} Cos\frac{(2n+1)}{L}\frac{\pi}{2}xdx$$

$$= \frac{4C_o}{\pi}\sum_{n=0}^{\infty}\frac{(-1)^n}{(2n+1)}\exp\left[\frac{-D_g(2n+1)^2\pi^2 t}{4L^2}\right]\left[\frac{Sin\frac{(2n+1)\pi x}{2L}}{\frac{(2n+1)\pi}{2L}}\right]_{-L}^{L}$$

$$= \frac{8C_oL}{\pi^2}\sum_{n=0}^{\infty}\frac{(-1)^n}{(2n+1)^2}\exp\left[\frac{-D_g(2n+1)^2\pi^2 t}{4L^2}\right]2Sin\frac{(2n+1)\pi L}{2L}$$

$$= \frac{16C_oL}{\pi^2}\sum_{n=0}^{\infty}\frac{(-1)^n}{(2n+1)^2}\exp\left[\frac{-D_g(2n+1)^2\pi^2 t}{4L^2}\right]Sin\frac{(2n+1)\pi}{2}$$

For any value of n;

$$(-1)^n Sin\frac{(2n+1)\pi}{2} = 1$$

Thus,

$$\int_{-L}^{L} C_{(x,t)}dx == 16C_oL\sum_{n=0}^{\infty}\frac{1}{(2n+1)^2\pi^2}\exp\left[\frac{-D_g(2n+1)^2\pi^2 t}{4L^2}\right]$$

Substituting this in equation 12, we obtain;

$$\boxed{\frac{\mathrm{M_t}}{\mathrm{M_\infty}} = 1 - 8\sum_{n=0}^{\infty}\frac{1}{(2n+1)^2\pi^2}\exp\left[\frac{-D_g(2n+1)^2\pi^2 t}{4L^2}\right]}$$